SOME CONTRIBUTIONS TO STOCHASTIC VOLATILITY MODELS

Thesis submitted to the University of Calicut

for the award of the degree of

DOCTOR OF PHILOSOPHY

in

STATISTICS

under the Faculty of Science

by

FATHIMA JAFNA

under the guidance of

Dr. KRISHNARANI S. D.

DEPARTMENT OF STATISTICS

UNIVERSITY OF CALICUT

KERALA- 673 635

INDIA

April - 2025

DEPARTMENT OF STATISTICS

UNIVERSITY OF CALICUT

Dr. Krishnarani S. D.
Associate Professor & Head

Calicut University (P.O.)
Kerala, India 673 635.
Phone: 0494 2407340, 341 (O)
Mob: 91-9496127836
Email: krishnaranisd@uoc.ac.in

CERTIFICATE

I hereby certify that the work presented in this thesis entitled **"Some Contributions to Stochastic Volatility Models"** is a bonafide work done by **Mrs. Fathima Jafna** under my guidance for the award of the degree of Doctor of Philosophy in the Department of Statistics, University of Calicut and that this work has not been included in any other thesis submitted previously for the award of any degree. Also, certified that the contents of the thesis have been checked using an anti-plagiarism database and no unacceptable similarity was found through the software check.

University of Calicut

25-04-2025

Dr. Krishnarani S. D.

Research Supervisor

Dr. Krishnarani S.D.
Associate Professor
Dept. of Statistics, University of Calicut
Calicut University P.O., Malappuram (Dist.)
Kerala - 673635

DEPARTMENT OF STATISTICS

UNIVERSITY OF CALICUT

Dr. Krishnarani S. D.
Associate Professor & Head

Calicut University (P.O.)
Kerala, India 673 635.
Phone: 0494 2407340, 341 (O)
Mob: 91-9496127836
Email: krishnaranisd@uoc.ac.in

CERTIFICATE

Certified that the corrections/suggestions recommended by the adjudicators of the Ph.D. thesis entitled **"Some Contributions to Stochastic Volatility Models"** submitted by **Mrs. Fathima Jafna**, Research Scholar, Department of Statistics, University of Calicut, under my supervision and guidance, have been incorporated in the thesis and that the contents in the thesis and the soft copy are one and the same.

University of Calicut

03-09-2025

Dr. Krishnarani S. D.

Research Supervisor

Dr. Krishnarani S.D.
Associate Professor
Dept. of Statistics, University of Calicut
Calicut University P.O., Malappuram (Dist.)
Kerala - 673635

DECLARATION

I, Fathima Jafna, hereby declare that the work presented in the thesis entitled **"Some Contributions to Stochastic Volatility Models"** is based on the original work done by me under the guidance of Dr. Krishnarani S. D., Department of Statistics, University of Calicut and has not been included in any other thesis submitted previously for the award of any degree. The contents of the thesis have undergone plagiarism check using the *iThenticate* software at C.H.M.K. Library, University of Calicut, and the similarity index found within the permissible limit. I also declare that the thesis is free from AI-generated content.

University of Calicut

25-04-2025

Fathima Jafna

Dr. Krishnarani S. D.

Research Supervisor

Dr. Krishnarani S.D.
Associate Professor
Dept. of Statistics, University of Calicut
Calicut University P.O., Malappuram (Dist.)
Kerala - 673635

Acknowledgements

First and foremost, I express my deepest gratitude to the Almighty for His blessings, guidance, and strength throughout this research journey.

I extend my heartfelt gratitude to my supervising guide, Dr. Krishnarani S. D., Associate Professor & Head, Department of Statistics, University of Calicut, for her invaluable supervision, scholarly guidance, constructive criticism, and unwavering support. Her encouragement and mentorship have been instrumental in shaping this research, and without her assistance, this thesis would not have been possible.

I am sincerely thankful to my teachers in the Department of Statistics Dr. M. Manoharan (Retired Senior Professor), Dr. K. Jayakumar (Senior Professor), and Dr. M. Dileepkumar (Assistant Professor) for their constant encouragement and invaluable support throughout my academic journey. I am also deeply grateful to the librarian and the non-teaching staff of the Department of Statistics, University of Calicut, for their timely help and cooperation. Furthermore, I would like to express my appreciation to all the teachers and non-teaching staff of Farook College (Autonomous) for their generous support and goodwill.

I would be remiss if I did not acknowledge and express my gratitude to my friends who have given me the joy of sharing my research experiences. I extend my heartfelt thanks to all my fellow research scholars at the Department of Statistics, University of Calicut, for their cooperation and warmth. I am also grateful to the research scholars at Farook College for their invaluable support.

I am profoundly grateful to my parents - to my late father, Subair, whose blessings have always been with me and who continues to inspire me at every step of this journey, and to my mother, Ramla, who has been a pillar of unwavering mental and emotional support throughout my academic life. I also extend my sincere gratitude to my brother and sister-in-law for their support. Additionally,

I am deeply thankful to my in-laws, including my brothers-in-law and sisters-in-law, for their understanding and for making my research journey smooth and stress-free.

I am especially grateful to my sweet daughter, Anfa Mehrin, for her understanding and patience during my academic endeavors. Finally, my love and deepest appreciation go to my husband, Basil P., whose motivation, encouragement, and continuous support have been the cornerstone of my ability to complete this research work.

Lastly, but certainly not least, I extend my heartfelt thanks once again to my extended family and friends for their patience, encouragement, and unwavering support throughout this research. This thesis would not have been possible without the support and help of numerous individuals, and I am forever grateful to each one of them.

25-04-2025 **Fathima Jafna**

Abstract

Stochastic volatility models are time series models that capture the time-varying nature of volatility in dynamic systems. Unlike traditional models with constant variance, stochastic volatility models allow volatility to evolve stochastically, offering a more realistic representation of uncertainty and risk. This thesis primarily focuses on the development of novel stochastic volatility models that extend classical frameworks by incorporating non-Gaussian distributions and alternative volatility structures, thereby increasing their adaptability across a wide range of applications. The proposed models are rigorously evaluated through parameter estimation methods, simulation studies, and real-world data analysis. In addition to financial modeling, this research explores the application of stochastic volatility models in non-traditional areas such as speech enhancement and image denoising, effectively bridging time series methodologies with signal processing techniques. Further, the stochastic volatility modeling approach is extended to multidimensional and spatial data structures to effectively capture complex spatial relationships, broadening its relevance to other applied fields. By expanding the theoretical foundation and demonstrating the practical versatility of stochastic volatility models, this work makes meaningful contributions to time series analysis, financial econometrics, signal processing, and spatial statistics. These innovations also lay the groundwork for future integration with machine learning frameworks and for applications in domains where accurately modeling uncertainty and variability is essential.

Keywords: Stochastic volatility, Induced Garima, Speech enhancement, Image denoising, Spatial volatility.

പഠനസംഗ്രഹം

ചലനാത്മക സംവിധാനങ്ങളിലെ അസ്ഥിരതയുടെ സമയ-വ്യതിയാന സ്വഭാവം പകർത്തുന്ന സമയ ശ്രേണി മാതൃകകളാണ് സ്റ്റോക്കാസ്റ്റിക് അസ്ഥിരത മാതൃകകൾ. സ്ഥിരമായ വ്യതിയാനങ്ങളുള്ള പരമ്പരാഗത മാതൃകകളിൽ നിന്ന് വ്യത്യസ്തമായി, അനിശ്ചിതത്വത്തിന്റെയും അപകടസാധ്യതയുടെയും കൂടുതൽ യാഥാർത്ഥ്യബോധമുള്ള പ്രാതിനിധ്യം വാഗ്ദാനം ചെയ്തുകൊണ്ട്, സ്റ്റോക്കാസ്റ്റിക് അസ്ഥിരത മാതൃകകൾ അസ്ഥിരതയെ സ്ഥിരമായി വികസിപ്പിക്കാൻ അനുവദിക്കുന്നു. നോൺ-ഗൗസിയൻ വിതരണങ്ങളും ഇതര അസ്ഥിരത ഘടനകളും ഉൾപ്പെടുത്തി പരമ്പരാഗത ചട്ടക്കൂടുകൾ വിപുലീകരിക്കുന്ന പുതിയ സ്റ്റോക്കാസ്റ്റിക് അസ്ഥിരത മാതൃകകളുടെ വികസനത്തിലാണ് ഈ പ്രബന്ധം പ്രാഥമികമായി ശ്രദ്ധ കേന്ദ്രീകരിക്കുന്നത്. അതുവഴി മാതൃകകളുടെ വിവിധ പ്രയോഗ മേഖലകളിലേക്കുള്ള അനുയോജ്യത വർധിപ്പിക്കുന്നു. പാരാമീറ്റർ അനുമാനനം, സൂക്ഷ്മാനുകരണ പഠനങ്ങൾ, യഥാർത്ഥ ലോകമായി ബന്ധപ്പെട്ട ഡാറ്റ വിശകലനം എന്നിവയിലൂടെ നിർദ്ദിഷ്ട മാതൃകകൾ കർശനമായി വിലയിരുത്തുകയും ചെയ്യുന്നു . സാമ്പത്തിക മാതൃക നിർമ്മാണത്തിന് പുറമേ, സംഭാഷണ മെച്ചപ്പെടുത്തൽ, ചിത്ര ശബ്ദനിർമാർജനം തുടങ്ങിയ പാരമ്പര്യേതര മേഖലകളിൽ സ്റ്റോക്കാസ്റ്റിക് അസ്ഥിരത മാതൃകകളുടെ പ്രയോഗവും സിഗ്നൽ സംസ്കരണ സാങ്കേതികതകൾ ഉപയോഗിച്ച് സമയ ശ്രേണി രീതിശാസ്ത്രത്തെ ഫലപ്രദമായി ബന്ധിപ്പിക്കുന്നതിനും ഈ ഗവേഷണം പര്യവേക്ഷണം ചെയ്യുന്നു. കൂടാതെ, സങ്കീർണ്ണമായ സ്ഥിതിഗതിക ബന്ധങ്ങൾ ഫലപ്രദമായി ഉൾക്കൊള്ളുന്നതിനും മറ്റ് പ്രായോഗിക മേഖലകളുമായുള്ള പ്രസക്തി വിപുലീകരിക്കുന്നതിനുമായി സ്റ്റോക്കാസ്റ്റിക് അസ്ഥിരത മാതൃക സമീപനം ബഹുമുഖ, സ്ഥലംവിതാന ഘടനകളിലേക്ക് വരെ വിപുലീകരിച്ചിരിക്കുന്നു. ഇതിലൂടെ മറ്റ് പ്രയോഗാത്മക മേഖലകളിലേക്കുള്ള അതിന്റെ പ്രസക്തിയും വ്യാപിപ്പിക്കപ്പെടുന്നു. സൈദ്ധാന്തിക അടിത്തറ വികസിപ്പിക്കുന്നതിലൂടെയും സ്റ്റോക്കാസ്റ്റിക് അസ്ഥിരത മാതൃകകളുടെ പ്രായോഗിക വൈവിധ്യം പ്രകടമാക്കുന്നതിലൂടെയും, ഈ പ്രബന്ധം സമയ ശ്രേണി വിശകലനം, സാമ്പത്തികശാസ്ത്രം, സിഗ്നൽ സംസ്കരണം, സ്ഥലംസ്ഥിതിവിവര ശാസ്ത്രം എന്നിവയിൽ അർത്ഥവത്തായ സംഭാവനകൾ നൽകുന്നു. ഈ പുതുമകൾ മെഷീൻ ലേണിംഗ് ചട്ടക്കൂടുകളുമായുള്ള ഭാവിയിലെ സംയോജനത്തിനും അനിശ്ചിതത്വവും വ്യതിയാനവും കൃത്യമായി മാതൃകയാക്കേണ്ട മേഖലകളിലെ പ്രയോഗങ്ങൾക്കും അടിത്തറയിടുന്നു.

സൂചകപദങ്ങൾ: സ്റ്റോകാസ്റ്റിക് അസ്ഥിരത, ഇൻഡ്യൂസ്ഡ് ഗരിമ , സംഭാഷണ മെച്ചപ്പെടുത്തൽ, ചിത്ര ശബ്ദനിർമാർജനം, സ്ഥലാസ്ഥിരത.

To my beloved parents

Contents

List of Figures

List of Tables

List of Abbreviations

ACF	Autocorrelation function
AR	Autoregressive
ARCH	Autoregressive conditional heteroskedasticity
ARIMA	Autoregressive integrated moving average
ARMA	Autoregressive moving average
DWT	Discrete wavelet transform
EMM	Efficient method of moments
EAR	Exponential autoregressive
EMARMIN	Exponential mixture of autoregressive and minification
GARCH	Generalized autoregressive conditional heteroskedasticity
GMM	Generalized method of moments
IMCRA	Improved minima controlled recursive averaging
iid	Independent and identically distributed
i-Garima	Induced-Garima
IDWT	Inverse discrete wavelet transform

K-S	Kolmogorov-Smirnov
LSD	Log-spectral distortion
MCMC	Markov chain Monte Carlo
MAE	Mean absolute error
MSE	Mean squared error
MSSIM	Mean structural similarity index measure
MMSE	Minimum mean squared error
MA	Moving average
NEAR	New exponential autoregressive
1-D	One-dimensional
OMLSA	Optimal modified log-spectral amplitude
PACF	Partial autocorrelation function
PSNR	Peak signal-to-noise ratio
PESQ	Perceptual evaluation of speech quality
FOM	Pratt's figure of merit
pdf	Probability density function
QML	Quasi-maximum likelihood
RMSE	Root mean squared error
STFT	Short-time Fourier transform
STOI	Short-time objective intelligibility
SNR	Signal-to-noise-ratio

SE	Standard error
SV	Stochastic volatility
SC	Structural content
2-D	Two-dimensional
VaR	Value at Risk

CHAPTER 1

Introduction

1.1 Introduction

The study of time series, which involves analyzing sequentially recorded observations over time, is crucial in understanding dynamic and evolving systems around us. The use of time series data is widespread in many fields, such as finance, economics, climate science, engineering, etc. A systematic analysis of these data allows researchers to develop empirical models that capture underlying patterns, deliver more accurate predictions, and inform their decisions.

Classical time series models, such as those proposed by Box & Jenkins (1970), are based on linearity and Gaussian assumptions, making them analytically convenient and computationally efficient. Despite these assumptions, financial data show characteristics such as nonlinearity, heavy tails (leptokurtosis), volatility clustering, and abrupt regime shifts. Consequently, conventional linear models fail to capture the complexity of financial time series dynamics. This has led researchers to turn to more advanced stochastic modeling techniques that are more flexible in dealing with these complexities.

Among these advanced methods, volatility modeling has emerged as a critical area in financial econometrics. Financial markets are inherently volatile, charac-

terized by high uncertainty, sudden fluctuations, and periods of extreme market behavior, especially during financial crises. Traditional models, such as the Black-Scholes model (Black & Scholes (1973)), assume constant volatility, a simplifying assumption that does not capture the reality of financial markets. Market volatility is typically time-dependent and has persistence and clustering properties, with episodes of high volatility usually followed by more volatility. This shortcoming in traditional models has prompted the evolution of more advanced frameworks, which has resulted in the formulation of stochastic volatility (SV) models.

SV models offer a more realistic approach, allowing volatility to evolve randomly over time. Unlike constant-volatility models, SV models introduce an additional latent process governing volatility, capturing the inherent randomness and fluctuations observed in financial returns. This makes SV models particularly useful for derivative pricing, risk management, and portfolio optimization, as they provide a more accurate representation of market uncertainty. These models align with empirical observations, effectively capturing key market phenomena such as volatility clustering, leverage effects, and non-Gaussian return distributions. By incorporating flexible distributional assumptions and dynamic volatility structures, these models can better represent financial risk and improve investment strategies. Their adaptability makes them particularly suitable for capturing the intricate behavior of real-world financial data, particularly during times of market turbulence or structural shifts. As a result, they have become an essential tool for financial analysts, risk managers, and quantitative researchers aiming to develop robust and responsive financial models.

1.2 Motivation

Studying SV models is crucial due to the intrinsic limitations of classical financial models. The classical models that are based on constant or deterministic volatility assumptions often tend to inadequately describe the real-world data, resulting in poor predictions and decision-making. By incorporating stochastic components into volatility modeling, researchers can provide more realistic depictions of complex systems, thus improving forecasting precision and risk evaluation. The need for SV models also arises from well-established market phenomena. Volatility generally exhibits time variation, clustering, and mean reversion. Periods of high volatility tend to persist, just as low volatility phases often endure. Furthermore, financial markets often display the leverage effect, where negative asset returns are typically associated with increased volatility. These characteristics, along with the growing availability of high-frequency and large-scale time series data in various fields, highlight the necessity of more sophisticated models that can manage nonlinearities as well as structural changes, leading to the development and refinement of SV frameworks.

The application of SV models in decision-making and risk management modeling is another important motivating factor. Accurate estimates of volatility are required for asset allocation, hedging, and capital adequacy planning in financial markets. Analogously, in other domains, precise modeling of uncertainty can improve forecasting, resource allocation, and adaptive control in dynamic systems. As data-driven methods are becoming increasingly common, robust SV models will be increasingly useful for handling the nonlinearities and diverse sources of uncertainty in a vast variety of applications.

Although SV models have been widely researched in finance, their potential applications across other domains have not been very well explored. Most real-world

systems exhibit time-varying uncertainty, and hence SV marks to be a valuable framework across a wide range of fields. For example, it can be employed in signal processing for denoising signals, and in spatial dynamics to analyze environmental variability, climate patterns, epidemiological spread, etc., where conventional models struggle to capture dynamic fluctuations effectively. Hence, by leveraging SV models, we can improve the analysis of uncertainty and variability in these contexts, paving the way for new research and practical applications, thereby addressing the gap in current research.

In the following sections, we introduce some basic concepts that form the foundation for the systematic development of the thesis in the subsequent chapters.

1.3 Some basic concepts

In this section, we define some basic definitions of stochastic processes, stationary processes, and key concepts such as autocorrelation and partial autocorrelation functions etc., which are essential for a proper understanding of time series models.

1.3.1 Stochastic processes

In probability theory, a stochastic process is defined as a collection of random variables $\mathcal{Z}(\omega, t)$ indexed by time t in a specified index set and ω in a sample space, defined on a probability space $(\Omega, \mathcal{F}, P)$, where Ω is the sample space, $\mathcal{F}$ is a sigma-algebra of subsets of Ω, and P is the probability measure. For a fixed outcome $\omega \in \Omega$, the function $\mathcal{Z}(\omega, t)$, which depends on t, is referred to as a sample function or realization of the process.

The complete set of all possible realizations constitutes the ensemble of the stochastic process. A time series is essentially one such realization or sample function drawn from a specific stochastic process. To simplify notation, the dependence

on ω is often omitted when referring to a stochastic process. Thus, $\mathcal{Z}(\omega, t)$ is generally written as $\mathcal{Z}(t)$ or $\mathcal{Z}_t$. The mean and variance functions of the stochastic process are $\mu_t = E(\mathcal{Z}_t)$, and $\sigma_t^2 = \text{Var}(\mathcal{Z}_t) = E\Big[(\mathcal{Z}_t - \mu_t)^2\Big]$ respectively.

1.3.2 Stationary processes

Stationarity is a form of invariance used to model data-dependence structures. There are two types of stationarity: weak stationarity and strict stationarity.

1.3.2.1 Strict stationarity

A time series $\{\mathcal{Z}_t\}$ is strictly stationary if the joint probability distribution of $(\mathcal{Z}_{t_1}, \mathcal{Z}_{t_2}, \ldots, \mathcal{Z}_{t_n})$ is identical to that of $(\mathcal{Z}_{t_1+k}, \mathcal{Z}_{t_2+k}, \ldots, \mathcal{Z}_{t_n+k})$ for all t and k, provided n is any positive integer and $(t_1, t_2, \ldots, t_n)$ is any collection of n time indices. That is, the distributions are invariant over time.

1.3.2.2 Weak stationarity

A time series $\{\mathcal{Z}_t\}$ is weakly stationary or covariance stationary if its mean remains constant over time, its variance is finite, and its autocovariance function depends only on the time lag, not on the specific time points.

It is evident that if $\{\mathcal{Z}_t\}$ is strictly stationary with finite first two moments, then it is also weakly stationary. The converse does not hold in general. Notably, in the case of a Gaussian process, weak stationarity is equivalent to strict stationarity.

1.3.3 Autocorrelation function

Let $\{\mathcal{Z}_t : t = 0, \pm 1, \pm 2, \ldots\}$ be a stochastic process. The autocovariance function at lag k is the covariance between $\mathcal{Z}_t$ and $\mathcal{Z}_{t-k}$ defined as,

$$\gamma_k = \text{Cov}\left(\mathcal{Z}_t, \mathcal{Z}_{t-k}\right) = E\left(\left(\mathcal{Z}_t - E\left(\mathcal{Z}_t\right)\right)\left(\mathcal{Z}_{t-k} - E\left(\mathcal{Z}_{t-k}\right)\right)\right), k = 0, \pm 1, \pm 2, \ldots.$$

The autocorrelation function (ACF) at lag k is then defined as the correlation coefficient between $\mathcal{Z}_t$ and $\mathcal{Z}_{t-k}$, $k > 0$, represented by $\rho_Z(k)$ and given by,

$$\rho_Z(k) = \text{Corr}\left(\mathcal{Z}_t, \mathcal{Z}_{t-k}\right) = \frac{\text{Cov}\left(\mathcal{Z}_t, \mathcal{Z}_{t-k}\right)}{\sqrt{\text{Var}\left(\mathcal{Z}_t\right)}\sqrt{\text{Var}\left(\mathcal{Z}_{t-k}\right)}}, \tag{1.1}$$

where Var(.) represents the variance function of the process, also denoted by ρ_k. For a strictly stationary process, since $\text{Var}\left(\mathcal{Z}_t\right)$ and $\text{Var}\left(\mathcal{Z}_{t-k}\right)$ are equal, we have ACF as,

$$\rho_Z(k) = \frac{\text{Cov}\left(\mathcal{Z}_t, \mathcal{Z}_{t-k}\right)}{\text{Var}\left(\mathcal{Z}_t\right)} = \frac{\gamma_k}{\gamma_0}.$$

1.3.4 Partial autocorrelation function

For a stationary process $\{\mathcal{Z}_t\}$, the partial autocorrelation function (PACF) denoted by $\phi_{k,k}$ for $k = 1, 2, 3, \ldots$, is defined as the correlation between $\mathcal{Z}_t$ and $\mathcal{Z}_{t-k}$ by fixing the effects of $\mathcal{Z}_{t-1}, \mathcal{Z}_{t-2}, \ldots, \mathcal{Z}_{t-(k-1)}$. That is,

$$\phi_{1,1} = \text{Corr}\left(\mathcal{Z}_1, \mathcal{Z}_0\right) = \rho_1,$$

and

$$\phi_{k,k} = \text{Corr}\left(\mathcal{Z}_k - \hat{\mathcal{Z}}_k, \mathcal{Z}_0 - \hat{\mathcal{Z}}_0\right), k \geq 2,$$

where $\hat{\mathcal{Z}}_k$ is the regression of $\mathcal{Z}_k$ on $\{\mathcal{Z}_1, \mathcal{Z}_2, ..., \mathcal{Z}_{k-1}\}$ and $\hat{\mathcal{Z}}_0$ is the regression of $\mathcal{Z}_0$ on $\{\mathcal{Z}_1, \mathcal{Z}_2, ..., \mathcal{Z}_{k-1}\}$.

1.3.5 White noise

A sequence $\{\eta_t : t \geq 1\}$ of independent and identically distributed (iid) random variables with mean zero and a constant variance σ_η^2 is called white noise. This process is also often referred to as innovation, shock, or noise at time t, and the

autocovariance function of $\{\eta_t\}$ is given by,

$$\gamma_k = \begin{cases} \sigma_\eta^2, & \text{if } k = 0, \\ 0, & \text{if } k \neq 0. \end{cases}$$

1.4 Box-Jenkins methodology

This section introduces the Box-Jenkins methodology, a paradigm for time series analysis and forecasting developed by Box & Jenkins (1970). It is a systematic approach to time series model building and forecasting, mainly consisting of four key steps. They are,

1. Identification
2. Estimation
3. Diagnostic Checking
4. Forecasting

1.4.1 Identification of the model

A tentative model is first identified by analyzing historical data, typically using tools like correlograms, to propose a parametric model of unknown parameters.

1.4.2 Estimation of the parameters

One of the most important steps in the model-building process is estimating the model's unknown parameters. Various methods of parameter estimation, based on different theoretical frameworks, are discussed in the literature (see Box & Jenkins (1970)). Although these methods produce comparable estimates, their

effectiveness may differ based on the particular model under study.

1.4.3 Model diagnostic checking

After estimating the model parameters, it is essential to evaluate the adequacy of the model by verifying the model assumptions made about the errors. Residuals, which are obtained after parameter estimation, act as a suitable basis for this validation. The model diagnostic checking commonly involves techniques like overfitting, examining residual plots, and, most importantly, ensuring that the residuals are approximately uncorrelated. In time series analysis, this is a crucial stage since a well-fitting model should accurately depict the dependence structure of the data. The ACF is a key measure of this dependence. In essence, a robust time series model should produce residuals that closely resemble white noise, indicating minimal correlation. The autocorrelation is tested using the portmanteau tests. It identifies if there is any dependence structure that is unexplained by the fitted model. In our study, we have used the Ljung-Box portmanteau test as the statistical test to check the autocorrelation structure of data.

Ljung-Box portmanteau test

Ljung & Box (1978) introduced the portmanteau statistic as,

$$Q(n) = m(m+2)\sum_{k=1}^{n}\frac{\hat{\rho}_k}{m-k},$$

where m is the sample size, n is the number of lags tested, and $\hat{\rho}_k$ is the sample ACF at lag k. The null hypothesis is $H_0 : \rho_1 = \rho_2 = \ldots = \rho_n = 0$ against the alternative hypothesis $H_1 : \rho_k \neq 0$ for some $k \in 1, 2, \ldots n$. We reject H_0 if $Q(n) > \chi^2_{n,\alpha}$ such that $\chi^2_{n,\alpha}$ is the $100(1-\alpha)$ percentile of the chi-squared distribution of n degrees of freedom.

For checking the normality assumption of residuals, we have considered the Jarque-Bera test in our study.

Jarque-Bera test

Jarque & Bera (1980) proposed the Jarque-Bera test statistic as,

$$JB = \frac{m}{6}\left(S^2 + \frac{(K-3)^2}{4}\right),$$

where m is the sample size, S and K are the skewness and kurtosis respectively. The null hypothesis is H_0 : The data follows a normal distribution, and the alternative hypothesis is H_1 : The data deviates from normality. We reject H_0 if $JB > \chi^2_{2,\alpha}$, where $\chi^2_{2,\alpha}$ is the $100(1-\alpha)$ percentile of the chi-squared distribution of 2 degrees of freedom.

Model diagnostic checking is often combined with model selection measures like the Akaike information criterion, Bayesian information criterion, etc., as these methodologies work in conjunction with one another. Diagnostic checks yield information on how to improve the current model, whereas information criteria provide an objective method of model selection from the same family. By exploring these diagnostic checking procedures, practitioners are in a better position to appreciate the relative merits of various models and how they can be properly estimated.

1.4.4 Forecasting

Predicting the future behavior of a time series is a fundamental objective in time series analysis. In particular, the objective is to use observations up to time t to estimate the value of the variable at an arbitrary future time. The minimum mean squared error (MMSE) approach is frequently used for forecasting when a linear model is appropriate. The MMSE forecast $\hat{\mathcal{Z}}_{t+l}$ at time t (the forecasting

origin) is determined by the conditional expectation $E(\mathcal{Z}_{t+l}|\mathcal{Z}_t, \mathcal{Z}_{t-1}, \dots)$, which utilizes past observations. Additionally, the forecast error $\hat{e}_{t+l} = \mathcal{Z}_{t+l} - \hat{Z}_{t+l}$ is an important component, as it quantifies the difference between the actual and predicted values. In financial time series, forecasting volatility is essential, especially since volatility models are intrinsically nonlinear and necessitate tailored approaches for different models.

1.5 Linear time series models

The Box-Jenkins methodology, a traditional framework for analyzing time series, assumes that the observed series is generated by a linear process. Time series that adhere to this presumption are called linear time series. Autoregressive (AR), moving average (MA), autoregressive moving average (ARMA), and autoregressive integrated moving average (ARIMA) models are a few examples of these types of models.

1.5.1 Autoregressive models

The AR model is a type of stochastic model that effectively captures the behavior of certain real-world time series. In this setup, the current value of the process is expressed as a linear combination of its past values and a random error term.
Let $\mathcal{Z}_t, \mathcal{Z}_{t-1}, \mathcal{Z}_{t-2}, \dots$, be the values of the process at equally spaced time points $t, t-1, t-2, \dots$. Define $\tilde{\mathcal{Z}}_t = \mathcal{Z}_t - \mu$ as the deviations of $\mathcal{Z}_t$ from its mean μ. The process is then defined as,

$$\tilde{\mathcal{Z}}_t = \phi_1 \tilde{\mathcal{Z}}_{t-1} + \dots + \phi_p \tilde{\mathcal{Z}}_{t-p} + \eta_t,$$

is the autoregressive process of order p, represented as AR(p). And $\{\eta_t\}$ represents white noise such that $\eta_t \sim WN(0, \sigma_\eta^2)$, and η_t is uncorrelated with $\tilde{\mathcal{Z}}_r$ for $r < t$. The above equation can also be represented equivalently as,

$$\Phi(B)\tilde{\mathcal{Z}}_t = \eta_t,$$

where $\Phi(B)$ is the characteristic polynomial associated with the AR process and is given by, $\Phi(B) = 1 - \phi_1 B - \phi_2 B^2 \ldots - \phi_p B^p$. This operator uses the backshift operator $B^k \tilde{\mathcal{Z}}_t = \tilde{\mathcal{Z}}_{t-k}$ to combine previous values. The AR(p) process is analogous to a multiple linear regression model, but instead of regressing on independent variables, $\tilde{\mathcal{Z}}_t$ is regressed on its own lagged values in the AR model, hence the term "auto." If all roots of the associated characteristic polynomial $\Phi(B) = 0$ lie outside the unit circle, then the AR(p) process is weakly stationary.
In particular, the AR model of order 1 (AR(1)) holds significant importance due to its simplicity and useful properties. It is defined as,

$$\tilde{\mathcal{Z}}_t = \phi\tilde{\mathcal{Z}}_{t-1} + \eta_t, \tag{1.2}$$

where $\eta_t \sim WN(0, \sigma_\eta^2)$. The sequence $\{\mathcal{Z}_t\}$ forms a weakly stationary AR(1) process when $|\phi| < 1$ and the ACF is given by,

$$\rho_z(k) = \phi^k, \quad k = 0, 1, 2, \ldots.$$

This highlights the exponential decay of autocorrelations as k increases, making the AR(1) model a fundamental building block for understanding more complex time series models.

1.5.2 Moving average models

The MA process is another widely used method for modeling the observed time series. In this model, the observation at time t, $\mathcal{Z}_t$, is expressed as a finite linear combination of current and past random shocks. A moving average process of order q, denoted by MA(q) is defined as,

$$\tilde{\mathcal{Z}}_t = \eta_t + \theta_1\eta_{t-1} + \theta_2\eta_{t-2} + \ldots + \theta_q\eta_{t-q},$$

where $\eta_t \sim WN(0, \sigma_\eta^2)$, and θ_i $(i = 1, 2, \ldots, q)$ are MA parameters. Equivalently, the above model can be written as,

$$\tilde{\mathcal{Z}}_t = \Theta(B)\eta_t,$$

where $\Theta(B) = 1+\theta_1 B+\theta_2 B^2+\ldots+\theta_q B^q$ is the characteristic polynomial associated with the MA(q) model and $B^k\tilde{\mathcal{Z}}_t = \tilde{\mathcal{Z}}_{t-k}$ is the backshift operator. In general, the MA(q) process is always weakly stationary as it is expressed as a finite linear combination of white noise terms, which are stationary by definition.
The simplest moving average process, MA(1) is defined as,

$$\tilde{\mathcal{Z}}_t = \eta_t + \theta_1\eta_{t-1}.$$

Here, $\tilde{\mathcal{Z}}_t$ is a linear function of the current shock η_t and the immediately preceding shock η_{t-1}. The MA(1) process is always stationary. However, it is invertible if $|\theta_1| < 1$.

1.5.3 Autoregressive moving average models

In some situations, higher-order models with additional parameters may be required to fully reflect the dynamic structure of the data, making the previously stated AR or MA models cumbersome. ARMA models are introduced to address this issue (See Box et al. (2015)). A general ARMA(p, q) model is defined as,

$$\tilde{\mathcal{Z}}_t = \sum_{i=1}^{p} \phi_i \tilde{\mathcal{Z}}_{t-i} + \eta_t + \sum_{j=1}^{q} \theta_j \eta_{t-j},$$

where $\eta_t \sim WN(0, \sigma_\eta^2)$, and p and q are non-negative integers. The model is stationary if the AR(p) component is stationary. For an in-depth review of linear time series models, one may refer to Box et al. (2015).

1.6 Financial time series models

Financial time series are characterized by uncertainty, particularly in the irregular behavior of financial indicators such as stock prices, exchange rates, and bond yields, which are subject to time-dependent fluctuations. This variability, also known as volatility, can generate high-frequency stochastic data. The dynamics of such series are best described using stochastic models, making statistical theory and methods essential in financial time series analysis to manage the inherent uncertainty.

In the following sections, we explore various aspects of financial time series, highlighting key models and their characteristics.

1.6.1 Stylized facts of financial time series

One primary goal of analyzing financial time series is to model and forecast the volatility, or time-varying conditional variance of asset returns. Conditional variances in financial time series are empirically shown to fluctuate over time, indicating the presence of conditional heteroskedasticity. According to Tsay (2005), the return series is more appropriate for financial analysis since it captures relative changes more accurately. It is often more effective to analyze the return series X_t defined by,

$$X_t = \frac{P_t - P_{t-1}}{P_{t-1}} = \frac{P_t}{P_{t-1}} - 1, \quad t = 1, 2, 3, \ldots,$$

rather than using raw price data. The main advantages of using this return series over the actual price series are

1. **Scale-Free Summary:** The return series makes it simpler to compare different assets by offering a standardized measure of investment performance.

2. **Statistical Properties:** Return series are easier to model than price series because they have better statistical properties.

The log-return series is defined as,

$$X_t = \log(P_t) - \log(P_{t-1}) = \log\left(\frac{P_t}{P_{t-1}}\right), \quad t = 1, 2, 3, \ldots,$$

is particularly well-suited for studying stochastic market behavior. Empirical studies (Mandelbrot (1997); Fama (1965); Cont (2001)) reveal that the return series $\{X_t\}$ possesses the following characteristics:

- No significant autocorrelation in $\{X_t\}$.

- Significant serial correlation in $\{X_t^2\}$.

- Heavy-tailed marginal distributions for $\{X_t\}$.
- Time-varying conditional variance (volatility) for $\{X_t\}$.
- **Volatility Clustering:** Large (small) price changes tend to follow large (small) price changes.
- **Leverage Effect:** Volatility is negatively correlated with asset returns.

The non-constant nature of conditional variances has led researchers to develop two major families of models to describe time-varying, autocorrelated volatility processes. The first category consists of observation-driven models, such as the autoregressive conditional heteroskedasticity (ARCH) model introduced by Engle (1982). These models assume that conditional variances are deterministic functions of the squared past returns. The second category includes parameter-driven models, such as the SV models proposed by Taylor (1986). According to these models, the conditional variance at time t follows a stochastic process controlled by latent variables. Next, we provide a detailed description of each of these models.

1.6.2 Autoregressive conditional heteroskedasticity models

In econometrics, the ARCH model, introduced by Engle (1982), was one of the earliest attempts to model clustered volatility in time series data. Engle (1982) utilized conditional variance to measure volatility and proposed a dynamic framework for modeling it. Since then, ARCH models have been widely applied in financial time series research for predicting time-varying confidence intervals and more efficient estimators in the presence of heteroskedasticity.

For a time series $\{X_t\}$, the ARCH(p) model is defined as,

$$X_t = w_t Y_t, \quad w_t = \alpha_0 + \sum_{i=1}^{p} \alpha_i X_{t-i}^2,$$

where $\{Y_t\}$ is an iid sequence of random variables with mean 0 and variance 1. Additionally, $\alpha_0 > 0$ and $\alpha_i \geq 0$ for all $i > 0$. If $\{Y_t\}$ follows a standard normal distribution, then X_t is conditionally normal with mean 0 and variance w_t. For the unconditional variance of X_t to be finite, the coefficients α_i must satisfy certain regularity conditions.

The model's structure highlights that squared past shocks significantly influence conditional variance. According to the ARCH framework, large shocks are often followed by other large shocks, a feature resembling the volatility clustering observed in asset return distributions. A primary use of ARCH models is to evaluate the accuracy of volatility estimates. The impact of ARCH on forecasting was first explored by Engle & Kraft (1983). Since conditional variance is closely related to the squares of past data, the MMSE approach, commonly used in standard AR models, can be employed for volatility prediction.

1.6.3 Generalized autoregressive conditional heteroskedasticity models

While the ARCH model is relatively straightforward to use, it often requires a large number of parameters to capture the volatility process of an asset returns adequately. In some cases, a higher-order ARCH(p) model may be necessary. To address this, Bollerslev (1986) proposed the generalized ARCH (GARCH) model as an extension of the ARCH family. The GARCH model simplifies the process by allowing the conditional variance to depend on both the prior conditional variance and the squares of previous returns. The GARCH(p, q) model for $\{X_t\}$ is defined

as,

$$X_t = w_t Y_t, \quad w_t = \alpha_0 + \sum_{i=1}^{p} \alpha_i X_{t-i}^2 + \sum_{j=1}^{q} \beta_j w_{t-j},$$

where $\{Y_t\}$ is an iid sequence of random variables with mean 0 and variance 1. And the parameters satisfy the conditions $\alpha_0 > 0$, $\alpha_i \geq 0$, and $\beta_j \geq 0$ for all $i, j > 0$, and $\sum_{i=1}^{\max(p,q)}(\alpha_i + \beta_i) < 1$. This constraint on $(\alpha_i + \beta_i)$ ensures that the unconditional variance of X_t is finite, while the conditional variance w_t evolves dynamically over time.

The GARCH model has several extensions such as log-GARCH, exponential GARCH, integrated GARCH, fractionally integrated GARCH, and threshold GARCH, among others (See Tsay (2005)).

1.6.4 Stochastic volatility models

This class of parameter-driven models assumes that volatility at time t is generated as a latent stochastic process, often modeled using an AR framework. A notable advantage of the SV model is its ability to incorporate random components in the evolution of volatility, offering a more realistic representation. The simple univariate SV model introduced by Taylor (1986) is defined as,

$$X_t = Y_t \exp\{w_t/2\}, \quad w_t = \alpha + \phi w_{t-1} + \eta_t, \quad t = 1, 2, \ldots, \tag{1.3}$$

where Y_t and η_t are independent Gaussian white noises having variances 1 and σ_η^2 respectively. This model is referred to as a normal log-normal SV model due to the Gaussian nature of η_t. The key properties of the basic SV model are discussed in Taylor (1986, 1994). Since $\{\eta_t\}$ is Gaussian, we have $\{w_t\}$ follows the Gaussian AR(1) process and is stationary when $|\phi| < 1$ with,

$$\mu_w = E(w_t) = \frac{\alpha}{1-\phi}, \quad \sigma_w^2 = \mathrm{Var}(w_t) = \frac{\sigma_\eta^2}{1-\phi^2}.$$

We have $\{Y_t\}$ is always stationary, then $\{X_t\}$ will be stationary provided $\{w_t\}$ is stationary. By using the properties of log-normal distribution, the odd moments of $\{X_t\}$ vanish, and even moments of $\{X_t\}$ exist when $\{w_t\}$ is stationary. The kurtosis, a measure of heavy tailedness is given by,

$$K_X = \frac{E(X_t^4)}{E(X_t^2)^2} = 3\exp(\sigma_w^2) \geq 3,$$

indicating that the SV model exhibits fatter tails compared to the corresponding normal distribution. The other distributional properties of $\{X_t\}$ are given below. The autocovariance function at lag k is,

$$\begin{aligned}\gamma_k = \text{Cov}\left(X_t^2, X_{t-k}^2\right) &= E\left(X_t^2 X_{t-k}^2\right) - E\left(X_t^2\right) E\left(X_{t-k}^2\right) \\ &= E\left(\exp\left(w_t + w_{t-k}\right)\right) - \left(E\left(\exp\left(w_t\right)\right)\right)^2 \\ &= \exp\left(2\mu_w + \sigma_w^2\right)\left(\exp\left(\sigma_w^2\phi^k\right) - 1\right),\end{aligned}$$

and the ACF at lag k is,

$$\begin{aligned}\rho_{X_t^2} = \text{Corr}\left(X_t^2, X_{t-k}^2\right)(k) =& \frac{\text{Cov}\left(X_t^2, X_{t-k}^2\right)}{\text{Var}\left(X_t^2\right)} \\ =& \frac{\exp\left(\sigma_w^2\phi^k\right) - 1}{3\exp\left(\sigma_w^2\right) - 1} \simeq \frac{\exp\left(\sigma_w^2\right) - 1}{3\exp\left(\sigma_w^2\right) - 1}\phi^k.\end{aligned}$$

The ACF of the $\{X_t^2\}$ can indeed be negative, provided that $\phi < 0$, unlike ARCH models. This is like the ACF of an ARMA(1,1) process with a GARCH(1,1) appearance in the SV model. Additionally, in comparison to GARCH models, the coefficients are not subject to non-negativity constraints or bounded kurtosis constraints, which is another key benefit. A comprehensive review of the properties of SV models can be found in Taylor (1994) and Tsay (2005). Theoretical advantages of SV models nevertheless did not lead to their popularity among practitioners compared to AR models. The main reason for this is that efficient estimation us-

ing the likelihood function for SV models is more difficult than for ARCH models. The likelihood function $L(\mathbf{\Lambda})$ of parameter vector $\mathbf{\Lambda} = \left(\alpha, \phi, \sigma_\eta^2\right)^T$ is

$$\begin{aligned} L(\mathbf{\Lambda}) &= \int_{\boldsymbol{w}} P_{\mathbf{\Lambda}}(\boldsymbol{X} \mid \boldsymbol{w}) P_{\mathbf{\Lambda}}(\boldsymbol{w}) d\boldsymbol{w} \\ &= \int_{w_n} \int_{w_{n-1}} \dots \int_{w_1} \prod_{t=1}^{n} P_{\mathbf{\Lambda}}\left(X_t \mid w_t\right) P_{\mathbf{\Lambda}}\left(w_t \mid w_{t-1}\right) dw_1 dw_2 \dots dw_n, \end{aligned} \tag{1.4}$$

where $\boldsymbol{X} = (X_1, X_2, \dots, X_n)^T$ is the observed returns and $\boldsymbol{w} = (w_1, w_2, \dots, w_n)^T$ is the vector of latent volatilities. Performing numerical integration is needed for the evaluation of this multi-dimensional integral, and as the sample size grows, it can become both very computationally intensive and time-consuming. When the conditional densities $P_{\mathbf{\Lambda}}(X_t \mid w_t)$ and $P_{\mathbf{\Lambda}}(w_t \mid w_{t-1})$ are Gaussian, the above-mentioned likelihood function can be computed using the Kalman filtering framework. Since volatility often exhibits a positively skewed distribution, the normal distribution, however, is unable to accurately depict the volatility evolution. To overcome this, various researchers have proposed several numerical methods. Some of the approaches are the generalized method of moments (GMM) (Melino & Turnbull (1990)), the quasi maximum likelihood (QML) method (Harvey et al. (1994); Ruiz (1994)), Markov chain Monte Carlo (MCMC) (Jacquier et al. (1994); Kim et al. (1998)), the efficient method of moments (EMM) (Gallant et al. (1997)). For a comprehensive review of these estimation techniques, see Ghysels et al. (1996), Broto & Ruiz (2004), and Bos (2012). Next, we discuss some of the estimation techniques that we utilized in our research.

1.6.4.1 Generalized method of moments

The simplest estimation procedure for SV models is the method of moments proposed by Taylor (1986). Later, Melino & Turnbull (1990) introduced the GMM approach, developed by Hansen (1982), to estimate the unknown parameters. The

main advantage of GMM is that it does not involve the specification of the likelihood function, instead, it only needs some moment conditions. This method is based on the fact that the theoretical population moments should match the corresponding sample moments. More specifically, given a sample $\boldsymbol{x} = (x_1, \ldots, x_T)$, the GMM procedure minimizes the criterion function,

$$Q = \boldsymbol{g}'\boldsymbol{G}\boldsymbol{g},$$

with respect to $\boldsymbol{\Lambda} = (\alpha, \phi, \sigma_\eta^2)^T$, where

$$\boldsymbol{g}' = \Big[\frac{1}{T}\sum x_t^2 - E(x_t^2), \frac{1}{T}\sum x_t^4 - E(x_t^4), \frac{1}{T}\sum x_t^2 x_{t-1}^2 - E(x_t^2 x_{t-1}^2), \ldots, \frac{1}{T}\sum x_t^2 x_{t-m}^2 - E(x_t^2 x_{t-m}^2)\Big],$$

(The theoretical values of $E(x_t^2 x_{t-m}^2)$ for $m \geq 1$ can be found inTaylor (1986); Ghysels et al. (1996)) and $\boldsymbol{G}$ is a symmetric, positive definite $(m+2) \times (m+2)$ weighting matrix that indicates the importance given to matching each one of the moments. Generally, numerical optimization approaches are used to minimize the criterion function Q.

The main advantage of the GMM method is that it does not require the computation of the likelihood function in (1.4). However, a notable drawback is that GMM may not always utilize the available sample information in the most efficient manner. Hansen (1982) proved the consistency and asymptotic normality of the GMM estimators under the following regularity conditions.

Regularity conditions for GMM estimators:

(i) $\{x_t : -\infty < t < \infty\}$ is a stationary and ergodic sequence having a finite-dimensional distribution that depends on a q-dimensional parameter vector.

(ii) The parameter space ζ is an open subset of $\mathbf{R}^q$ that contains the true pa-

rameter $\mathbf{\Lambda}_0$.

(iii) The function $g : \mathbf{R}^q \times \zeta \to \mathbf{R}^r, r \geq q$ and $g(., \mathbf{\Lambda})$ and $\frac{\partial g}{\partial \mathbf{\Lambda}}$ are Borel measurable for each $\mathbf{\Lambda} \in \zeta$ and $\frac{\partial g(x.)}{\partial \mathbf{\Lambda}}$ is continuous on ζ for each r.

(iv) $\frac{\partial g(x_t, \mathbf{\Lambda})}{\partial \mathbf{\Lambda}}$ is first moment continuous at true value $\mathbf{\Lambda}_0$ and $D = E\left(\frac{\partial g(x_t, \mathbf{\Lambda})}{\partial \mathbf{\Lambda}}\right)$ exists and has full rank.

(v) Let $\omega_t = g\left(x_t, x_{t-1}, \mathbf{\Lambda}\right), -\infty < t < \infty$ and

$$\vartheta_j = E\left(\omega_0 \mid \omega_{-j}, \omega_{-j-1}, \ldots\right) - E\left(\omega_0 \mid \omega_{-j-1}, \omega_{-j-2}, \ldots\right) \geqslant 0,$$

and $E\left(\omega_0 \omega_0^T\right)$ exists and finite. $E\left(\omega_0 \mid \omega_{-j}, \omega_{-j-1}, \ldots\right) \xrightarrow{MSE} 0$, and the series

$$\sum^{\infty} E\left({\vartheta^T}_j \vartheta_j\right)^{1/2} < \infty.$$

1.6.4.2 Bayesian method via Markov chain Monte Carlo

SV model estimation using MCMC was initially put forth by Shephard (1996); Jacquier et al. (1994). This method involves the generation of observations from the posterior distribution without finding the likelihood function. The main concept is to model the system as a hierarchical structure of conditional distributions. We have $\mathbf{\Lambda} = \left(\alpha, \phi, \sigma_\eta^2\right)^T$ is vector of hyperparameters. The hierarchy involves, first finding the distribution of observations conditioned on log volatilities $p(\boldsymbol{X}|\boldsymbol{w})$, second finding the conditional distribution of log volatilities on hyperparameters $p(\boldsymbol{w}|\mathbf{\Lambda})$, and third involves the prior distribution of hyperparameters. Thus, the joint posterior distribution of $\boldsymbol{w}$ and $\mathbf{\Lambda}$ is

$$p(\mathbf{\Lambda}, \boldsymbol{w}|\boldsymbol{X}) \propto p(\boldsymbol{X} \mid \boldsymbol{w}) p(\boldsymbol{w} \mid \mathbf{\Lambda}) p(\mathbf{\Lambda}).$$

That is, in a Bayesian framework, the posterior distribution of $\boldsymbol{\Lambda}$ is obtained as the product of the likelihood of the observations $\boldsymbol{X}$ and the prior distribution of $\boldsymbol{\Lambda}$. Since the likelihood function in (1.4) is intractable, the direct analysis of the posterior density $p(\boldsymbol{\Lambda} \mid \boldsymbol{X})$ via MCMC methods is ruled out. To overcome this problem, the hyperparameters vector $\boldsymbol{\Lambda}$ is augmented with the vector $\boldsymbol{w}$.
There are several methods for sampling $p(\boldsymbol{\Lambda}, \boldsymbol{w} \mid \boldsymbol{X})$. Some of them are Gibbs sampler (Geman & Geman (1984); Gelfand & Smith (1990)), Metropolis algorithm (Metropolis & Ulam (1949)), Metropolis-Hesting algorithm (Jacquier et al. (1994)), and so on. Since the posterior density $p(\boldsymbol{\Lambda}, \boldsymbol{w} \mid \boldsymbol{X})$ is multivariate, the direct sampling becomes challenging. In some cases, the Gibbs sampler acts as a flexible approach to split a high-dimensional problem into lower-dimensional problems. It involves producing samples by alternating between the posterior distributions $p(\boldsymbol{w} \mid \boldsymbol{X}, \boldsymbol{\Lambda})$ and $p(\boldsymbol{\Lambda} \mid \boldsymbol{X}, \boldsymbol{w})$ such that it will converge to approximate samples generated from $p(\boldsymbol{\Lambda}, \boldsymbol{w} \mid \boldsymbol{X})$. The general algorithm of the Gibbs sampler for the SV model is described as follows.

Algorithm 1 Gibbs sampling for the SV model

1: Initialize $\boldsymbol{\Lambda}^{(0)}$ and $\boldsymbol{w}^{(0)}$ and let $i = 0$.
2: Sample $\boldsymbol{w}^{(i+1)} \sim p(\boldsymbol{w} \mid \boldsymbol{X}, \boldsymbol{\Lambda}^{(i)})$.
3: Sample $\boldsymbol{\Lambda}^{(i+1)} \sim p(\boldsymbol{\Lambda} \mid \boldsymbol{X}, \boldsymbol{w}^{(i+1)})$.
4: Set $i = i + 1$ and go to step 1.

For more details, one may refer to Jacquier et al. (1994); Shephard (1996).

1.6.4.3 Kalman filter in state-space models

The state-space formulation provides a flexible framework for time series analysis with many linear and non-linear models. Some examples are regression models with time-varying coefficients, ARIMA models, and unobserved component models. State-space models consist of two main equations: the first is the state

equation, which governs the temporal dynamics of the latent state variables, while the second is the observation equation that relates the observed data to the hidden state vector. Estimation of the state variables and model parameters from data is required, and maximum likelihood estimation can be performed using the Kalman filter. This recursive algorithm provides successive estimates of the unobserved components at time t based on available information at that time. Many dynamic economic and financial time series models can be easily formulated in state-space form. Once a model is represented in state-space form, the Kalman filter can be applied to recursively update estimates of the state variable as new data becomes available. It is especially well-suited to real-time prediction and estimation due to its recursive nature. The Kalman filter relies on the assumption that the underlying random variables are normally distributed, enabling computationally efficient calculation and optimal linear estimation. Here we provide a brief overview and the derivation of the Kalman filter and smoothing algorithms using the trend method.

Let r_t represent a univariate time series holding,

$$r_t = \mu_t + y_t, \quad \mu_t = \mu_{t-1} + a_t, \tag{1.5}$$

where $\{y_t\}$ and $\{a_t\}$ are independent Gaussian white noises having mean 0 and variances σ_y^2 and σ_a^2 respectively. Let $\mathcal{F}_t = \{r_1, r_2, \ldots, r_t\}$ is the information available at time t. We denote the conditional mean of μ_t given $\mathcal{F}_j$ as $\mu_{t|j} = E(\mu_t \mid \mathcal{F}_j)$ and the conditional variance of μ_t given $\mathcal{F}_j$ as $\Lambda_{t|j} = \mathrm{Var}(\mu_t \mid \mathcal{F}_j)$. Also, $r_{t|j}$ represents the conditional mean of r_t given $\mathcal{F}_j$. Additionally, let $\nu_t = r_t - r_{t|t-1}$ be the 1-step ahead forecast error and $g_t = \mathrm{Var}(\nu_t \mid \mathcal{F}_{t-1})$ be the variance of ν_t given $\mathcal{F}_{t-1}$. We have the forecast error ν_t is independent of $\mathcal{F}_{t-1}$ making the conditional variance same as the unconditional variance, that is, $\mathrm{Var}(\nu_t \mid \mathcal{F}_{t-1}) =$

$\mathrm{Var}(\nu_t)$. From (1.5),

$$r_{t|t-1} = E(r_t \mid \mathcal{F}_{t-1}) = E(\mu_t + y_t \mid \mathcal{F}_{t-1}) = E(\mu_t \mid \mathcal{F}_{t-1}) = \mu_{t|t-1}.$$

Consequently,

$$\nu_t = r_t - r_{t|t-1} = r_t - \mu_{t|t-1},$$

and

$$\begin{aligned} g_t = \mathrm{Var}(\nu_t \mid \mathcal{F}_{t-1}) &= \mathrm{Var}\left(r_t - \mu_{t|t-1} \mid \mathcal{F}_{t-1}\right) = \mathrm{Var}\left(\mu_t + y_t - \mu_{t|t-1} \mid \mathcal{F}_{t-1}\right) \\ &= \mathrm{Var}\left(\mu_t - \mu_{t|t-1} \mid \mathcal{F}_{t-1}\right) + \mathrm{Var}(y_t \mid \mathcal{F}_{t-1}) \\ &= \Lambda_{t|t-1} + \sigma_y^2. \end{aligned}$$

To derive the Kalman filter, we need to first obtain the joint conditional distribution of $(\mu_t, \nu_t)^T$ given $\mathcal{F}_{t-1}$. We have the conditional distribution of ν_t given $\mathcal{F}_{t-1}$ follows normal distribution with mean zero and variance g_t and that of μ_t given $\mathcal{F}_{t-1}$ also follows normal distribution with mean $\mu_{t|t-1}$ and variance $\Lambda_{t|t-1}$. Therefore, the joint distribution of $(\mu_t, \nu_t)^T$ given $\mathcal{F}_{t-1}$ is also normal. Using the definition we have,

$$\begin{aligned} \mathrm{Cov}(\mu_t, \nu_t \mid \mathcal{F}_{t-1}) &= E(\mu_t \nu_t \mid \mathcal{F}_{t-1}) = E\left[\mu_t\left(r_t - \mu_{t|t-1}\right) \mid \mathcal{F}_{t-1}\right] \\ &= E\left[\mu_t\left(\mu_t + y_t - \mu_{t|t-1}\right) \mid \mathcal{F}_{t-1}\right] \\ &= E\left[\mu_t\left(\mu_t - \mu_{t|t-1}\right) \mid \mathcal{F}_{t-1}\right] + E(\mu_t y_t \mid F_{t-1}) \\ &= E\left[\left(\mu_t - \mu_{t|t-1}\right)^2 \mid \mathcal{F}_{t-1}\right] = \mathrm{Var}(\mu_t \mid \mathcal{F}_{t-1}) = \Lambda_{t|t-1}, \end{aligned}$$

These results yield

$$\begin{bmatrix} \mu_t \\ \nu_t \end{bmatrix}_{\mathcal{F}_{t-1}} \sim N\left(\begin{bmatrix} \mu_{t|t-1} \\ 0 \end{bmatrix}, \begin{bmatrix} \Lambda_{t|t-1} & \Lambda_{t|t-1} \\ \Lambda_{t|t-1} & g_t \end{bmatrix}\right).$$

Thus, the conditional distribution of μ_t given $\mathcal{F}_t$ follows normal distribution with mean and variance

$$\mu_{t|t} = \mu_{t|t-1} + \frac{\Lambda_{t|t-1}\nu_t}{g_t} = \mu_{t|t-1} + K_t\nu_t,$$
$$\Lambda_{t|t} = \Lambda_{t|t-1} - \frac{\Lambda^2_{t|t-1}}{g_t} = \Lambda_{t|t-1}\left(1 - K_t\right),$$

where $K_t = \Lambda_{t|t-1}/g_t$ is the Kalman gain. It is the regression coefficient of μ_t on ν_t and it determines the influence of the new shock ν_t on the state variable μ_t. Furthermore, we can use of the knowledge of μ_t given $\mathcal{F}_t$ to predict μ_{t+1}. That is,

$$\mu_{t+1|t} = E\left(\mu_t + a_t \mid \mathcal{F}_t\right) = E\left(\mu_t \mid \mathcal{F}_t\right) = \mu_{t|t},$$
$$\Lambda_{t+1|t} = \mathrm{Var}\left(\mu_{t+1} \mid \mathcal{F}_t\right) = \mathrm{Var}\left(\mu_t \mid \mathcal{F}_t\right) + \mathrm{Var}\left(a_t\right) = \Lambda_{t|t} + \sigma^2_a.$$

Once the new data r_{t+1} is observed, this procedure can be repeated to update the knowledge of μ_{t+1}. This iterative procedure is the Kalman filtering algorithm introduced by Kalman (1960).

1.7 Spatial analysis

Spatial econometrics is a specialized econometric discipline dealing with the analysis of spatial interdependencies between observations scattered over geographic areas or space points. Spatial econometrics inherently includes location-based variables, spatial structure, and distance-related factors in model specification, estimation, diagnostic checking, and prediction (Anselin (2003)). Over the past few decades, the construction and implementation of spatial econometric models have received considerable interest, with extensive applications in geography, geology, biology, and agriculture. Researchers in these areas utilize spatial econometric methods to examine dependencies and spatial heterogeneity, revealing patterns, re-

lationships, and underlying structures in spatial data (Cliff & Ord (1973); Anselin (2003); LeSage & Pace (2009)).

Identification of spatial dependence is one of the crucial steps in spatial econometric analysis that determines whether to incorporate spatial interactions into the model. Moran's I test is one of the most widely used statistical tests employed to measure spatial autocorrelation. It determines whether a given variable shows a systematic spatial pattern. It is defined as given below.

Moran's I test

Moran (1950) proposed the Moran's I test statistic as,

$$I = \frac{N}{\sum_i \sum_j g_{ij}} \times \frac{\sum_i \sum_j g_{ij}(x_i - \bar{x})(x_j - \bar{x})}{\sum_i (x_i - \bar{x})^2},$$

where N is the total number of observations, x_i is the variable at location i, $\bar{x}$ is its mean, g_{ij} is the spatial weights between i and j. The null hypothesis is H_0 : There is no spatial autocorrelation, and the alternative hypothesis is H_1 : There is significant spatial autocorrelation. We have $z = \frac{I - E(I)}{\sqrt{\text{Var}\,(I)}}$ and we reject H_0 if $|z| > z_{\alpha/2}$, where $z_{\alpha/2}$ is the $100(1-\alpha)$ percentile value of standard normal distribution.

The spatial models that account for these dependencies, variability, and spatial structure have been increasingly introduced in the literature. Notably, these models have demonstrated great potential in fields such as signal and image processing, where capturing spatial interactions is crucial for tasks like anomaly detection and pattern recognition.

In the following subsections, we will discuss some of the spatial models that we encountered during our study.

1.7.1 Two-Dimensional autoregressive model

To model the spatial dependencies, certain random fields are considered with respect to the two-dimensional (2-D) framework. One among them is the 2-D AR models (Choi & Politis (2007); Aksasse & Radouane (1999)) which is given by,

$$w_{ij} = \sum_{(k,l)\in\Gamma} \phi_{kl} w_{i-k,j-l} + \eta_{ij}, \tag{1.6}$$

where η_{ij} is a 2-D white noise process with variance σ_η^2 defined on a 2-D neighborhood of location (i, j), that is, $\Gamma = \{k\ell \mid k \leq i, \ell \leq j\}$ and we have $|\phi_{kl}| < 1$. This 2-D model has many applications in image processing and analysis. The simplest 2-D AR process of order 1 (2-D AR(1))is given by,

$$w_{ij} = \phi_{00} + \phi_{01} w_{i,j-1} + \phi_{10} w_{i-1,j} + \phi_{11} w_{i-1,j-1} + \eta_{ij}, \tag{1.7}$$

where, ϕ_{00}, ϕ_{01}, ϕ_{10}, and ϕ_{11} represents the 2-D AR(1) parameters.

1.7.2 Two-Dimensional generalized autoregressive conditional heteroskedasticity model

Several extensions of GARCH models are discussed in Tsay (2005). To account for the variability of variance across space, the standard GARCH models are further extended to 2-D GARCH by Noiboar & Cohen (2005) so that it can model spatial interactions and spatial structures. This 2-D GARCH family stands out as a significant spatial volatility model capable of capturing conditional spatial heteroskedasticity. Now, we define the 2-D GARCH model.

Let $q_1, q_2, p_1, p_2 \geq 0$ be the order of the GARCH model, and let Γ_1 and Γ_2 be two

neighborhood sets which are defined by,

$$\Gamma_1 = \{k\ell \mid 0 \leq k \leq q_1, 0 \leq \ell \leq q_2, (k\ell) \neq (0,0)\},$$
$$\Gamma_2 = \{k\ell \mid 0 \leq k \leq p_1, 0 \leq \ell \leq p_2, (k\ell) \neq (0,0)\}.$$

Let X_{ij} represent a 2-D stochastic process, and let w_{ij} be the variance conditioned upon the information set $\mathcal{F}_{ij} = \left\{\{X_{i-k,j-\ell}\}_{k\ell\in\Gamma_1}, \{w_{i-k,j-\ell}\}_{k\ell\in\Gamma_2}\right\}$. Let the 2-D neighborhood of location (i,j) is $\Gamma = \{k\ell \mid k \leq i, \ell \leq j\}$ and let $Y_{ij} \overset{iid}{\sim} N(0,1)$ be a 2-D stochastic process which is independent of $w_{k\ell}, \forall k\ell \in \Gamma$. Then the 2-D GARCH (p_1, p_2, q_1, q_2) process is given by,

$$X_{ij} = \sqrt{w_{ij}} Y_{ij},$$
$$w_{ij} = \alpha_0 + \sum_{k\ell\in\Gamma_1} \alpha_{k\ell} X^2_{i-k,j-\ell} + \sum_{k\ell\in\Gamma_2} \beta_{k\ell} w_{i-k,j-\ell},$$

and X_{ij} is conditionally distributed as,

$$X_{ij} \mid \mathcal{F}_{ij} \sim N(0, w_{ij}),$$

with $\alpha_0 > 0, \quad \alpha_{kl} \geq 0$, such that $k\ell \in \Gamma_1$ and $\beta_{kl} \geq 0$, such that $k\ell \in \Gamma_2$. This model has been effectively applied in image processing, specifically because of the "heavy-tailed" characteristic of wavelet representations of natural images. Important applications of the 2-D GARCH model are anomaly detection and noise filtering (Noiboar & Cohen (2005); Amirmazlaghani & Amindavar (2007a,b)). For inference regarding 2-D GARCH, refer to Kharfouchi (2014); Kharfouchi & Mili (2023); Raslain et al. (2018).

1.7.3 Spatial stochastic volatility model

One of the most widely used spatial econometric models is the spatial AR model (Cliff & Ord (1973); Anselin (2003)), in which a spatial lag of the dependent variable accounts for the spatial dependencies between neighboring regions. Another model is the spatial MA process (Hepple (1995); Fingleton (2008a,b)), which offers a compelling approach by capturing the localized transmission of shocks. The spatial dependence in volatilities was initially considered as a secondary observation by Bera & Simlai (2005). Since then, significant developments have been made in addressing this phenomenon. Otto et al. (2018) introduced spatial ARCH models, which were later refined and extended in Otto et al. (2021), by expanding the standard ARCH framework to account for spatial interactions. Concurrently, Sato & Matsuda (2017) developed spatial log-ARCH models to capture ARCH-like variance dependencies in spatial processes. Later, Robinson (2009) and Taşpınar et al. (2021) further advanced this area by developing spatial SV models, by integrating additional stochastic elements into the volatility process to better capture complex spatial dynamics. In these models, spatial SV is often driven by the spatial AR process, which allows the diffusion of shocks through global spillovers accumulated from higher-order neighboring units (LeSage & Pace (2009)). The spatial SV model defined by Taşpınar et al. (2021) is given as,

$$\begin{aligned} x_i =& e^{\frac{1}{2}w_i} y_i, \\ w_i - \mu_w =& \phi \sum_{j=1}^{n} g_{ij}(w_j - \mu_w) + \eta_i, \end{aligned} \tag{1.8}$$

where x_i for $i = 1, 2, ..., n$ is the outcome variable, $\{y_i\}_{i=1}^n$ is an iid normal random variable with mean zero and unit variance, μ_w represents the constant mean, $\{g_{ij}\}_{i=1}^n$ denotes non-stochastic spatial weights, and $\{\eta_i\}$ is an iid normal random

variable with mean zero and variance σ_η^2. We assume that η_i and y_j are independent for all i, j. The scalar parameter ϕ measures the spatial dependence and influence between spatial units. For a comprehensive review of spatial SV models, one may refer to Otto et al. (2024).

In the next section, we will discuss some other models that we have used in our chapters.

1.8 Models used in the study

1.8.1 Minification model

Minification models are introduced as a viable and efficient alternative to non-Gaussian time series models. Unlike traditional approaches that rely on generating functions and often lack closed-form solutions, minification models offer a distinct methodology. These models assume a stochastic framework with a stationary sequence of random variables following a specified marginal distribution, subject to certain conditions. Notably, minification models share several properties with additive AR models. Their existence and key characteristics can be analyzed using the survival function of the underlying random variables, providing valuable insights into their behavior.

The study of minification processes originated with Tavares (1980), laying the foundation for further developments in this area. Tavares (1980) developed the AR minification process as,

$$w_t = \begin{cases} w_0, & \text{if } t = 0, \\ \text{kmin}\left(w_{t-1}, \epsilon_t\right), & \text{if } t \geq 1, \end{cases} \tag{1.9}$$

provided the constant $k > 1$ and $\{\epsilon_t\}$ is a sequence of iid random variables with $\{w_t\}$ being a stationary Markov process of a specified marginal distribution function. Later, Lawrance & Lewis (1981) provided a comprehensive analysis of minification processes, exploring their fundamental properties and various transformations. In subsequent studies, some authors made modifications to the basic model structure to accommodate heavy-tailed distributions. For additional insights into minification models, refer to Krishnarani (2007); Joseph (2009). Further, a mixture of minification and AR models is explored by Popović et al. (2017).

1.9 Review of literature

Volatility is vital in financial markets and is the amount of variation in a financial instrument's price over time. It acts as an indicator of risk involving an asset during a specific period. Understanding volatility in depth is important for realistic option pricing, financial risk assessment, hedging strategy optimization, and asset allocation decision-making within portfolio management. A widely used class of models for modeling this conditional volatility is the ARCH (Engle (1982)), and its extension, GARCH (Bollerslev (1986)). These models effectively capture the stylized features of financial time series data and capture variations in volatility. Since their inception, numerous studies have expanded their original specifications to better capture the empirical patterns found in real-world data. Some notable extensions include the nonlinear GARCH model (Engle & Ng (1993)), the exponential GARCH model (Nelson (1991)), the Glosten-Jagannathan-Runkle GARCH model (Glosten et al. (1993)), the threshold GARCH model (Zakoian (1994)), and among others. A comprehensive review of early GARCH models can be found in Tsay (2005).

An alternative to ARCH-based models is the SV model. The notion of SV models

originated from continuous-time financial models, especially those based on diffusion processes. The Black-Scholes model, developed by Black & Scholes (1973), initially assumed constant volatility, which was later generalized by Hull & White (1987) by allowing volatility to follow a diffusion process. However, later empirical evidence revealed that volatility exhibits clustering effects and persistence, demanding more adaptable modeling techniques. Taylor (1986, 1994) was among the first to introduce SV models in a discrete-time setup, by modeling log-volatility through an AR process. These early developments laid the foundation for modern SV research. Comparative research, such as those by Ghysels et al. (1996) and Kim et al. (1998), has shown that SV models effectively capture long-memory and leverage effects commonly observed in financial returns.

Even though the standard SV model captures volatility clustering found in financial time series, Liesenfeld & Jung (2000) found that its implied kurtosis is often not sufficient to match the empirical sample kurtosis. Consequently, many studies have incorporated heavy-tailed distributions to improve the SV model performance. Liesenfeld & Jung (2000) examined Student-t and generalized error distributions, concluding that the Student-t distribution provides a better fit. Other studies that considered Student-t distribution are Harvey et al. (1994), Meyer & Yu (2000), Jacquier et al. (2004), Omori et al. (2007), among others. Other developments on non-normal SV models include, Nakajima & Omori (2012) employed a generalized hyperbolic skew Student-t error distribution, Barndorff-Nielsen (1997); Andersson (2001) used normal inverse Gaussian distribution, Wang et al. (2013) utilized generalized student-t distribution and so on, to capture both asymmetry and heavy-tailed behavior in returns.

Several other extensions of the SV model are also available in the literature. Chib et al. (2002) modified the standard SV model to incorporate covariates, thereby offering more explanatory variables in volatility modeling. Similar to this, Harvey

et al. (1994); Shephard (1996) improved the model's capacity to capture time-dependent volatility structures by incorporating two independent AR processes into the observation equation. Furthermore, SV models with jumps were explored by Berg et al. (2004); Nakajima & Omori (2009). And SV models with leverage effect were developed by Meyer & Yu (2000); Omori et al. (2007) and they assumed a bivariate normal distribution, while Choy et al. (2009) assumed a bivariate Student-t distribution for greater flexibility. Additionally, Asai & McAleer (2005) proposed an alternative asymmetric SV model that combines the leverage effect, providing a more comprehensive framework for capturing asymmetries in financial data.

Extensions of the SV models based on volatilities generated by some non-Gaussian AR processes have also been widely studied in the literature. For example, Abraham et al. (2006) introduced SV models where volatilities are generated by linear exponential and Gamma AR processes, Balakrishna & Shiji (2014) proposed an SV model generated by a first-order extreme value AR process, Sri Ranganath (2018) developed a Lindley-based SV model, Balakrishna & Thekkedath (2019) proposed Birnbaum- Saunders based SV models, Kavungal & Thekkedath (2022) developed SV model based on normal-Laplace distribution, Sujith & Balakrishna (2023) introduced SV model generated by inverse Gaussian AR process, and so on. Other extensions include Chan (2013) constructed SV models using MA processes, Muhammed Anvar et al. (2019) developed using product AR processes, among others. The univariate SV model is also extended to multivariate SV models, although research in this area remains relatively limited. Notable studies include those by Harvey et al. (1994); Chib et al. (2006). Extending to spatial dynamics, one may refer to Otto et al. (2021, 2024); Taşpınar et al. (2021) for a comprehensive review.

Estimation of these SV models is another well-explored area in the literature.

Some of the contributions include, GMM by Melino & Turnbull (1990); Hansen (1982), the QML developed by Harvey et al. (1994); Ruiz (1994), MCMC by Jacquier et al. (1994); Kim et al. (1998), the EMM by Gallant et al. (1997); Andersen et al. (1999), simulated maximum likelihood by Danielsson (1994), and so on. Further advancements include the efficient importance sampling technique developed by Liesenfeld & Richard (2003), which was later refined by Liesenfeld & Richard (2008) by introducing an improved MCMC approach using the Metropolis-Hastings algorithm in conjunction with efficient importance sampling. For a comprehensive review of the estimation methods, along with their key advantages and limitations in the context of univariate SV models, refer to Ghysels et al. (1996); Broto & Ruiz (2004); Bos (2012); Shephard (1996).

1.10 Objectives of the research

The main objectives of our research study are outlined below.

- ➤ To develop new SV models incorporating long and short memory, periodic volatility, and other structural properties.
- ➤ To study the theoretical properties and structural characteristics of the proposed SV models and evaluate their performances.
- ➤ To address the inferential problems, specifically parameter estimation associated with the proposed SV models considered in this study.
- ➤ To propose a systematic criterion for choosing the best model when the forecast is similar for two or more models.
- ➤ To explore the application of the models in real-life financial data or simulated data.

- To extend SV modeling frameworks to multidimensional and spatial data for capturing complex dependencies.
- To employ the SV models in a variety of domains, including signal processing in addition to the traditional time series analysis.

1.11 Research significance

The significance of this research is both theoretical and practical. Theoretically, SV models enhance the development of financial econometrics as they deal with the inadequacies of conventional time series models and deliver more accurate representations of financial market dynamics. These models provide a better insight into volatility clustering, leverage effects, and heavy-tailed return distributions, which are crucial features of financial time series. Furthermore, advancements in SV modeling lead to the development of more robust estimation techniques and computational methodologies, enriching the broader field of quantitative finance. The theoretical contributions spill over into other fields, with the underlying stochastic concepts being adopted into other disciplines, promoting interdisciplinary research and innovation.

Practically, improved volatility modeling has significant implications for risk management and financial decision-making. More precise volatility predictions allow for improved pricing of financial derivatives, lowering risk uncertainty in options and futures markets. Portfolio managers and investors gain from improved risk assessment tools, enabling more reasonable asset allocation and hedging strategies. Regulators and policymakers also depend on reliable volatility estimates to maintain financial stability and construct efficient monetary policies. Apart from finance, the practical significance extends to fields such as energy, healthcare, engineering, signal processing, image analysis, spatial analysis, etc., where under-

standing and managing volatility can lead to better resource allocation, improved predictive models, and optimized operational strategies. By exploring some of these cross-domain applications, this research broadens the scope of SV models, demonstrating their utility in a wide range of real-world problems.

1.12 Structural outline of the thesis

The present research study focuses on developing new SV models and exploring their statistical properties and applications in other interdisciplinary domains. Chapter 1 presents an introduction to the research area and a detailed review of existing literature. It also includes an overview of some basic preliminaries, Box-Jenkins methodology, linear time series models, financial time series models, and spatial models encountered in our study. Additionally, the research objectives and their significance are also provided.

In Chapter 2, we develop new SV models generated by a new exponential AR model, an exponential minification model, and an exponential mixture of AR and minification processes. The statistical properties of the proposed models are studied, and for estimation, we carry out the GMM technique and discuss its asymptotic properties. To validate the performance of estimators, a Monte Carlo simulation study of each model is done.

The real-time applications of the models developed in Chapter 2 are thoroughly analyzed in Chapter 3. Two real financial data sets are considered for the study, and the performance of the models in capturing key volatility features is evaluated. For model diagnostics, we employ the Kalman filtering technique and a non-linear filtering approach. A comparative study of these models is also done using some risk assessment and prediction metrics.

In Chapter 4, we propose and develop an SV model based on induced Garima

Markov sequences. The distributional and time-series properties of the proposed model are studied. Estimation of the model parameters is done using GMM, and its asymptotic properties are discussed. A Monte Carlo simulation study and real-time applications of the model are done. Additionally, the proposed model is compared with an existing SV model.

The application of the SV model in signal processing, especially in speech enhancement, is explored in Chapter 5. An overview of the speech quality and intelligibility metrics utilized in the study is provided. We develop a new modeling technique in the short-time Fourier transform (STFT) domain for speech signals. Speech enhancement technique using an improved minima-controlled recursive averaging (IMCRA) for noise estimation and an optimally modified log-spectral amplitude (OMLSA) estimator associated with an SV model is proposed. The speech variances modeled using SV are estimated by a Bayesian method via the MCMC techniques. The IMCRA and OMLSA approaches are also explored. To validate the effectiveness of the proposed technique, experiments are conducted and compared with existing approaches.

In Chapter 6, we explore the application of the SV models in image processing, especially for noise reduction in images using wavelet transforms. We extend the one-dimensional (1-D) SV model to a new 2-D SV model and study its application in image denoising. The properties of the proposed model are studied, and for estimation, we employ the Kalman filtering technique in 2-D space. To estimate the clean wavelet image coefficients, an MMSE estimator based on the proposed 2-D SV model is developed. The image denoising algorithm based on the proposed model is discussed, and its efficacy is demonstrated and compared with existing conventional techniques. The image quality metrics utilized in the study are also summarised.

The application of SV models in capturing complex spatial dependencies and vari-

able dynamics in real-world processes is explored in Chapter 7. A novel spatial SV model generated using a spatial MA approach is proposed. It models the spatially correlated random effects through spatially weighted averages of latent stochastic processes. The properties of the model are discussed, and estimation is carried out using a Bayesian MCMC algorithm. A comprehensive simulation study is performed to evaluate the model's performance, and its practical utility is demonstrated using real-world data.

In Chapter 8, the key findings and contributions of the research are summarised. The recommendations for future work are also presented. It highlights the potential directions for further advancements in SV modeling and its applications.

Following this, a comprehensive bibliography is presented, listing all references cited throughout the study, ensuring proper acknowledgment of previous research and providing a valuable resource for further exploration.

CHAPTER 2

Exponential Stochastic Volatility Models and their Variants

2.1 Introduction

[1] Time-varying volatility, in the framework of economic and financial time series modeling, is an indispensable concept that allows one to explain the inherent variations in market behavior and economic indicators. Econometricians and financial economists have then thoroughly explored SV models and their diverse extensions to gain greater insight and predict such dynamic patterns that are happening in the economy. In Chapter 1, we discussed SV models that incorporate non-normal conditional distributions for the return series, as well as models where volatility sequences are generated by some non-Gaussian AR(1) processes.

For non-negative random variables, several AR models have been presented within the context of non-Gaussian time series. We employ some of these models to demonstrate the dynamics of volatilities that vary with time. This chapter mainly focuses on developing SV models with Laplace-distributed returns, taking into account that the volatility sequences are generated by an exponential minification

[1] Some parts of this chapter are based on Krishnarani & Jafna (2024).

model (Tavares (1980)), a new exponential AR model (Lawrance & Lewis (1981)), and an exponential mixture of AR and minification processes (Popović et al. (2017)).

Minification models capture most of the key features of AR models and are well-suited for modeling a variety of real-world scenarios. However, their use in volatility modeling hasn't been thoroughly explored yet. Hence, in this chapter, we extend the application of the minification process to model SV. Additionally, we incorporate an extension of the minification model that combines both AR and minification processes to model volatilities within the SV framework and investigates its application in financial time series. In order to produce volatilities, we also take into consideration a new exponential AR process with a two-parameter structure, which has advantages over the standard exponential AR process but is rarely used in financial modeling.

The chapter is organized as follows. Section 2.2 introduces a new SV model generated using exponential Markov sequences and analyzes its distributional characteristics and properties. The volatility models used to derive this SV model are explored, and its time series behavior is also studied in its subsections. Section 2.3 focuses on the parameter estimation for each of these models and discusses its asymptotic properties. Finally, Section 2.4 presents simulation analysis, and the summary of the chapter is given in Section 2.5.

2.2 Exponential stochastic volatility model with Laplace distributed returns

Let X_t represent a series of returns for a financial asset, and the SV model corresponding to it is defined by,

$$X_t = \sqrt{w_t} Y_t, \tag{2.1}$$

such that $\{Y_t,\ t \geq 1\}$ is a sequence of iid standard normal random variables and is independent of $\{w_t\}$ for every t. The volatility sequences $\{w_t\}$ are assumed to follow exponential random variables having probability density function (pdf),

$$f(w_t;\lambda) = \lambda e^{-\lambda w_t}; \quad w_t \geq 0, \quad \lambda > 0, \tag{2.2}$$

denoted by $w_t \sim Exp(\lambda)$.

The characteristic function of X_t is given by,

$$\begin{aligned}\Phi_X(s) &= E\left(e^{isX_t}\right)\\ &= \frac{2\lambda}{2\lambda + s^2},\end{aligned}$$

and the pdf corresponding to it is,

$$f_L(x) = \sqrt{\frac{\lambda}{2}}\exp\{-|x|\sqrt{2\lambda}\}; \quad -\infty < x < \infty, \quad \lambda > 0,$$

which represents the pdf of a Laplace distribution with mean 0 and variance $\frac{1}{\lambda}$. Next, we examine some of the distributional properties of this suggested SV model as well as the time series models employed to generate the unobserved volatility sequences $\{w_t\}$.

2.2.1 Properties

Based on the model defined in (2.1), all odd moments of the returns X_t are zero, while the even moments are given by,

$$E\left(X_t^{2r}\right) = \left(\frac{r!}{\lambda^r}\right)\prod_{j=1}^{r}(2j-1); \quad r = 1, 2, \ldots. \tag{2.3}$$

To assess the tail behavior of the returns' marginal distribution, we calculate the kurtosis of X_t as,

$$K_X = \frac{E(X_t^4)}{E(X_t^2)^2} = 6 > 3,$$

indicating that the returns are leptokurtic. This suggests that the exponential SV model can effectively capture the heavy-tailed nature of the return series.

The volatility sequences following exponential distribution, as described in (2.2), can be derived using various time series models. A detailed analysis of each of these models is provided below.

2.2.2 New exponential autoregressive model

The new exponential autoregressive (NEAR(1)) process introduced by Lawrance & Lewis (1981) is defined by,

$$w_t = \eta_t + \begin{cases} \beta_0 w_{t-1}, & \text{with probability} \quad \alpha_0, \\ 0, & \text{with probability} \quad 1-\alpha_0, \end{cases} \qquad t = 0, 1, 2, \ldots, \tag{2.4}$$

where $\{\eta_t\}$ is an iid sequence following a mixed exponential distribution, specified as,

$$\eta_t = \begin{cases} E_t, & \text{with probability} \quad \frac{1-\beta_0}{1-(1-\alpha_0)\beta_0}, \\ (1-\alpha_0)\beta_0 E_t, & \text{with probability} \quad \frac{\alpha_0\beta_0}{1-(1-\alpha_0)\beta_0}, \end{cases} \qquad t = 0, 1, \ldots, \tag{2.5}$$

provided $0 \leq \alpha_0 \leq 1$, $0 \leq \beta_0 \leq 1$, and $\{w_t\}$ have stationary exponential marginals. These NEAR(1) models are characterized by simple linear combinations of independent exponential random variables, making them easy to simulate, and their two-parameter structure allows flexibility in adjusting directional impacts on sample path behavior.

The SV model developed using this process is denoted as SV-NEAR(1), and it assumes that $\{\eta_t\}$ and $\{Y_t\}$ are independent of each other for every t.

The mean of squared returns $\{X_t^2\}$ is given by,

$$E\left(X_t^2\right) = \frac{1}{\lambda}, \tag{2.6}$$

and the higher-order moments of this SV-NEAR(1) model are obtained as follows,

$$E\left(X_t^2 X_{t-1}^2\right) = \frac{\alpha_0\beta_0 + 1}{\lambda^2}, \tag{2.7}$$

and

$$E\left(X_t^4 X_{t-1}^2\right) = \frac{3\sqrt{20}\alpha_0\beta_0(1 - \alpha_0\beta_0 + 2\beta_0)}{\lambda^3}. \tag{2.8}$$

The structure of the model in (2.1) suggests that the ACF of $\{X_t\}$ is zero, whereas the ACF of $\{X_t^2\}$ at lag j is significant and is given by,

$$\rho_{X_t^2}(j) = Corr\left(X_t^2, X_{t-j}^2\right) = \frac{(\alpha_0\beta_0)^j}{5}.$$

2.2.3 Minification model

The minification model introduced by Tavares (1980) is given in (1.9). We have $k > 1$ is a constant and we assume that $\{\varepsilon_t\}$ is an innovation process of iid random variables with $\varepsilon_t \sim Exp(\lambda(k-1))$. This ensures that $\{w_t\}$ forms a stationary Markov sequence with exponential marginals. This model generates a first-order AR exponential process and is particularly useful in hydrological applications where processes like river flow exhibit reduction effects over time. Additionally, models with minification structures retain many characteristics of additive AR models.

The SV model generated using this process is denoted by SV-MIN(1) and we assume that $\{\varepsilon_t\}$ is independent of $\{Y_t\}$ for every t.

The mean of squared returns of this model is,

$$E\left(X_t^2\right) = \frac{1}{\lambda}, \tag{2.9}$$

and the second order moments is given by,

$$E\left(X_t^2 X_{t-1}^2\right) = \frac{k+1}{\lambda^2 k}. \tag{2.10}$$

The ACF of $\{X_t\}$ is zero while that of $\{X_t^2\}$ at lag j is,

$$\rho_{X_t^2}(j) = Corr\left(X_t^2, X_{t-j}^2\right) = \frac{1}{5k^j}.$$

The decay rate of the above ACF is governed by the parameter k, which controls how quickly volatility shocks dissipate over time.

2.2.4 Exponential mixture of autoregressive and minification process

In Popović et al. (2017) the exponential mixture of autoregressive and minification (EMARMIN(1)) process is introduced as,

$$w_t = \begin{cases} \alpha w_{t-1}, & \text{with probability } \alpha\beta, \\ \alpha w_{t-1} + \xi_t, & \text{with probability } (1-\alpha)\beta, \quad t \geq 1, \\ \frac{1}{\alpha}\min\left(w_{t-1}, \frac{\alpha}{1-\alpha}\xi_t\right), & \text{with probability } 1-\beta, \end{cases} \tag{2.11}$$

where $\{\xi_t\}$ is an iid sequence of random variables with exponential marginals, ξ_t is independent of w_{t-i} for all $i > 0$, and the parameters $\alpha \in (0,1)$ and $\beta \in [0,1]$. Then the process $\{w_t, t \geq 0\}$ is strictly stationary, ergodic, and follows an exponential marginal distribution. The model is characterized as a mixture of

a first-order AR process and a minification process, offering more flexibility by encompassing two standard models as special cases.

The SV model developed using this process is denoted by SV-EMARMIN(1) with the assumption that $\{\xi_t\}$ is independent of $\{Y_t\}$ for every t.

The mean of squared returns is,

$$E\left(X_t^2\right) = \frac{1}{\lambda}, \tag{2.12}$$

and the higher-order moments are obtained as,

$$E\left(X_t^2 X_{t-1}^2\right) = \frac{\alpha+1}{\lambda^2}, \tag{2.13}$$

and

$$E\left(X_t^4 X_{t-1}^2\right) = \frac{12\alpha - 6\alpha\beta + 6\alpha\beta^2 + 6}{\lambda^3}. \tag{2.14}$$

The ACF of $\{X_t^2\}$ at lag 1 is given by,

$$\rho_{X_t^2}(1) = Corr\left(X_t^2, X_{t-1}^2\right) = \frac{\alpha}{5},$$

while the higher-order ACFs are more complex to derive.

Once the model structure and its characteristics have been assessed, our next objective is to study the estimation of the parameters of the model. Hence, in the following section, we explore the estimation of parameters for each model.

2.3 Estimation of the parameters

The GMM technique discussed in Subsection 1.6.4.1 is used to estimate the developed SV models. GMM provides more flexibility in handling potential nonlinearity within the models and is frequently preferred over the simple method of moments

since it can deal with a wider range of moment conditions. This method creates a framework for the estimation of parameters by minimizing a criterion function using these moments.

Consider an observed return series $(x_1, x_2, \ldots, x_n)$ of length n from the exponential SV model described in (2.1) and let $g(x_t, x_{t-1}, \mathbf{\Lambda})$ represent the moment function, with $\mathbf{\Lambda}$ being the parameter vector that needs to be estimated. The estimates of the parameters are then obtained by solving the following equation,

$$E\left(g\left(x_t, x_{t-1}, \mathbf{\Lambda}\right)\right) = 0. \tag{2.15}$$

Next, we will outline the GMM procedure applied to each SV model.

2.3.1 SV-NEAR(1)

The parameter vector to be estimated is $\mathbf{\Lambda} = (\lambda, \alpha_0, \beta_0)^T$. The moment function $g(x_t, x_{t-1}, \mathbf{\Lambda})$ is given by,

$$g\left(x_t, x_{t-1}, \mathbf{\Lambda}\right) = \begin{pmatrix} x_t^2 - \frac{1}{\lambda} \\ x_t^2 x_{t-1}^2 - \frac{\alpha_0\beta_0+1}{\lambda^2} \\ x_t^4 x_{t-1}^2 - \frac{3\sqrt{20}\alpha_0\beta_0(1-\alpha_0\beta_0+2\beta_0)}{\lambda^3} \end{pmatrix}.$$

Then, (2.15) results in the following system of non-linear equations in terms of unknown parameters,

$$\bar{x}_2 = \frac{\sum_{t=1}^n x_t^2}{n} = \frac{1}{\lambda},$$

$$\bar{x}_{22} = \frac{\sum_{t=2}^n x_t^2 x_{t-1}^2}{n-1} = \frac{\alpha_0\beta_0 + 1}{\lambda^2},$$

and

$$\bar{x}_{42} = \frac{\sum_{t=2}^n x_t^4 x_{t-1}^2}{n-1} = \frac{3\sqrt{20}\alpha_0\beta_0(1 - \alpha_0\beta_0 + 2\beta_0)}{\lambda^3}.$$

These equations are then solved numerically to obtain $\hat{\lambda}$, $\hat{\alpha_0}$ and $\hat{\beta_0}$.

2.3.2 SV-MIN(1)

In this setup, the parameter vector to be estimated is $\mathbf{\Lambda} = (\lambda, k)^T$ and the moment function $g(x_t, x_{t-1}, \mathbf{\Lambda})$ is obtained as,

$$g\left(x_t, x_{t-1}, \mathbf{\Lambda}\right) = \begin{pmatrix} x_t^2 - \frac{1}{\lambda} \\ x_t^2 x_{t-1}^2 - \frac{k+1}{\lambda^2 k} \end{pmatrix}.$$

Using (2.15), we solve the set of equations

$$\bar{x}_2 = \frac{\sum_{t=1}^{n} x_t^2}{n} = \frac{1}{\lambda},$$

and

$$\bar{x}_{22} = \frac{\sum_{t=2}^{n} x_t^2 x_{t-1}^2}{n-1} = \frac{k+1}{\lambda^2 k},$$

to obtain the estimates of λ and k as,

$$\hat{\lambda} = \frac{1}{\bar{x}_2},$$

and

$$\hat{k} = \frac{\bar{x}_2^2}{\bar{x}_{22} - \bar{x}_2^2}.$$

2.3.3 SV-EMARMIN(1)

The parameter vector to be estimated is $\mathbf{\Lambda} = (\lambda, \alpha, \beta)^T$ and the moment function $g(x_t, x_{t-1}, \mathbf{\Lambda})$ is given by,

$$g\left(x_t, x_{t-1}, \mathbf{\Lambda}\right) = \begin{pmatrix} x_t^2 - \frac{1}{\lambda} \\ x_t^2 x_{t-1}^2 - \frac{\alpha+1}{\lambda^2} \\ x_t^4 x_{t-1}^2 - \frac{12\alpha - 6\alpha\beta + 6\alpha\beta^2 + 6}{\lambda^3} \end{pmatrix}.$$

The moment equations derived from (2.15) are

$$\bar{x}_2 = \frac{\sum_{t=1}^{n} x_t^2}{n} = \frac{1}{\lambda},$$

$$\bar{x}_{22} = \frac{\sum_{t=2}^{n} x_t^2 x_{t-1}^2}{n-1} = \frac{\alpha+1}{\lambda^2},$$

and

$$\bar{x}_{42} = \frac{\sum_{t=2}^{n} x_t^4 x_{t-1}^2}{n-1} = \frac{12\alpha - 6\alpha\beta + 6\alpha\beta^2 + 6}{\lambda^3}.$$

These equations are then solved numerically to obtain the estimates $\hat{\lambda}$, $\hat{\alpha}$, and $\hat{\beta}$.

2.3.4 Asymptotic properties of estimators

We state the following theorem for the suggested exponential SV models using the regularity constraints discussed in Subsection 1.6.4.1.

Theorem 2.3.1. *Suppose the sequence* $\{x_t : -\infty < t < \infty\}$ *satisfies the regularity conditions (i) to (v) stated by Hansen (1982). Then* $\{\sqrt{n}(\hat{\mathbf{\Lambda}} - \mathbf{\Lambda}), n \geq 1\}$ *converges in distribution to a normal random vector with mean 0 and dispersion matrix* $\left[DS^{-1}D^T\right]^{-1}$*, where D is given in (iv), and* $S = \sum_{j=-\infty}^{\infty} \Gamma_{(j)}$, $\Gamma_{(j)} = E\left(\omega_t \omega_{t-j}^T\right)$.

The sequences w_t considered in all cases are ergodic, stationary, and have finite moments; likewise, the sequence $\{X_t\}$ defined in (2.1) also exhibits these properties. Additionally, all moments of $\{X_t\}$ and $\{w_t\}$ are finite and $\frac{\partial g(x_t, x_{t-1}, \mathbf{\Lambda})}{\partial \mathbf{\Lambda}}$ exist and are continuous for all values of $\mathbf{\Lambda}$ in each case. Consequently, our proposed SV model adheres to the specified regularity criteria.

The asymptotic dispersion matrix for each model to determine the asymptotic standard errors (SE) of the estimators is computed as follows.

➤ **SV-NEAR(1)**

The moment function of SV-NEAR(1) is given by,

$$g\left(x_t, x_{t-1}, \mathbf{\Lambda}\right) = \begin{pmatrix} x_t^2 - a_1 \\ x_t^2 x_{t-1}^2 - a_2 \\ x_t^4 x_{t-1}^2 - a_3 \end{pmatrix},$$

where $a_1 = \frac{1}{\lambda}$, $a_2 = \frac{\alpha_0\beta_0+1}{\lambda^2}$, and $a_3 = \frac{3\sqrt{20}\alpha_0\beta_0(1-\alpha_0\beta_0+2\beta_0)}{\lambda^3}$.

Also,

$$\frac{\partial g}{\partial \lambda} = \begin{pmatrix} \frac{1}{\lambda^2} \\ \frac{2(\alpha_0\beta_0+1)}{\lambda^3} \\ \frac{9\sqrt{20}\alpha_0\beta_0(1-\alpha_0\beta_0+2\beta_0)}{\lambda^4} \end{pmatrix},$$

$$\frac{\partial g}{\partial \alpha_0} = \begin{pmatrix} 0 \\ \frac{-\beta_0}{\lambda^2} \\ \frac{-3\sqrt{20}\beta_0+6\sqrt{20}\beta_0^2(1-\alpha_0)}{\lambda^3} \end{pmatrix},$$

and

$$\frac{\partial g}{\partial \beta_0} = \begin{pmatrix} 0 \\ \frac{-\alpha_0}{\lambda^2} \\ \frac{-3\sqrt{20}\alpha_0+6\sqrt{20}\alpha_0^2\beta_0-12\sqrt{20}\alpha_0\beta_0}{\lambda^3} \end{pmatrix},$$

indicates that $\frac{\partial g(x_t, x_{t-1}, \mathbf{\Lambda})}{\partial \mathbf{\Lambda}}$ exists and are continuous for all $\mathbf{\Lambda}$.

Let

$$\Gamma_{(k)} = \begin{bmatrix} \gamma_{11}^{(k)} & \gamma_{12}^{(k)} & \gamma_{13}^{(k)} \\ \gamma_{21}^{(k)} & \gamma_{22}^{(k)} & \gamma_{23}^{(k)} \\ \gamma_{31}^{(k)} & \gamma_{32}^{(k)} & \gamma_{33}^{(k)} \end{bmatrix}, \quad k = 0, \pm 1, \pm 2, \ldots,$$

with $\Gamma_{(k)} = \Gamma_{(-k)}, \quad k = 1, 2, \ldots$. Then the matrix S is obtained by $S = \Gamma_{(0)} + 2\sum_{k=1}^{\infty}\Gamma_{(k)}$.

For $k = 0$ the elements of $\Gamma_{(0)} = E\left(\omega_t\omega_t'\right)$ are found as,

$$\gamma_{11}^{(0)} = \frac{5}{\lambda^2},$$

$$\gamma_{12}^{(0)} = \gamma_{21}^{(0)} = a_3 - a_1a_2,$$

$$\gamma_{13}^{(0)} = \gamma_{31}^{(0)} = 15b_3c_1 + 45\alpha_0\beta_0^2b_1c_3 + 45\alpha_0\beta_0b_2c_2 + 15\alpha_0\beta_0^3c_4 - a_1a_3,$$

$$\gamma_{22}^{(0)} = 9b_2c_2 + 9\alpha_0\beta_0^2c_4 + 18\alpha_0\beta_0b_1c_3 - a_2^2,$$

$$\gamma_{23}^{(0)} = \gamma_{32}^{(0)} = 45b_3c_2 + 135\alpha_0\beta_0^2b_1c_4 + 135\alpha_0\beta_0b_2c_3 + 45\alpha_0\beta_0^3c_5 - a_2a_3,$$

$$\gamma_{33}^{(0)} = 225(b_4c_2 + 3\alpha_0\beta_0^2b_2c_4 + 3\alpha_0\beta_0b_3c_3 + \alpha_0\beta_0^3b_1c_5 + \alpha_0\beta_0b_3c_3 + 3\alpha_0\beta_0^3b_1c_5 + 3\alpha_0\beta_0^2b_2c_4 + \alpha_0\beta_0^4c_6) - a_3^2,$$

where $b_1 = E(\eta_t)$, $b_2 = E(\eta_t^2)$, $b_3 = E(\eta_t^3)$, $b_4 = E(\eta_t^4)$, $c_1 = E(w_t)$, $c_2 = E(w_t^2)$, $c_3 = E(w_t^3)$, $c_4 = E(w_t^4)$, $c_5 = E(w_t^5)$, and $c_6 = E(w_t^6)$.

The elements of $\Gamma_{(k)}$, for $k = 1, 2, \ldots,$ are obtained as,

$$\gamma_{11}^{(k)} = \sum_{i=0}^{k-1}\beta_0^i\alpha_0^ib_1c_1 + \alpha_0^k\beta_0^kc_2 - a_1^2,$$

$$\gamma_{12}^{(k)} = \gamma_{21}^{(k)} = \sum_{i=0}^{k}\alpha_0^i\beta_0^ib_2c_1 + \sum_{i=0}^{k}\alpha_0^{i+1}\beta_0^{i+1}b_1c_2 + \alpha_0^{k+1}\beta_0^{k+1}b_1c_2 + \alpha_0^{k+2}\beta_0^{k+2}c_3 - a_1a_2,$$

$$\gamma_{13}^{(k)} = \gamma_{31}^{(k)} = 3\sum_{i=0}^{k}\alpha_0^i\beta_0^ib_3c_1 + 3\alpha_0^{k+1}\beta_0^{k+1}b_2c_2 + 6\sum_{i=0}^{k}\alpha_0^{i+1}\beta_0^{i+1}b_1c_2 + 6\alpha_0^{k+2}\beta_0^{k+2}b_1c_3 + 3\sum_{i=0}^{k}\alpha_0^i\beta_0^ib_1c_3 + 3\alpha_0^{k+1}\beta_0^{k+1}c_4 - a_1a_3,$$

$$\gamma_{22}^{(k)} = \left(\sum_{i=0}^{k-1}\alpha_0^i\beta_0^ib_1\right)^2\alpha_0^k\beta_0^kb_2c_1 + \left(\sum_{i=0}^{k-1}\alpha_0^i\beta_0^ib_1\right)^2\alpha_0^{k+1}\beta_0^{k+1}c_2 + \alpha_0^{k+1}\beta_0^k\sum_{i=0}^{k-1}\alpha_0^i\beta_0^ib_2c_2 + \alpha_0^{k+2}\beta_0^{k+1}\sum_{i=0}^{k-1}\alpha_0^i\beta_0^ib_1c_3 + \alpha_0^k\beta_0^k\sum_{i=0}^{k}\alpha_0^i\beta_0^ib_2c_2 + \alpha_0^{k+1}\beta_0^{k+1}\sum_{i=0}^{k}\alpha_0^i\beta_0^ib_1c_3 - a_2^2,$$

$$\gamma_{23}^{(k)} = \gamma_{32}^{(k)} = 3\left(\sum_{i=0}^{k-1}\alpha_0^i\beta_0^ib_4\right)^2\alpha_0^k\beta_0^kc_1 + 3\alpha_0^k\beta_0^kb_3c_2\sum_{i=0}^{k}\alpha_0^i\beta_0^i + 3\alpha_0^{k+1}\beta_0^{k+1}b_3c_2\sum_{i=0}^{k-1}\alpha_0^i\beta_0^i + 3\alpha_0^{k+2}\beta_0^{k+2}b_2c_3 + 6\sum_{i=0}^{k}\alpha_0^{i+1}\beta_0^{i+1}\sum_{i=0}^{k-1}\alpha_0^i\beta_0^ib_2c_2 + 6\sum_{i=0}^{k}\alpha_0^{i+1}\beta_0^{i+1}b_1c_3\alpha_0^{k+1}\beta_0^{k+1} + 6\alpha_0^{k+2}\beta_0^{k+2}b_2c_3\sum_{i=0}^{k-1}\alpha_0^i\beta_0^i + 6\alpha_0^{k+3}\beta_0^{k+3}b_1c_4$$

$$
\begin{aligned}
&+\left(\sum_{i=0}^{k-1}\alpha_0^i\beta_0^i b_1\right)^2\alpha_0^k\beta_0^k c_3+\sum_{i=0}^{k}\alpha_0^i\beta_0^i\alpha_0^k\beta_0^k b_1c_4+\alpha_0^{k+1}\beta_0^{k+1}c_4c_1\sum_{i=0}^{k-1}\alpha_0^i\beta_0^i\\
&+\alpha_0^{k+2}\beta_0^{k+2}c_5,
\end{aligned}
$$

$$
\begin{aligned}
\gamma_{33}^{(k)} &= 27\left(\sum_{i=0}^{k-1}\alpha_0^i\beta_0^i b_4\right)^3\alpha_0^k\beta_0^k c_1\sum_{i=0}^{k}\alpha_0^i\beta_0^i b_1+27\left(\sum_{i=0}^{k}\alpha_0^i\beta_0^i b_4\right)^2\alpha_0^k\beta_0^k b_1b_3c_2\\
&+27\sum_{i=0}^{k}\alpha_0^i\beta_0^i\sum_{i=0}^{k-1}\alpha_0^i\beta_0^i\alpha_0^{k+1}\beta_0^{k+1}b_1b_3c_2+27\alpha_0^{k+2}\beta_0^{k+2}b_1b_2c_3\sum_{i=0}^{k}\alpha_0^i\beta_0^i\\
&+54b_1b_2c_2\sum_{i=0}^{k}\alpha_0^{i+1}\beta_0^{i+1}\sum_{i=0}^{k-1}\alpha_0^i\beta_0^i\sum_{i=0}^{k}\alpha_0^i\beta_0^i+54\sum_{i=0}^{k}\alpha_0^{i+1}\beta_0^{i+1}\sum_{i=0}^{k}\alpha_0^i\beta_0^i\alpha_0^k\beta_0^k b_1^2c_3\\
&+54\sum_{i=0}^{k-1}\alpha_0^i\beta_0^i\sum_{i=0}^{k}\alpha_0^i\beta_0^i\alpha_0^{k+2}\beta_0^{k+2}b_1b_2c_3+54\sum_{i=0}^{k}\alpha_0^i\beta_0^i\alpha_0^{k+3}\beta_0^{k+3}b_1^2c_4\\
&+9\left(\sum_{i=0}^{k-1}\alpha_0^i\beta_0^i b_1\right)^3\alpha_0^{2k}\beta_0^{2k}b_1^2c_3+9\left(\sum_{i=0}^{k}\alpha_0^i\beta_0^i\right)^2\alpha_0^k\beta_0^k b_1^2c_4\\
&+9\left(\sum_{i=0}^{k}\alpha_0^i\beta_0^i b_1\right)^2\alpha_0^{2k+1}\beta_0^{2k+1}b_1c_4+9\sum_{i=0}^{k}\alpha_0^i\beta_0^i\alpha_0^{k+2}\beta_0^{k+2}b_1c_5\\
&+27\left(\sum_{i=0}^{k-1}\alpha_0^i\beta_0^i b_4\right)^2\alpha_0^{2k+1}\beta_0^{2k+1}c_2+27\sum_{i=0}^{k}\alpha_0^i\beta_0^i\alpha_0^{2k+1}\beta_0^{2k+1}b_3c_3\\
&+27\sum_{i=0}^{k-1}\alpha_0^i\beta_0^i\alpha_0^{2k+2}\beta_0^{2k+2}b_3c_3+27\alpha_0^{2k+3}\beta_0^{2k+3}b_3c_4\\
&+54\sum_{i=0}^{k}\alpha_0^{i+1}\beta_0^{i+1}\sum_{i=0}^{k-1}\alpha_0^i\beta_0^i\alpha_0^{k+1}\beta_0^{k+1}b_3c_3+54\alpha_0^{2k+1}\beta_0^{2k+1}\sum_{i=0}^{k}\alpha_0^{i+1}\beta_0^{i+1}b_1c_4\\
&+54\alpha_0^{2k+3}\beta_0^{2k+3}\sum_{i=0}^{k-1}\alpha_0^i\beta_0^i b_2c_4+54\alpha_0^{2k+4}\beta_0^{2k+4}b_1c_5\\
&+9\left(\sum_{i=0}^{k-1}\alpha_0^i\beta_0^i b_1\right)^2\alpha_0^{2k+1}\beta_0^{2k+1}b_1c_4\\
&+\alpha_0^{2k+1}\beta_0^{2k+1}\sum_{i=0}^{k}\alpha_0^i\beta_0^i b_1c_5+\alpha_0^{2k+2}\beta_0^{2k+2}\sum_{i=0}^{k-1}\alpha_0^i\beta_0^i b_1c_5+\alpha_0^{2k+3}\beta_0^{2k+3}c_6.
\end{aligned}
$$

The elements of matrix D are given below,

$$
\begin{aligned}
d_{11} &= E\left(\frac{\partial g\left(x_t, x_{t-1}; \mathbf{\Lambda}\right)}{\partial \lambda}\right) = \frac{1}{\lambda^2}, \\
d_{12} &= E\left(\frac{\partial g\left(x_t, x_{t-1}; \mathbf{\Lambda}\right)}{\partial \alpha_0}\right) = 0, \\
d_{13} &= E\left(\frac{\partial g\left(x_t, x_{t-1}; \mathbf{\Lambda}\right)}{\partial \beta_0}\right) = 0, \\
d_{21} &= E\left(\frac{\partial g\left(x_t, x_{t-1}; \mathbf{\Lambda}\right)}{\partial \lambda}\right) = \frac{2(\alpha_0\beta_0 + 1)}{\lambda^3}, \\
d_{22} &= E\left(\frac{\partial g\left(x_t, x_{t-1}; \mathbf{\Lambda}\right)}{\partial \alpha_0}\right) = \frac{-\beta_0}{\lambda^2}, \\
d_{23} &= E\left(\frac{\partial g\left(x_t, x_{t-1}; \mathbf{\Lambda}\right)}{\partial \beta_0}\right) = \frac{-\alpha_0}{\lambda^2}, \\
d_{31} &= E\left(\frac{\partial g\left(x_t, x_{t-1}; \mathbf{\Lambda}\right)}{\partial \lambda}\right) = \frac{9\sqrt{20}\alpha_0\beta_0(1 - \alpha_0\beta_0 + 2\beta_0)}{\lambda^4}, \\
d_{32} &= E\left(\frac{\partial g\left(x_t, x_{t-1}; \mathbf{\Lambda}\right)}{\partial \alpha_0}\right) = \frac{-3\sqrt{20}\beta_0 + 6\sqrt{20}\beta_0^2(1 - \alpha_0)}{\lambda^3}, \\
d_{33} &= E\left(\frac{\partial g\left(x_t, x_{t-1}; \mathbf{\Lambda}\right)}{\partial \beta_0}\right) = \frac{-3\sqrt{20}\alpha_0 + 6\sqrt{20}\alpha_0^2\beta_0 - 12\sqrt{20}\alpha_0\beta_0}{\lambda^3}.
\end{aligned}
$$

➤ **SV-MIN(1)**

The moment function of SV-MIN(1) is given by,

$$
g\left(x_t, x_{t-1}, \mathbf{\Lambda}\right) = \begin{pmatrix} x_t^2 - d_1 \\ x_t^2 x_{t-1}^2 - d_2 \end{pmatrix}.
$$

where $d_1 = \frac{1}{\lambda}$, and $d_2 = \frac{k+1}{\lambda^2 k}$. Also,

$$
\frac{\partial g}{\partial \lambda} = \begin{pmatrix} \frac{1}{\lambda^2} \\ \frac{2(k+1)}{\lambda^3 k} \end{pmatrix},
$$

$$
\frac{\partial g}{\partial k} = \begin{pmatrix} 0 \\ \frac{1}{\lambda^2 k^2} \end{pmatrix},
$$

indicating that $\frac{\partial g(x_t, x_{t-1}, \mathbf{\Lambda})}{\partial \mathbf{\Lambda}}$ exists and are continuous for all $\mathbf{\Lambda}$.

Let

$$\Gamma_j = \begin{bmatrix} \gamma_{11}^{(j)} & \gamma_{12}^{(j)} \\ \gamma_{21}^{(j)} & \gamma_{22}^{(j)} \end{bmatrix}, \quad j = 0, \pm 1, \pm 2, \ldots,$$

with $\Gamma_{(j)} = \Gamma_{(-j)}, \quad j = 1, 2, \ldots$. Then the matrix S is obtained by $S = \Gamma_{(0)} + 2\sum_{j=1}^{\infty} \Gamma_{(j)}$.

For $j = 0$ the elements of $\Gamma_{(0)} = E(\omega_t \omega_t')$ are found as,

$$\begin{aligned}
\gamma_{11}^{(0)} &= \frac{5}{\lambda^2}, \\
\gamma_{12}^{(0)} &= \gamma_{21}^{(0)} = \frac{6k\lambda - 18 - 6k^2 + 12k}{k^2\lambda^3} - d_1 d_2, \\
\gamma_{22}^{(0)} &= \frac{36k^2 + 36k^2 + 36k - 108}{\lambda^4 k^2 (k-1)} - d_2^2.
\end{aligned}$$

The elements of $\Gamma_{(j)}$, for $j = 1, 2, \ldots$ are obtained as,

$$\begin{aligned}
\gamma_{11}^{(j)} &= \frac{1 + k^j}{\lambda^2 k^j} - d_1^2, \\
\gamma_{12}^{(j)} &= \gamma_{21}^{(j)} = E(w_t w_{t-j} w_{t-j-1}) - d_1 d_2, \\
\gamma_{22}^{(j)} &= E(w_t w_{t-1} w_{t-j} w_{t-j-1}) - d_2^2.
\end{aligned}$$

The elements of matrix D are given below,

$$\begin{aligned}
d_{11} &= E\left(\frac{\partial g(x_t, x_{t-1}; \mathbf{\Lambda})}{\partial \lambda}\right) = \frac{1}{\lambda^2}, \\
d_{12} &= E\left(\frac{\partial g(x_t, x_{t-1}; \mathbf{\Lambda})}{\partial k}\right) = 0, \\
d_{21} &= E\left(\frac{\partial g(x_t, x_{t-1}; \mathbf{\Lambda})}{\partial \lambda}\right) = \frac{2(k+1)}{\lambda^3 k}, \\
d_{22} &= E\left(\frac{\partial g(x_t, x_{t-1}; \mathbf{\Lambda})}{\partial k}\right) = \frac{1}{\lambda^2 k^2}.
\end{aligned}$$

➤ **SV-EMARMIN(1)**

The moment function of SV-EMARMIN(1) is given by,

$$g\left(x_t, x_{t-1}, \mathbf{\Lambda}\right) = \begin{pmatrix} x_t^2 - e_1 \\ x_t^2 x_{t-1}^2 - e_2 \\ x_t^4 x_{t-1}^2 - e_3 \end{pmatrix},$$

where $e_1 = \frac{1}{\lambda}$, $e_2 = \frac{\alpha+1}{\lambda^2}$, and $e_3 = \frac{12\alpha-6\alpha\beta+6\alpha\beta^2+6}{\lambda^3}$.

Also,

$$\frac{\partial g}{\partial \lambda} = \begin{pmatrix} \frac{1}{\lambda^2} \\ \frac{2(\alpha+1)}{\lambda^3} \\ \frac{3(12\alpha-6\alpha\beta+6\alpha\beta^2+6)}{\lambda^4} \end{pmatrix},$$

$$\frac{\partial g}{\partial \alpha} = \begin{pmatrix} 0 \\ \frac{-1}{\lambda^2} \\ \frac{-12+6\beta-6\beta^2}{\lambda^3} \end{pmatrix},$$

and

$$\frac{\partial g}{\partial \beta} = \begin{pmatrix} 0 \\ 0 \\ \frac{6\alpha-12\alpha\beta}{\lambda^3} \end{pmatrix},$$

indicates that $\frac{\partial g(x_t, x_{t-1}, \mathbf{\Lambda})}{\partial \mathbf{\Lambda}}$ exists and are continuous for all $\mathbf{\Lambda}$.

Let

$$\Gamma_{(k)} = \begin{bmatrix} \gamma_{11}^{(k)} & \gamma_{12}^{(k)} & \gamma_{13}^{(k)} \\ \gamma_{21}^{(k)} & \gamma_{22}^{(k)} & \gamma_{23}^{(k)} \\ \gamma_{31}^{(k)} & \gamma_{32}^{(k)} & \gamma_{33}^{(k)} \end{bmatrix}, \quad k = 0, \pm 1, \pm 2, \ldots,$$

with $\Gamma_{(k)} = \Gamma_{(-k)}$, $k = 1, 2, \ldots$. Then the matrix S is obtained by $S = \Gamma_{(0)} + 2\sum_{k=1}^{\infty} \Gamma_{(k)}$.

For $k = 0$ the elements of $\Gamma_{(0)} = E\left(\omega_t \omega_t'\right)$ are found as,

$$\gamma_{11}^{(0)} = \frac{5}{\lambda^2},$$
$$\gamma_{12}^{(0)} = \gamma_{21}^{(0)} = \frac{11\alpha_6\alpha\beta(\alpha-1)+5}{\lambda^3},$$
$$\gamma_{13}^{(0)} = \gamma_{31}^{(0)} = \frac{90\alpha^3\beta+84+258\alpha-174\alpha\beta+90\alpha^2\beta-6\alpha\beta^2}{\lambda^4},$$
$$\gamma_{22}^{(0)} = \frac{\lambda^3(18\alpha+27\alpha^2)+175-5\alpha^2-10\alpha}{5\lambda^4},$$
$$\gamma_{23}^{(0)} = \gamma_{32}^{(0)} = \frac{6\beta+6+48\alpha+48\alpha^3\beta+72\alpha^2-6\alpha-18\alpha\beta-36\alpha^2\beta}{\lambda^5} - e_2e_3,$$
$$\gamma_{33}^{(0)} = \frac{240\alpha^4\beta+192\alpha^3\beta-336\alpha^2\beta+480\alpha^2-96\alpha\beta+192\alpha+48}{\lambda^6} - e_3^2.$$

The elements of matrix D are given below,

$$d_{11} = E\left(\frac{\partial g\left(x_t, x_{t-1}; \mathbf{\Lambda}\right)}{\partial\lambda}\right) = \frac{1}{\lambda^2},$$
$$d_{12} = E\left(\frac{\partial g\left(x_t, x_{t-1}; \mathbf{\Lambda}\right)}{\partial\alpha}\right) = 0,$$
$$d_{13} = E\left(\frac{\partial g\left(x_t, x_{t-1}; \mathbf{\Lambda}\right)}{\partial\beta}\right) = 0,$$
$$d_{21} = E\left(\frac{\partial g\left(x_t, x_{t-1}; \mathbf{\Lambda}\right)}{\partial\lambda}\right) = \frac{2(\alpha+1)}{\lambda^3},$$
$$d_{22} = E\left(\frac{\partial g\left(x_t, x_{t-1}; \mathbf{\Lambda}\right)}{\partial\alpha}\right) = \frac{-1}{\lambda^2},$$
$$d_{23} = E\left(\frac{\partial g\left(x_t, x_{t-1}; \mathbf{\Lambda}\right)}{\partial\beta}\right) = 0,$$
$$d_{31} = E\left(\frac{\partial g\left(x_t, x_{t-1}; \mathbf{\Lambda}\right)}{\partial\lambda}\right) = \frac{3(12\alpha-6\alpha\beta+6\alpha\beta^2+6)}{\lambda^4},$$
$$d_{32} = E\left(\frac{\partial g\left(x_t, x_{t-1}; \mathbf{\Lambda}\right)}{\partial\alpha}\right) = \frac{-12+6\beta-6\beta^2}{\lambda^3},$$
$$d_{33} = E\left(\frac{\partial g\left(x_t, x_{t-1}; \mathbf{\Lambda}\right)}{\partial\beta}\right) = \frac{6\alpha-12\alpha\beta}{\lambda^3}.$$

The asymptotic dispersion matrix is $\frac{1}{n}(\Sigma)$, where $\Sigma = \left[DS^{-1}D^T\right]^{-1}$ and the diagonal elements of Σ are used to compute the asymptotic SE of the estimators of each model. This estimation algorithm of the developed exponential SV model is validated in the following section through simulation studies.

2.4 Simulation study

In this section, the performance of the suggested estimation method is evaluated, and we use R software (version 4.3.2) to carry out this. The steps for the simulation analysis are outlined as follows,

1. Generate samples of sizes 100, 500, 1000, 2500, and 5000 from exponential Markov sequence based on the models described in (2.4), (1.9), and (2.11).
2. Simulate samples from a standard normal distribution.
3. Generate return sequences $\{X_t\}$ using these samples.
4. Solve the moment equations for each model to estimate the parameters.
5. For the SV-MIN(1) model, solve the moment equations directly. For the SV-NEAR(1) model, we use the *BBsolve* function from the R package BB (Varadhan & Gilbert (2009)), and for the SV-EMARMIN(1) model, we use the *gmm* function from the R package gmm (Chausse (2010)).
6. Repeat the process 1000 times for a fixed set of parameter values.
7. Compute the mean estimates with corresponding root mean squared errors (RMSE), and SE.

The RMSE is defined as,

$$\mathrm{RMSE} = \sqrt{\frac{1}{\mathrm{n}}\sum_{\mathrm{i}=1}^{\mathrm{n}}(\mathrm{a_i} - \hat{\mathrm{a}}_\mathrm{i})^2},$$

where a_i represents actual values and $\hat{a}_i$ represents the predicted values.
The mean estimates, along with their corresponding RMSE and SE for each model, are presented in Tables 2.1, 2.2, and 2.3. The relatively low RMSE values indicate

high precision and accuracy, with minimal bias and very low standard errors. The results in the tables show that as the sample size increases, the bias, RMSE, and SE decrease significantly for the given parameter values. This demonstrates the stability and reliability of the estimation method.

Table 2.1: The mean estimates, corresponding RMSE, and SE based on the SV-NEAR(1) model for samples of sizes 100, 500, 1000, 2500, and 5000.

	True Values			**Mean Estimate Values with RMSE and SE**								
Sample size (n)	λ	α_0	β_0	$\hat{\lambda}$	**RMSE**	**SE**	$\hat{\alpha_0}$	**RMSE**	**SE**	$\hat{\beta_0}$	**RMSE**	**SE**
100	0.5	0.5	0.5	0.4362	0.1335	0.1424	0.4537	0.1232	0.2031	0.4591	0.1187	0.1075
		0.7	0.7	0.4426	0.1251	0.1138	0.6621	0.1029	0.1162	0.6645	0.1135	0.1023
		0.9	0.9	0.4482	0.1066	0.1105	0.8631	0.1125	0.1213	0.8565	0.1242	0.1281
	4.5	0.5	0.5	4.3244	0.1654	0.1713	0.4411	0.1459	0.1342	0.4624	0.1209	0.1265
		0.7	0.7	4.4215	0.1533	0.1435	0.6673	0.1272	0.1136	0.6524	0.1352	0.1258
		0.9	0.9	4.4132	0.1518	0.1352	0.8593	0.2014	0.1936	0.8677	0.1174	0.1112
	6	0.5	0.5	5.6732	0.1671	0.1543	0.4521	0.1220	0.1229	0.4601	0.1039	0.1022
		0.7	0.7	5.7213	0.1242	0.1113	0.6654	0.1152	0.1202	0.6691	0.1098	0.1067
		0.9	0.9	5.6987	0.1320	0.1254	0.8651	0.1627	0.1631	0.8681	0.1120	0.1094
500	0.5	0.5	0.5	0.4631	0.0921	0.0954	0.4689	0.0892	0.0868	0.4628	0.0836	0.0982
		0.7	0.7	0.4672	0.0835	0.0763	0.6783	0.0934	0.1054	0.6702	0.0734	0.0767
		0.9	0.9	0.4619	0.0964	0.0947	0.8699	0.0876	0.0901	0.8695	0.0983	0.0884
	4.5	0.5	0.5	4.3977	0.0893	0.0827	0.4580	0.0729	0.1223	0.4699	0.1004	0.1027
		0.7	0.7	4.4380	0.0780	0.0706	0.6695	0.0674	0.0982	0.6631	0.1203	0.1170
		0.9	0.9	4.4341	0.0905	0.0887	0.8667	0.0806	0.0842	0.8721	0.0735	0.0663
	6	0.5	0.5	5.7712	0.0732	0.0627	0.4681	0.0531	0.0679	0.4705	0.0892	0.0871
		0.7	0.7	5.8102	0.0771	0.0768	0.6783	0.0658	0.0624	0.6740	0.0547	0.0572
		0.9	0.9	5.7993	0.0506	0.0530	0.8746	0.0685	0.0527	0.8722	0.0405	0.0367
1000	0.5	0.5	0.5	0.4812	0.0514	0.0826	0.4834	0.0665	0.0580	0.4797	0.0925	0.0501
		0.7	0.7	0.4829	0.0501	0.0514	0.6891	0.0701	0.0753	0.6885	0.0678	0.0643
		0.9	0.9	0.4889	0.0671	0.0636	0.8799	0.0562	0.0643	0.8845	0.0453	0.0582
	4.5	0.5	0.5	4.4326	0.0523	0.0528	0.4793	0.0498	0.0563	0.4820	0.0452	0.0543
		0.7	0.7	4.4487	0.0583	0.0503	0.6835	0.0671	0.0596	0.6873	0.0562	0.0459
		0.9	0.9	4.4536	0.0437	0.0410	0.8845	0.0525	0.0532	0.8897	0.0392	0.0431
	6	0.5	0.5	5.8832	0.0623	0.0527	0.4834	0.0501	0.0539	0.4883	0.0512	0.0496
		0.7	0.7	5.8910	0.0446	0.0575	0.6885	0.0457	0.0317	0.6867	0.0527	0.0468
		0.9	0.9	5.9102	0.0102	0.0200	0.8897	0.0210	0.0233	0.8859	0.0186	0.0285
2500	0.5	0.5	0.5	0.4905	0.0065	0.0105	0.4937	0.0128	0.0165	0.4911	0.0142	0.0097
		0.7	0.7	0.4911	0.0101	0.0096	0.6902	0.0102	0.0112	0.6923	0.0093	0.0087
		0.9	0.9	0.4941	0.0117	0.0127	0.8912	0.0078	0.0067	0.8945	0.0056	0.0072
	4.5	0.5	0.5	4.4621	0.0143	0.0138	0.4899	0.0128	0.0049	0.4903	0.0051	0.0082
		0.7	0.7	4.4682	0.0092	0.0110	0.6910	0.0102	0.0092	0.6936	0.0034	0.0081
		0.9	0.9	4.4781	0.0082	0.0057	0.8931	0.0047	0.0062	0.8925	0.0035	0.0052
	6	0.5	0.5	5.9210	0.0049	0.0076	0.4900	0.0100	0.0092	0.4915	0.0078	0.0069
		0.7	0.7	5.9002	0.0078	0.0101	0.6901	0.0091	0.0082	0.6933	0.0064	0.0056
		0.9	0.9	5.9229	0.0068	0.0101	0.8918	0.0087	0.0076	0.8931	0.0058	0.0072
5000	0.5	0.5	0.5	0.5021	0.0021	0.0034	0.4971	0.0005	0.0010	0.4982	0.0003	0.0012
		0.7	0.7	0.5018	0.0018	0.0016	0.6992	0.0008	0.0010	0.6997	0.0003	0.0007
		0.9	0.9	0.4998	0.0010	0.0013	0.9017	0.0017	0.0026	0.8989	0.0018	0.0014
	4.5	0.5	0.5	4.4938	0.0086	0.0078	0.4932	0.0087	0.0035	0.4926	0.0045	0.0052
		0.7	0.7	4.4971	0.0023	0.0035	0.7011	0.0011	0.0016	0.7031	0.0031	0.0042
		0.9	0.9	4.4957	0.0037	0.0034	0.8992	0.0009	0.0010	0.8981	0.0023	0.0036
	6	0.5	0.5	5.9834	0.0027	0.0021	0.5006	0.0006	0.0016	0.5031	0.0031	0.0037
		0.7	0.7	5.9993	0.0008	0.0021	0.7038	0.0038	0.0041	0.7011	0.0011	0.0023
		0.9	0.9	6.0017	0.0017	0.0043	0.9018	0.0018	0.0020	0.9007	0.0007	0.0010

Table 2.2: The mean estimates, corresponding RMSE, and SE based on the SV-MIN(1) model for samples of sizes 100, 500, 1000, 2500, and 5000.

	True Values		**Mean Estimate Values with RMSE and SE**					
Sample size (n)	λ	k	$\hat{\lambda}$	**RMSE**	**SE**	$\hat{k}$	**RMSE**	**SE**
100	0.5	1.2	0.4503	0.1513	0.1374	1.0128	0.2027	0.1993
		1.5	0.4591	0.1431	0.1729	1.3109	0.2173	0.2005
		1.8	0.4618	0.1364	0.1450	1.6781	0.2819	0.2374
	4.5	1.2	4.2473	0.1623	0.1935	1.0731	0.1071	0.1265
		1.5	4.2807	0.1207	0.1520	1.3870	0.1005	0.1248
		1.8	4.2781	0.1786	0.1625	1.7100	0.1153	0.1136
	6	1.2	5.7209	0.1730	0.1542	1.1429	0.1428	0.1369
		1.5	5.7281	0.1367	0.1548	1.7108	0.1213	0.1010
		1.8	5.6455	0.1755	0.1742	1.9282	0.2178	0.2001
500	0.5	1.2	0.4674	0.1204	0.1156	1.1671	0.1027	0.0917
		1.5	0.4703	0.1053	0.1105	1.3999	0.0989	0.0992
		1.8	0.4738	0.1028	0.1057	1.6910	0.1032	0.1004
	4.5	1.2	4.3712	0.1127	0.0982	1.1237	0.1167	0.1205
		1.5	4.3548	0.1288	0.1193	1.3984	0.0948	0.0932
		1.8	4.4001	0.1021	0.1007	1.7204	0.0936	0.0912
	6	1.2	5.8134	0.1204	0.1027	1.1777	0.1021	0.1007
		1.5	5.8209	0.0979	0.1078	1.6523	0.0923	0.0937
		1.8	5.7353	0.1230	0.1321	1.7017	0.0915	0.0931
1000	0.5	1.2	0.4851	0.0950	0.0931	1.1734	0.0502	0.0552
		1.5	0.4801	0.0982	0.0917	1.4102	0.0481	0.0499
		1.8	0.4888	0.0918	0.0891	1.7100	0.0471	0.0521
	4.5	1.2	4.4286	0.0878	0.8310	1.1912	0.0512	0.0584
		1.5	4.4664	0.0866	0.0857	1.4001	0.0437	0.0411
		1.8	4.4103	0.0910	0.0915	1.7465	0.0420	0.0415
	6	1.2	5.8847	0.0987	0.0882	1.1856	0.0456	0.0394
		1.5	6.2781	0.0871	0.0792	1.4210	0.0417	0.0386
		1.8	5.8850	0.0905	0.0912	1.7256	0.0395	0.0371
2500	0.5	1.2	0.4911	0.0401	0.0447	1.1907	0.0127	0.0174
		1.5	0.4927	0.0311	0.0384	1.4489	0.0089	0.0117
		1.8	0.5104	0.0214	0.0275	1.7633	0.0078	0.0126
	4.5	1.2	4.4563	0.0358	0.0341	1.1959	0.0179	0.0158
		1.5	4.4700	0.0270	0.0203	1.4507	0.0105	0.0125
		1.8	4.4636	0.0212	0.0239	1.7859	0.0098	0.0107
	6	1.2	5.9111	0.0211	0.0187	1.1963	0.0027	0.0034
		1.5	5.9583	0.0141	0.0138	1.4637	0.0110	0.0087
		1.8	6.1791	0.0171	0.0203	1.7781	0.0087	0.0101
5000	0.5	1.2	0.4970	0.0083	0.0070	1.1978	0.0027	0.0031
		1.5	0.4961	0.0101	0.0097	1.4913	0.0013	0.0017
		1.8	0.5012	0.0012	0.0018	1.7971	0.0016	0.0009
	4.5	1.2	4.4916	0.0036	0.0041	1.1988	0.0018	0.0027
		1.5	5.0013	0.0013	0.0042	1.4891	0.0073	0.0081
		1.8	4.4991	0.0004	0.0035	1.7976	0.0046	0.0094
	6	1.2	6.0032	0.0032	0.0023	1.2170	0.0007	0.0017
		1.5	5.9971	0.0037	0.0016	1.4925	0.0056	0.0051
		1.8	5.9980	0.0011	0.0020	1.7910	0.0087	0.0092

Table 2.3: The mean estimates, corresponding RMSE, and SE based on the SV-EMARMIN(1) model for samples of sizes 100, 500, 1000, 2500, and 5000.

	True Values			**Mean Estimate Values with RMSE and SE**								
Sample size (n)	$\boldsymbol{\lambda}$	$\boldsymbol{\alpha}$	$\boldsymbol{\beta}$	$\hat{\boldsymbol{\lambda}}$	**RMSE**	**SE**	$\hat{\boldsymbol{\alpha}}$	**RMSE**	**SE**	$\hat{\boldsymbol{\beta}}$	**RMSE**	**SE**
100	0.5	0.5	0.5	0.4671	0.1043	0.0982	0.4632	0.0965	0.0982	0.4612	0.1041	0.1005
		0.7	0.7	0.4698	0.0991	0.0974	0.6790	0.0937	0.0922	0.6711	0.0970	0.1001
		0.9	0.9	0.4739	0.0804	0.0892	0.8713	0.0906	0.0931	0.8615	0.0910	0.0898
	4.5	0.5	0.5	4.3682	0.0908	0.0911	0.4616	0.0830	0.0803	0.4741	0.0785	0.0790
		0.7	0.7	4.4571	0.0896	0.0893	0.6810	0.0846	0.0824	0.6736	0.0850	0.0804
		0.9	0.9	4.4101	0.0901	0.0912	0.8678	0.0912	0.0926	0.8518	0.0995	0.0987
	6	0.5	0.5	5.7446	0.0861	0.0737	0.4688	0.0742	0.0800	0.4710	0.0891	0.0802
		0.7	0.7	5.7915	0.0797	0.0801	0.6834	0.0781	0.0771	0.6765	0.0818	0.0796
		0.9	0.9	5.7561	0.0812	0.0827	0.8782	0.0623	0.0761	0.8711	0.0746	0.0721
500	0.5	0.5	0.5	0.4726	0.0624	0.0671	0.4788	0.0518	0.0571	0.4791	0.0459	0.0501
		0.7	0.7	0.4744	0.0667	0.0684	0.6837	0.0791	0.0737	0.6816	0.0635	0.0623
		0.9	0.9	0.4813	0.0517	0.0603	0.8810	0.0510	0.0519	0.8781	0.0719	0.0724
	4.5	0.5	0.5	4.4127	0.0432	0.0478	0.4689	0.0671	0.0614	0.4801	0.0591	0.0604
		0.7	0.7	4.4673	0.0468	0.0481	0.6879	0.0580	0.0576	0.6802	0.0657	0.0612
		0.9	0.9	4.4368	0.0432	0.0465	0.8839	0.0389	0.0401	0.8746	0.0469	0.0471
	6	0.5	0.5	5.8051	0.0581	0.0599	0.4790	0.0431	0.0464	0.4814	0.0501	0.0494
		0.7	0.7	5.8275	0.0562	0.0520	0.6895	0.0595	0.0586	0.6837	0.0476	0.0498
		0.9	0.9	5.8091	0.0478	0.0462	0.8875	0.0498	0.0503	0.8836	0.0489	0.0521
1000	0.5	0.5	0.5	0.4887	0.0231	0.0302	0.4867	0.0379	0.0325	0.4874	0.0293	0.0287
		0.7	0.7	0.4893	0.0356	0.0327	0.6901	0.0198	0.0221	0.6899	0.0279	0.0256
		0.9	0.9	0.4898	0.0325	0.0312	0.8884	0.0294	0.0286	0.8870	0.0306	0.0291
	4.5	0.5	0.5	4.4370	0.0280	0.0289	0.4744	0.0341	0.0356	0.4891	0.0278	0.0294
		0.7	0.7	4.4731	0.0231	0.0245	0.6890	0.0256	0.0234	0.6887	0.0223	0.0237
		0.9	0.9	4.4532	0.0236	0.0256	0.8869	0.0269	0.0260	0.8847	0.0303	0.0298
	6	0.5	0.5	5.8275	0.0359	0.0331	0.4839	0.0310	0.0317	0.4894	0.0341	0.0319
		0.7	0.7	5.8880	0.0281	0.0286	0.6900	0.0190	0.0201	0.6899	0.0213	0.0221
		0.9	0.9	5.9100	0.0210	0.0221	0.8910	0.0201	0.0226	0.8901	0.0156	0.0204
2500	0.5	0.5	0.5	0.4912	0.0108	0.0114	0.4917	0.0117	0.0114	0.4931	0.0131	0.0120
		0.7	0.7	0.4934	0.0098	0.0093	0.6956	0.0078	0.0084	0.6967	0.0062	0.0067
		0.9	0.9	0.4919	0.0119	0.0129	0.8947	0.0061	0.0072	0.8947	0.0057	0.0066
	4.5	0.5	0.5	4.4671	0.0171	0.0167	0.4846	0.0146	0.0101	0.4928	0.0087	0.0086
		0.7	0.7	4.4813	0.0113	0.0117	0.6927	0.0127	0.0097	0.6958	0.0058	0.0076
		0.9	0.9	4.4834	0.0074	0.0083	0.8910	0.0101	0.0091	0.8951	0.0056	0.0061
	6	0.5	0.5	5.8998	0.0108	0.0098	0.4931	0.0071	0.0073	0.4927	0.0087	0.0062
		0.7	0.7	5.9100	0.0100	0.0108	0.6961	0.0061	0.0072	0.6938	0.0038	0.0047
		0.9	0.9	5.9451	0.0091	0.0112	0.8937	0.0047	0.0041	0.8951	0.0051	0.0068
5000	0.5	0.5	0.5	0.4978	0.0028	0.0027	0.5012	0.0012	0.0011	0.4981	0.0018	0.0021
		0.7	0.7	0.5029	0.0024	0.0019	0.6980	0.0020	0.0027	0.6991	0.0008	0.0010
		0.9	0.9	0.5010	0.0010	0.0015	0.8986	0.0016	0.0028	0.9015	0.0015	0.0018
	4.5	0.5	0.5	4.4977	0.0077	0.0067	0.4981	0.0021	0.0022	0.4960	0.0060	0.0051
		0.7	0.7	4.4956	0.0036	0.0038	0.7020	0.0020	0.0011	0.7012	0.0012	0.0018
		0.9	0.9	5.0036	0.0031	0.0026	0.8980	0.0010	0.0018	0.9017	0.0017	0.0014
	6	0.5	0.5	6.0032	0.0032	0.0027	0.5019	0.0019	0.0009	0.5010	0.0010	0.0013
		0.7	0.7	5.9969	0.0029	0.0039	0.7024	0.0024	0.0027	0.7007	0.0007	0.0011
		0.9	0.9	6.0024	0.0024	0.0041	0.9010	0.0010	0.0012	0.8997	0.0006	0.0005

2.5 Summary

In this chapter, an exponential Markov sequence-based SV model with Laplace returns is introduced to analyze the financial data. The volatilities are modeled using a series of non-negative random variables generated by the NEAR(1), minification, and EMARMIN(1) processes. These SV models capture many of the typical characteristics found in financial time series data and serve as viable alternatives to existing models, featuring volatilities with an exponential distribution and a kurtosis of 6. The model parameters are estimated using the GMM, and the estimates are both consistent and asymptotically normal. Simulation analysis confirms that the estimation technique is reliable and stable.

CHAPTER 3

Exponential Stochastic Volatility Models: Applications and Comparisons

3.1 Introduction

[1] In the previous chapter, we have set up the theoretical framework, estimation methods, and simulation analysis of three SV models, namely, SV-MIN(1), SV-NEAR(1), and SV-EMARMIN(1). With this groundwork, we now proceed to explore the real-world applications of these models, especially in modeling and forecasting financial market volatility.

Financial markets are inherently dynamic and complex, with the presence of volatility clustering, sudden jumps, and persistent fluctuations. The ability to capture these aspects of volatility would be important in risk management, asset pricing, and portfolio optimization. This chapter shows how the SV-MIN(1) model, which incorporates the minification processes, the SV-NEAR(1) model, with a two-parameter exponential structure, and the SV-EMARMIN(1) model, which combines AR and minification dynamics, can be efficiently used to describe and forecast the volatility of financial markets.

[1] Some parts of this chapter are based on Krishnarani & Jafna (2024).

This chapter mainly focuses on evaluating the performance of these models through empirical analysis in terms of capturing key volatility features such as persistence, abrupt changes, and clustering effects. By comparing their forecasting accuracy and robustness, we will be able to provide deeper insights into their practical applicability in financial systems. This assessment also demonstrates how these sophisticated volatility models can be used to improve risk management techniques and volatility forecasts.

To evaluate the precision of these models' volatility forecasts, we use metrics such as mean absolute error (MAE) and RMSE. Furthermore, we also employ Value at Risk (VaR) to evaluate how well each model captures the potential losses at specified confidence levels. For comparison purposes, we also consider the SV model generated by the exponential AR(1) process (Gaver & Lewis (1980)), which was previously studied by Abraham et al. (2006). The volatility sequences for this model are given by,

$$w_t = \alpha w_{t-1} + I_t E_t; \quad t = 1, 2, \ldots, \quad 0 < \alpha < 1, \tag{3.1}$$

where $\{I_t\}$ and $\{E_t\}$ are mutually independent iid sequences such that the sequences $\{E_t\}$ follows an exponential distribution and $P(I_t = 0) = 1 - P(I_t = 1) = \alpha$. Then $\{w_t\}$ forms a stationary Markov sequence of exponential marginals. The SV model generated using this process is represented by SV-EAR(1), and we have also incorporated this model into the data analysis section of this chapter for a comprehensive comparison.

The chapter is organized as follows. Section 3.2 provides a brief overview of the performance metrics used for comparison of models. Section 3.3 demonstrates the application of each model using the first dataset, and in Section 3.4, we apply them to the second dataset. Finally, the summary of the chapter is given in

Section 3.5.

3.2 Risk assessment and prediction metrics

In this section, we give an overview of some of the evaluation metrics that we have employed in this chapter for assessing the accuracy of predictive models and measuring financial risk.

➤ **Mean absolute error**

The MAE is a well-known metric used to assess the accuracy of prediction models and is defined as,

$$\text{MAE} = \frac{1}{n}\sum_{j=1}^{n} |x_j - \hat{x}_j| \,,$$

where x_j and $\hat{x}_j$ are the actual and predicted returns respectively.

➤ **Value at Risk**

VaR is a common risk management measure employed to estimate the potential loss from a portfolio over a specified period at a given confidence level. The VaR at time t with level of significance α is defined as,

$$\text{VaR}_t(\alpha) = F^{-1}\left(\alpha \mid x_t\right),$$

where $F^{-1}\left(\cdot \mid x_t\right)$ is the quantile function of the returns at time t (See Zhang & Nadarajah (2018)). The accuracy of VaR forecasts is then verified through backtesting, which involves a comparison of predicted and actual losses at the end of a specified time horizon. In backtesting, one method to assess model efficiency is to examine VaR violations or the number of times in which losses are larger than the VaR threshold and outside the expected

confidence interval.

In the following sections, we will discuss the practical applications of the models described in Chapter 2.

3.3 Data analysis-1

We consider the daily exchange rate of returns for US dollars to Canadian dollars (USD/CAD) from January 1, 2010, to December 30, 2022, using data from https://www.marketwatch.com. Here we assess the applicability of the proposed models and compare the results to identify which model is the most effective.
Let P_t denote the daily exchange rate, and the returns are computed using the formula,

$$X_t = 100\left[\log\left(\frac{P_t}{P_{t-1}}\right) - \frac{1}{n}\sum_{t=1}^{n}\log\left(\frac{P_t}{P_{t-1}}\right)\right]; \quad t = 1, 2, \ldots, n. \tag{3.2}$$

where P_0 is the starting value of the exchange rate.
The time series plot of both the original exchange rate series and the computed returns is illustrated in Figure 3.1, and the descriptive statistics for the return series are given in Table 3.1. The ACF plot of the return series shows that serial correlations are negligible, while the squared return series shows significant serial correlations that decay gradually (See Figure 3.2). This is further supported by the Ljung-Box portmanteau test with lag 20. That is, autocorrelations in the returns are insignificant, with a p-value of 0.1621, and the autocorrelations in squared returns are significant with a p-value less than 0.05. Also, the returns exhibit leptokurtosis, with a kurtosis value exceeding three and nearing six. This suggests that the developed exponential SV model might fit the data well.

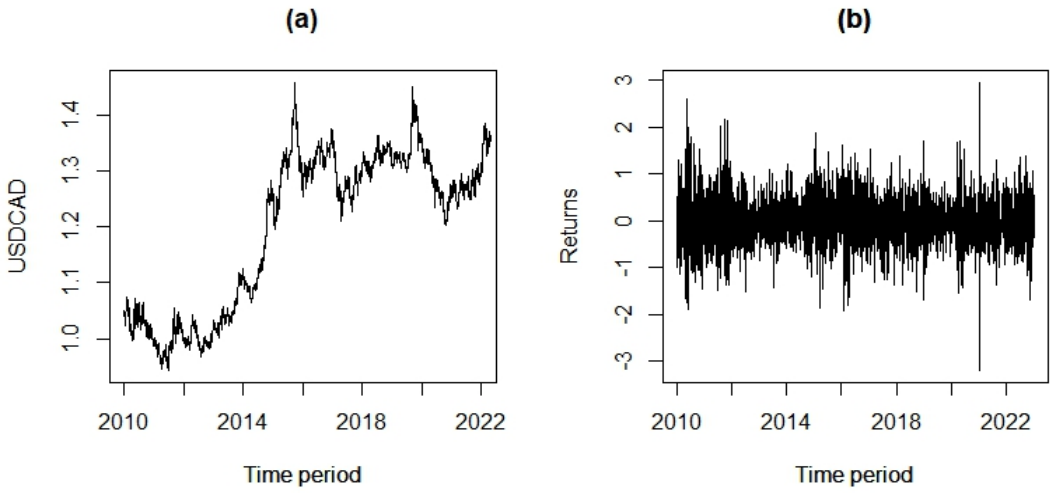

Figure 3.1: (a). USD/CAD exchange rate time series data. (b). Return series of the USD/CAD exchange rate data.

Table 3.1: Descriptive statistics of the return series.

Statistics	**USD/CAD**	**GH**
Sample size	3384	1166
Std. Dev	0.4955	4.3878
Minimum	-3.2013	-31.6375
Maximum	2.9617	25.1668
Kurtosis	5.9955	6.1121
Ljung-Box p-value for returns.	0.1621	0.8347
Ljung-Box p-value for squared returns.	2.2×10^{-16}	6.38×10^{-5}

The model parameters are then estimated using GMM as described in Section 2.3, and the estimates for each model are presented in Table 3.2.

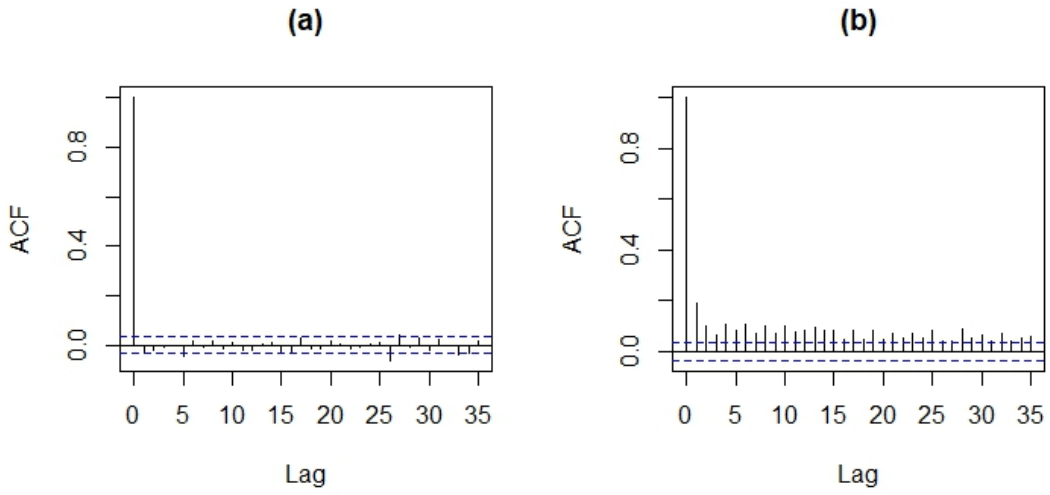

Figure 3.2: (a). ACF of USD/CAD returns data. (b). ACF of USD/CAD squared returns data.

Table 3.2: Estimates of parameters and their corresponding SE (in parentheses) of SV-EAR(1), SV-MIN(1), SV-NEAR(1), SV-EMARMIN(1) models.

		Estimates					
Data	**Model**	$\hat{\lambda}$	$\hat{k}$	$\hat{\alpha}$	$\hat{\alpha_0}$	$\hat{\beta}$	$\hat{\beta}_0$
USD/CAD	SV-EAR(1)	4.0740 (0.1420)		0.7918 (0.0691)			
	SV-MIN(1)	3.9019 (0.1434)	1.6549 (0.0617)				
	SV-NEAR(1)	4.0704 (0.1451)			0.8054 (0.0564)		0.8229 (0.0614)
	SV-EMARMIN(1)	4.0740 (0.1425)		0.7918 (0.0706)		0.8100 (0.0785)	
GH	SV-EAR(1)	0.5197 (0.0592)		0.8712 (0.0456)			
	SV-MIN(1)	0.4840 (0.0582)	1.1017 (0.0225)				
	SV-NEAR(1)	0.5197 (0.0581)			0.7893 (0.0384)		0.8326 (0.0411)
	SV-EMARMIN(1)	0.5917 (0.0570)		0.8712 (0.0278)		0.7983 (0.0249)	

After completing the estimation process, we should carry out the model diagnostic tests so that our model assumptions are aligned with the data. For this, a comprehensive residual analysis is required. However, since the SV model in (2.1) is expressed in terms of non-observable volatilities, the diagnostic process

is more complex. We usually use the Kalman filtering technique to handle this, which allows us to represent the model in state-space form. This is straightforward for the SV-EAR(1) and SV-NEAR(1) models. But for the SV-MIN(1) and SV-EMARMIN(1) models, we must use a non-linear filtering technique introduced by Watanabe (1999) to derive the residuals for model diagnostics since there is a non-linearity in the volatility terms in these models. This approach is based on conditional pdf. For both techniques, we first estimate the unobservable volatilities and then utilize those estimates of volatilities for the calculation of the residuals. That is, the residuals are derived as $\hat{Y}_t = X_t/\sqrt{\hat{w}_t}$, where $\hat{w}_t$ represents the estimated volatilities. The model diagnostics for each SV model are detailed below.

3.3.1 SV-EAR(1):

The state space representation of the exponential SV model is given by,

$$\log X_t^2 = -1.2704 + \log w_t + \tau_t, \tag{3.3}$$

where, $\tau_t = logY_t^2 + 1.2704$ with $E(\tau_t) = 0$, and $Var(\tau_t) = \frac{\pi^2}{2}$. The volatility process here is, $w_t = \alpha w_{t-1} + I_t E_t$. Using the Kalman filtering method, we approximate the distribution of E_t by a normal distribution with mean $1/\lambda$ and variance $1/\lambda^2$. The following equations are then used for prediction and updating steps in the Kalman filter,

Prediction:

$$\bar{w}_{t|t-1} = \alpha \bar{w}_{t-1|t-1} + (1-\alpha)/\lambda,$$

$$\Lambda_{t|t-1} = \alpha^2 \Lambda_{t-1|t-1} + \alpha(1-\alpha)/\lambda^2,$$

Updating:

$$\bar{w}_{t|t} = \bar{w}_{t|t-1} + \frac{\Lambda_{t|t-1}}{g_t}\left[\log X_t^2 + 1.27 - \log(\bar{w}_{t|t-1})\right],$$
$$\Lambda_{t|t} = \Lambda_{t|t-1}\left(1 - \frac{\Lambda_{t|t-1}}{g_t}\right),$$

where $\bar{w}_{t|t-1}$, $\Lambda_{t|t-1}$, $\bar{w}_{t|t}$, $\Lambda_{t|t}$ represent the predicted value of w_t and its variance at time $t-1$ and t respectively. The term $g_t = \Lambda_{t|t-1} + \frac{\pi^2}{2}$ captures the variance prediction component. The initial values for the system are chosen as $\Lambda_{0|0} = 1/\lambda^2$ and $\bar{w}_{0|0} = 1/\lambda$ and the parameters λ and α are updated using their respective estimates $\hat{\lambda}$ and $\hat{\alpha}$ which are provided in Table 3.2.

Figure 3.3 depicts the ACF plot of the residuals, which confirms the absence of significant serial correlations. This is verified by the Ljung-Box test with lag 20. The test statistic value for residuals is 5.584 with a p-value of 0.1898, and for squared residuals, the test statistic value is 1.326 with a p-value of 0.097, indicating no significant serial correlations. To check whether the residuals are normally distributed, we plotted the histogram of residuals against the normal distribution curve and observed that the normal distribution is a good approximation of the residuals (See Figure 3.3). This is also supported by the Jarque-Bera test with a p-value equal to 0.5623 for supporting the normality of the residuals. Based on these analyses, we infer that the SV-EAR(1) model is a good fit and adequate for this data.

3.3.2 SV-NEAR(1):

For this model, the volatility sequence is given by, $w_t = \beta_0 I_t w_{t-1} + \eta_t$. To apply the Kalman filtering method, we approximate the distribution of η_t using a normal distribution with mean $\frac{(1-\beta_0)+\alpha_0\beta_0^2(1-\alpha_0)}{(1-(1-\alpha_0)\beta_0)\lambda}$ and variance $\mathrm{Var}(\eta_t)$. The predictions and updates for the volatility sequences are obtained as follows,

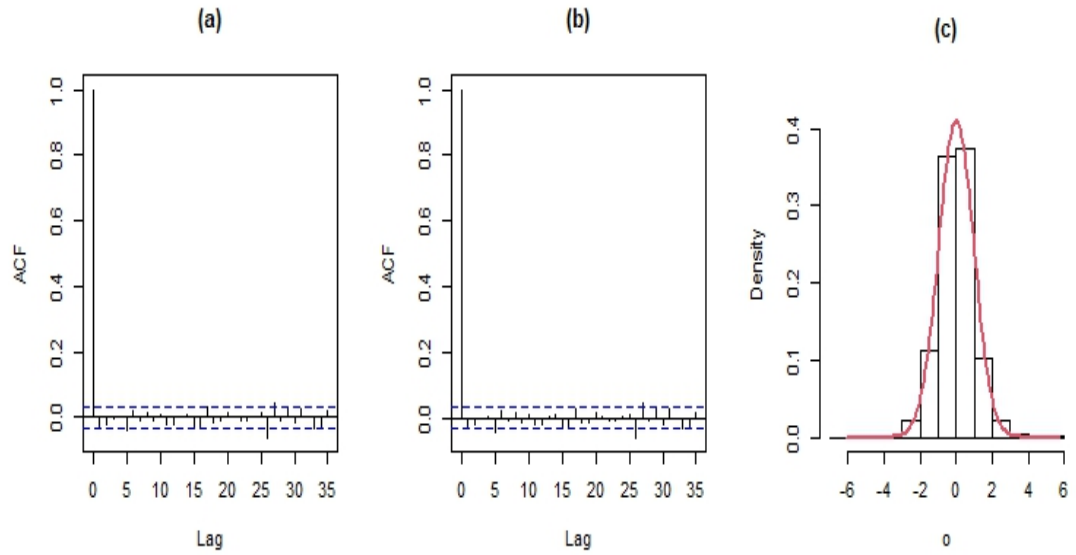

Figure 3.3: For USD/CAD data, (a). ACF of residuals for SV-EAR(1) model. (b). ACF of squared residuals for SV-EAR(1) model. (c). Histogram of residuals for SV-EAR(1) model.

Prediction:

$$\bar{w}_{t|t-1} = \beta_0\alpha_0\bar{w}_{t-1|t-1} + \frac{((1-\beta_0)+\alpha_0\beta_0^2(1-\alpha_0))}{(1-(1-\alpha_0)\beta_0)\lambda},$$
$$\Lambda_{t|t-1} = \beta_0^2\alpha_0(1-\alpha_0)\Lambda_{t-1|t-1} + Var(\eta_t),$$

Updating:

$$\bar{w}_{t|t} = \bar{w}_{t|t-1} + \frac{\Lambda_{t|t-1}}{g_t}\left[\log X_t^2 + 1.27 - \log(\bar{w}_{t|t-1})\right],$$
$$\Lambda_{t|t} = \Lambda_{t|t-1}\left(1 - \frac{\Lambda_{t|t-1}}{g_t}\right),$$

The initial values are set as $\Lambda_{0|0} = 1/\lambda^2$ and $\bar{w}_{0|0} = 1/\lambda$ and the parameters α_0, β_0, and λ are replaced by their respective estimates from Table 3.2.

The ACF plot of residuals and squared residuals is presented in Figure 3.4, indicating the lack of significant serial correlations in them. Additionally, the Ljung-Box test with a lag 20 confirmed the absence of significant serial correlations in the

residuals and squared residuals. That is, in residuals with a test statistic value of 5.346 and a p-value of 0.1885 and in the squared residuals with a test statistic value of 2.07 and a p-value of 0.088. Also from Figure 3.4, it is evident that the residuals follow a normal distribution, which is further validated using the Jarque-Bera test, with a p-value of 0.6121. Thus, confirming that the model is adequate and performs well for the given data.

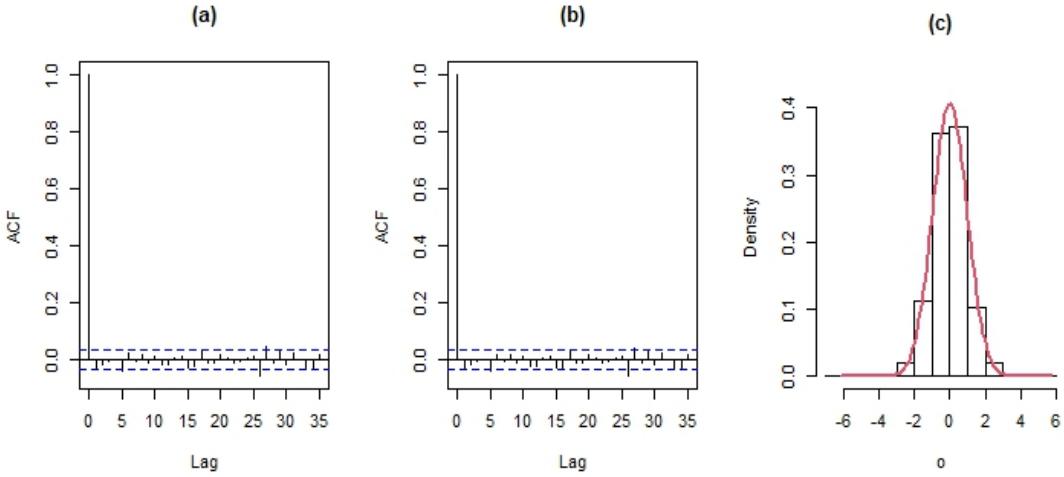

Figure 3.4: For USD/CAD data, (a). ACF of residuals for SV-NEAR(1) model. (b). ACF of squared residuals for SV-NEAR(1) model. (c). Histogram of residuals for SV-NEAR(1) model.

3.3.3 SV-MIN(1):

Since the volatilities in the SV-MIN(1) model are stated as non-linear functions, standard Kalman filtering is not effective. Consequently, we utilize a non-linear filtering approach based on the Bayes theorem, more precisely on the conditional pdf. For approximating the filter, Kitagawa (1987) developed a linear spline technique, and Watanabe (1999) suggested using this approach for SV model analysis. We derive the conditional densities for the minification model given in

(1.9) as follows,

$$\begin{aligned} p\left(w_t \mid w_{t-1}, \mathbf{X}_{t-1}\right) &= \frac{\lambda(k-1)}{k} \exp\left[\frac{-\lambda(k-1)w_{t-1}}{k}\right], \\ p\left(x_t \mid w_t, \mathbf{X}_{t-1}\right) &= \frac{1}{\sqrt{2\pi w_t}} \exp\left[-\frac{x_t^2}{2w_t}\right], \end{aligned} \tag{3.4}$$

where $\mathbf{X}_t \equiv (x_1, x_2, \ldots, x_t)$. For each period, we select N+1 number of nodes and denote them as $w_t^{(0)}, w_t^{(1)}, w_t^{(2)}, \ldots, w_t^{(N)}$ for $t = 1, 2, \ldots, L$. Then,

One-step-ahead prediction:

$$\begin{aligned} & p\left(w_t^{(i)} \mid \mathbf{X}_{t-1}\right) \\ & \quad \int_{-\infty}^{\infty} p\left(w_t^{(i)} \mid w_{t-1}, \mathbf{X}_{t-1}\right) p\left(w_{t-1} \mid \mathbf{X}_{t-1}\right) \mathrm{d}w_{t-1} \\ & \approx \sum_{n=1}^{N} \int_{w_{t-1}^{(n-1)}}^{w_{t-1}^{(n)}} p\left(w_t^{(i)} \mid w_{t-1}, \mathbf{X}_{t-1}\right) p\left(w_{t-1} \mid \mathbf{X}_{t-1}\right) \mathrm{d}w_{t-1} \\ & \approx \frac{1}{2} \sum_{n=1}^{N} \left(w_{t-1}^{(n)} - w_{t-1}^{(n-1)}\right) \left[p\left(w_t^{(i)} \mid w_{t-1}^{(n-1)}, \mathbf{X}_{t-1}\right) p\left(w_{t-1}^{(n-1)} \mid \mathbf{X}_{t-1}\right)\right. \\ & \left. + p\left(w_t^{(i)} \mid w_{t-1}^{(n)}, \mathbf{X}_{t-1}\right) p\left(w_{t-1}^{(n)} \mid \mathbf{X}_{t-1}\right)\right]; \quad i = 0, 1, \ldots, N. \end{aligned} \tag{3.5}$$

Updating:

$$p\left(w_t^{(i)} \mid \mathbf{X}_t\right) = \frac{p\left(x_t \mid w_t^{(i)}, \mathbf{X}_{t-1}\right) p\left(w_t^{(i)} \mid \mathbf{X}_{t-1}\right)}{p\left(x_t \mid \mathbf{X}_{t-1}\right)}; \quad i = 0, 1, \ldots, N, \tag{3.6}$$

where

$$\begin{aligned} p\left(x_t \mid \mathbf{X}_{t-1}\right) &= \int_{-\infty}^{\infty} p\left(x_t \mid w_t, \mathbf{X}_{t-1}\right) p\left(w_t \mid \mathbf{X}_{t-1}\right) \mathrm{d}w_t \\ & \quad \sum_{n=1}^{N} \int_{w_t^{(n-1)}}^{w_t^{(n)}} p\left(x_t \mid w_t, \mathbf{X}_{t-1}\right) p\left(w_t \mid \mathbf{X}_{t-1}\right) \mathrm{d}w_t \\ &\approx \frac{1}{2} \sum_{n=1}^{N} \left(w_t^{(n)} - w_t^{(n-1)}\right) \left[p\left(x_t \mid w_t^{(n-1)}, \mathbf{X}_{t-1}\right) p\left(w_t^{(n-1)} \mid \mathbf{X}_{t-1}\right)\right. \\ & \quad \left. + p\left(x_t \mid w_t^{(n)}, \mathbf{X}_{t-1}\right) p\left(w_t^{(n)} \mid \mathbf{X}_{t-1}\right)\right], \end{aligned} \tag{3.7}$$

and $p\left(w_t^{(i)} \mid w_{t-1}^{(n)}, \mathbf{X}_{t-1}\right)$ and $p\left(x_t \mid w_t^{(j)}, \mathbf{X}_{t-1}\right)$ $(i, j, n = 0, 1, \ldots, N)$ are derived from the conditional densities in (3.4).

The log-likelihood function is given by,

$$\begin{aligned} \log L &= \log\left[p(\mathbf{X_t})\right] \\ &= \sum_{t=1}^{T} \log\left[p\left(x_t \mid \mathbf{X}_{t-1}\right)\right]. \end{aligned} \tag{3.8}$$

Using the GMM parameter estimates, we apply the filter to calculate $p\left(x_t \mid \mathbf{X}_{t-1}\right)$ for each period and use these values to evaluate the likelihood. The SV parameters are then estimated by maximizing this exact log-likelihood. The residuals obtained using these estimates are analyzed to check the models' adequacy. Figure 3.5 illustrates the ACF plot and the histogram of the residuals. The Ljung-Box test (with lag 20) indicates no significant serial correlations in the residuals, with a p-value of 0.2117, and similarly, no significant serial correlations in the squared residuals, with a p-value of 0.1342. The histogram in Figure 3.5 suggests that the residuals are well-fitted by a normal distribution and is further validated by the Jarque-Bera test, which has a p-value of 0.5238, confirming the adequacy of the model.

3.3.4 SV-EMARMIN(1):

Since the volatilities of this model are also represented as non-linear functions, we apply the same non-linear filtering approach outlined above. The conditional densities for this model are given by,

$$P\left(w_t \mid w_{t-1}\right) = \begin{cases} (1-\alpha)\beta\lambda \exp\left(-\lambda w_t + \lambda\alpha w_{t-1}\right) + \\ (1-\beta)\lambda(1-\alpha)\exp\left(-\lambda(1-\alpha)w_t\right), & \text{if} \quad w_{t-1} > w_t\alpha, \\ -(1-\alpha)\beta\lambda \exp\left(-\lambda w_t + \lambda\alpha w_{t-1}\right), & \text{if} \quad w_{t-1} < w_t\alpha, \end{cases}$$

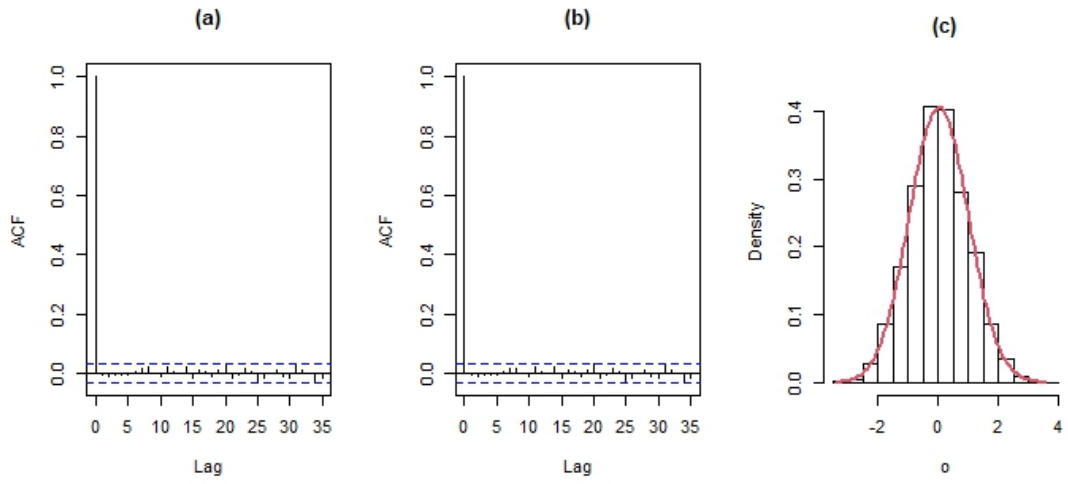

Figure 3.5: For USD/CAD data, (a). ACF of residuals for SV-MIN(1) model. (b). ACF of squared residuals for SV-MIN(1) model. (c). Histogram of residuals for SV-MIN(1) model.

$$p\left(x_t \mid w_t, \mathbf{X}_{t-1}\right) = \frac{1}{\sqrt{2\pi w_t}} \exp\left[-\frac{x_t^2}{2w_t}\right].$$

The predictions and updates are obtained by executing the equations (3.5)-(3.7). The log-likelihood function, as given in (3.8), is then evaluated to obtain the estimates and corresponding residuals. Figure 3.6 displays the ACF plot and histogram of residuals. The Ljung-Box test (lag 20) confirms the absence of significant serial correlations in residuals with a p-value of 0.1788 and in squared residuals with a p-value of 0.0957. The histogram depicts that the residuals are well-fit by a normal distribution, and this is supported by the Jarque-Bera test, which gives a p-value of 0.7234. Overall, the model's adequacy is confirmed, indicating that it performs satisfactorily.

Next, we conduct a comparative analysis of the proposed SV models to determine which one performs better. We compute the out-of-sample analysis using the squared returns. The parameters were estimated for the period from January 1, 2010, to December 30, 2022, and the out-of-sample analysis was carried out for the period from January 1, 2023, to December 18, 2023, covering 250 trading

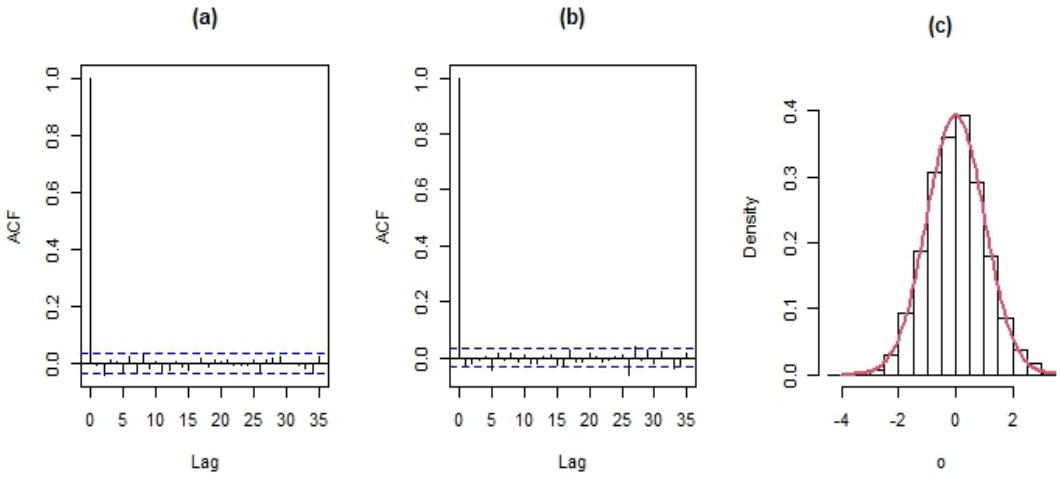

Figure 3.6: For USD/CAD data, (a). ACF of residuals for SV-EMARMIN(1) model. (b). ACF of squared residuals for SV-EMARMIN(1) model. (c). Histogram of residuals for SV-EMARMIN(1) model.

days.

For each SV model, the one-step-ahead prediction of w_{t+j} given $X_{t+j-1}, X_{t+j-2}, \ldots$, is determined by $\hat{w_{t+j}} = E\left(w_{t+j} \mid X_{t+j-1}, X_{t+j-2} \ldots\right)$. The predictions for $j = 1, 2, \ldots, 250$ are then computed by estimating the model parameters at each point in the post-sample period.

The one-step-ahead predictions for each SV model are as follows,

(i) SV-EAR(1),

$$E\left(w_{t+1} \mid X_t, X_{t-1} \ldots\right) = \alpha w_t + \frac{1-\alpha}{\lambda}.$$

(ii) SV-NEAR(1),

$$E\left(w_{t+1} \mid X_t, X_{t-1} \ldots\right) = \alpha_0\beta_0 w_t + \frac{(1-\beta_0) + \alpha_0\beta_0^2(1-\alpha_0)}{(1-(1-\alpha_0)\beta_0)\lambda}.$$

(iii) SV-MIN(1),

$$E\left(w_{t+1} \mid X_t, X_{t-1} \ldots\right) = kw_t e^{-\lambda(k-1)w_t} + \frac{k}{\lambda(k-1)}(1 - e^{-\lambda(k-1)w_t}).$$

(iv) SV-EMARMIN(1),

$$E\left(w_{t+1} \mid X_t, X_{t-1} \ldots\right) = \alpha\beta w_t + \frac{\beta}{\lambda}(1-\alpha) + \frac{1-\beta}{\lambda(1-\alpha)}\left[1 - e^{\frac{-\lambda(1-\alpha)w_t}{\alpha}}\right].$$

After obtaining these predictions for each model, we calculate the MAE and the RMSE to evaluate and compare the performance of each SV model. The computed values are provided in Table 3.3. From the table, it is observed that the SV-EMARMIN(1) model exhibits the lowest RMSE and MAE values compared to the other SV models, indicating that it outperforms the others in terms of forecasting accuracy. This suggests that the SV-EMARMIN(1) model provides higher forecasting performance.

Table 3.3: RMSE and MAE of SV-EAR(1), SV-MIN(1), SV-NEAR(1), SV-EMARMIN(1) models.

Data	**Model**	**RMSE**	**MAE**
USD/CAD	SV-EAR(1)	0.8261	0.5865
	SV-MIN(1)	0.7108	0.5350
	SV-NEAR(1)	0.6732	0.5118
	SV-EMARMIN(1)	0.6647	0.5028
GH	SV-EAR(1)	0.5312	0.3498
	SV-MIN(1)	0.5287	0.3234
	SV-NEAR(1)	0.4990	0.3113
	SV-EMARMIN(1)	0.4593	0.2994

The volatility estimated by our developed SV models can be applied to assess market risk for a portfolio of assets using the VaR metric. For all of the models, VaR was estimated at the 99th percentile for a 250-day horizon. To evaluate the accuracy of these estimates, we employed a backtesting procedure based on the Basel Committee on Banking Supervision's "traffic light" approach (Basel Committee on Banking Supervision (1996)). This approach compares the predicted VaR with actual returns, counting the number of exceptions-cases where the ac-

tual return falls below the VaR estimate over the past 250 days.

The Basel Committee categorizes VaR model performance based on the number of exceptions as follows,

- ➤ Green Zone: 0-4 exceptions (acceptable performance).
- ➤ Yellow Zone: 5 to 9 exceptions (potential concerns).
- ➤ Red Zone: ten or more exceptions (the model is inadequate).

The performance of the models was now evaluated by counting the number of exceptions and calculating the hit rate (the proportion of exceptions over a 250-day period). The backtesting results for each model over the last 250 days are as follows,

(i) SV-EAR(1): 1 exception (Green Zone).

(ii) SV-NEAR(1): 1 exception (Green Zone).

(iii) SV-MIN(1): 1 exception (Green Zone).

(iv) SV-EMARMIN(1): 0 exceptions (Green Zone).

These backtesting results demonstrate that all four models accurately predict VaR within the acceptable range set by the Basel Committee. On the other hand, the SV-EMARMIN(1) model had the fewest exceptions, indicating that it may be the most effective in predicting risk for the given data. We plotted the actual returns alongside the VaR estimates for each model over the last 250 days in Figure 3.7 to compare the performance of these models, and it highlights how often actual returns fell below the VaR thresholds, identifying the exceptions. Furthermore, from Figure 3.7, we can observe that the SV-EMARMIN(1) model performs better, with fewer violations, whereas the SV-EAR(1), SV-NEAR(1), and SV-MIN(1) models illustrate similar performance. In the next section, we analyze these models using another dataset and compare them.

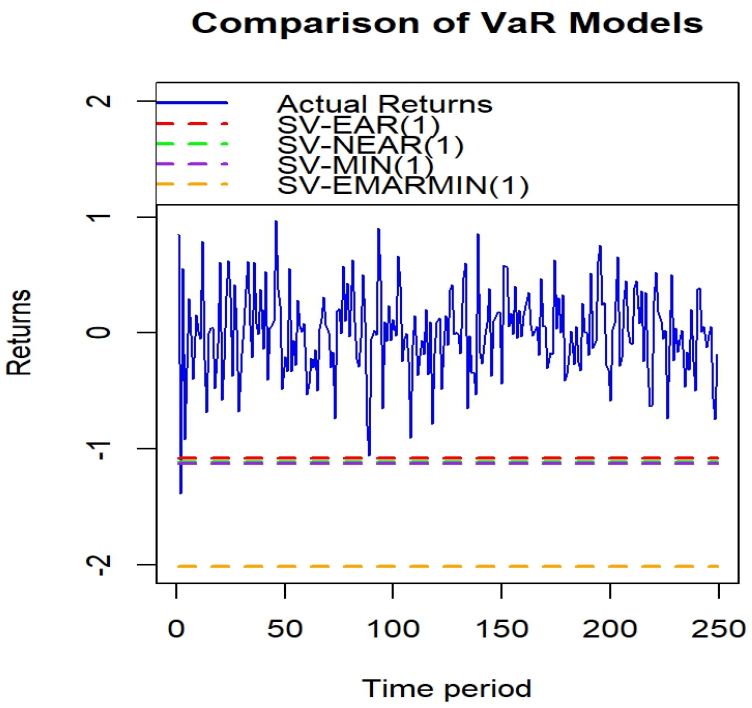

Figure 3.7: Daily returns and VaR estimates of USD/CAD data for each model.

3.4 Data analysis-2

We analyze the daily returns of Guardant Health, Inc. (GH) from October 4, 2018 to May 24, 2023 (https://finance.yahoo.com). We have P_t representing the price, and the returns for GH are calculated using (3.2). Figure 3.8 displays the time series plot of the original series and the returns, and the descriptive statistics of the GH return series are summarized in Table 3.1. The ACF plots of both the returns and squared returns in Figure 3.9 reveal that the return series exhibits negligible serial correlation, whereas the squared returns exhibit significant correlations that decay gradually. Moreover, this is corroborated by the Ljung-Box portmanteau test with lag 20, and it confirms no serial correlation in the returns, with a p-value of 0.8347, and significant autocorrelation in the squared returns, with a p-value below 0.05.

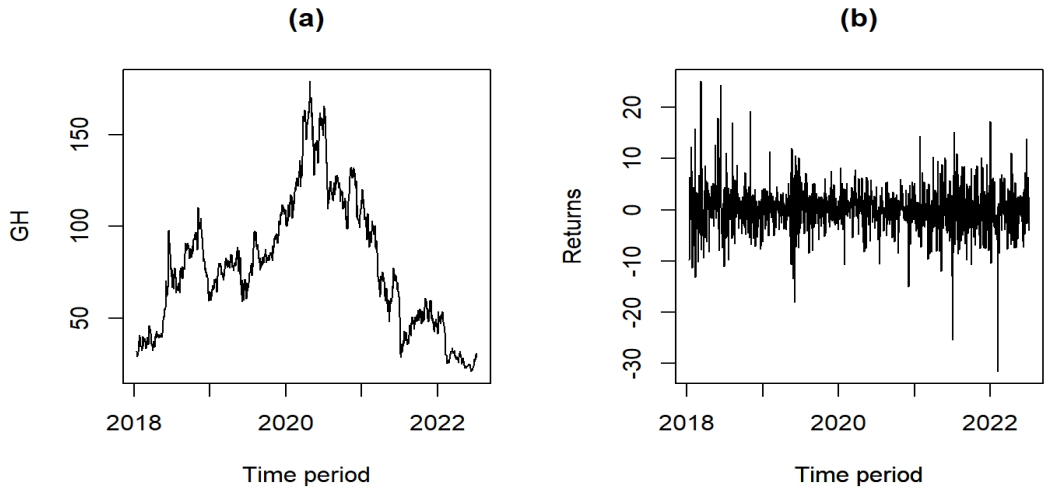

Figure 3.8: (a). GH time series data. (b). Return series of the GH data.

The kurtosis value in Table 3.1 indicates a leptokurtic distribution for the returns, suggesting that the proposed exponential SV models may be a good fit for this data. The parameter estimates for each model obtained using the GMM are provided in Table 3.2, and following the steps in Section 3.3, we perform model diagnostics for each of the SV models.

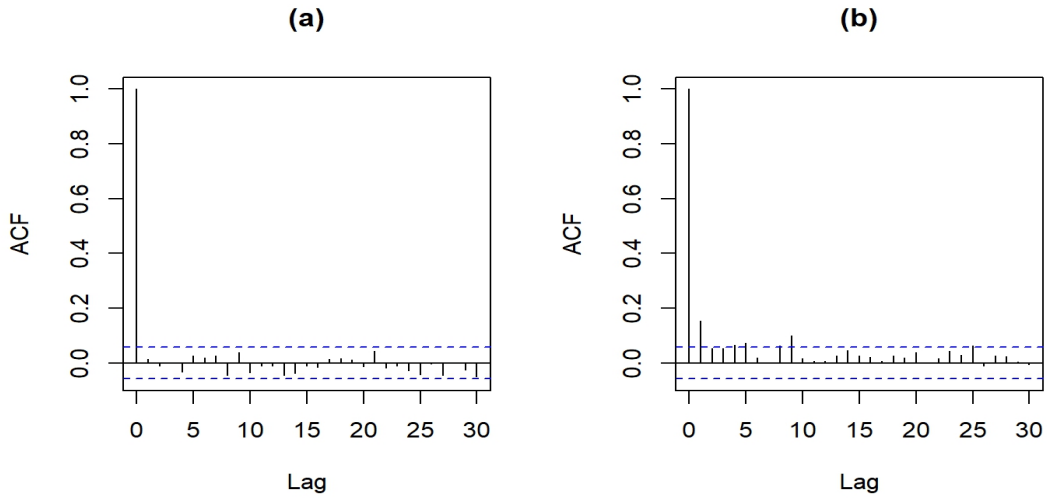

Figure 3.9: (a). ACF of GH returns data. (b). ACF of GH squared returns data.

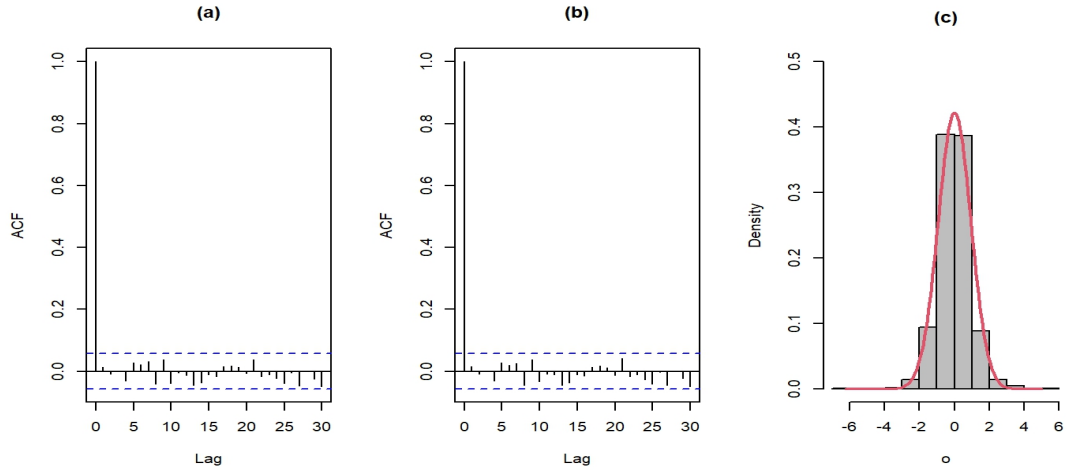

Figure 3.10: For GH data, (a). ACF of residuals for SV-EAR(1) model. (b). ACF of squared residuals for SV-EAR(1) model. (c). Histogram of residuals for SV-EAR(1) model.

3.4.1 SV-EAR(1)

Using the technique mentioned in Subsection 3.3.1, the residuals are computed. The ACF plots of the residuals and squared residuals are shown in Figure 3.10. The Ljung-Box test with lag 20 confirms the lack of significant serial correlations in residuals and squared residuals with p-values 0.8029 and 0.3291 respectively. The histogram of residuals superimposed with the normal variate is shown in Figure 3.10, and we can see that the normal distribution fits the residuals well. This is validated using the Jarque-Bera test with a p-value of 0.6428, confirming the normality of residuals. Thus, we examined the SV-EAR(1) model's adequacy and found that it works adequately.

3.4.2 SV-NEAR(1)

We perform the model diagnostics checks using the same diagnostic process as mentioned in Subsection 3.3.2. The ACF plots and histogram of residuals are displayed in Figure 3.11. Using the Ljung-Box test with a lag 20, we confirmed no

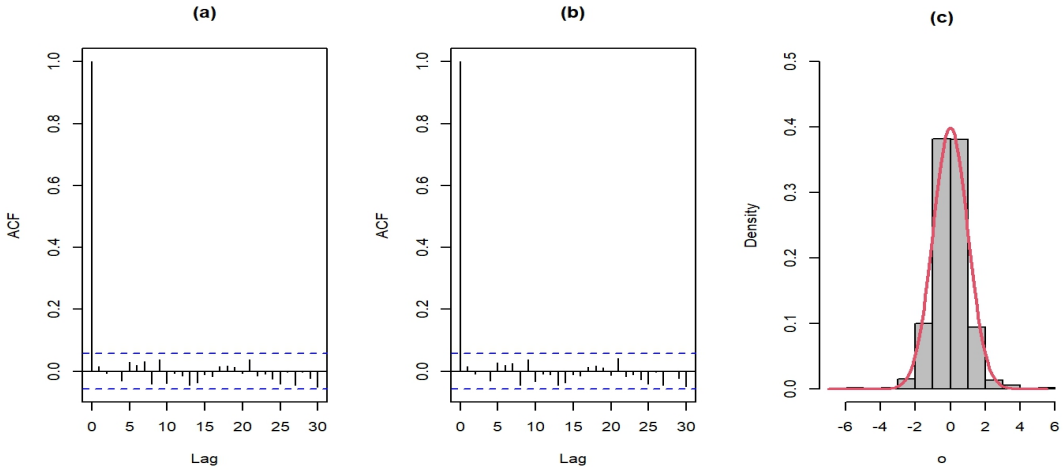

Figure 3.11: For GH data, (a). ACF of residuals for SV-NEAR(1) model. (b). ACF of squared residuals for SV-NEAR(1) model. (c). Histogram of residuals for SV-NEAR(1) model.

significant serial correlations in the residuals, with a p-value of 0.8628, and in the squared residuals, with a p-value of 0.3548. Further, Figure 3.11 clearly illustrates that the residuals follow a normal distribution. The Jarque-Bera test further supported this, with a p-value of 0.5490, implying that the model is adequate and performs well.

3.4.3 SV-MIN(1)

For the SV-MIN(1) model, we carried out the residual analysis as described in Subsection 3.3.3. The ACF plots of the residuals and squared residuals are shown in Figure 3.12. The Ljung-Box test with lag 20 confirmed the absence of significant serial correlations in the residuals, with a p-value of 0.8227, and in the squared residuals, with a p-value of 0.3313. Additionally, the adequacy of the model is confirmed by the residuals following a normal distribution, as shown by Figure 3.12 and by the Jarque-Bera test yielding a p-value of 0.5671. Thus, proving the model performs well for the data.

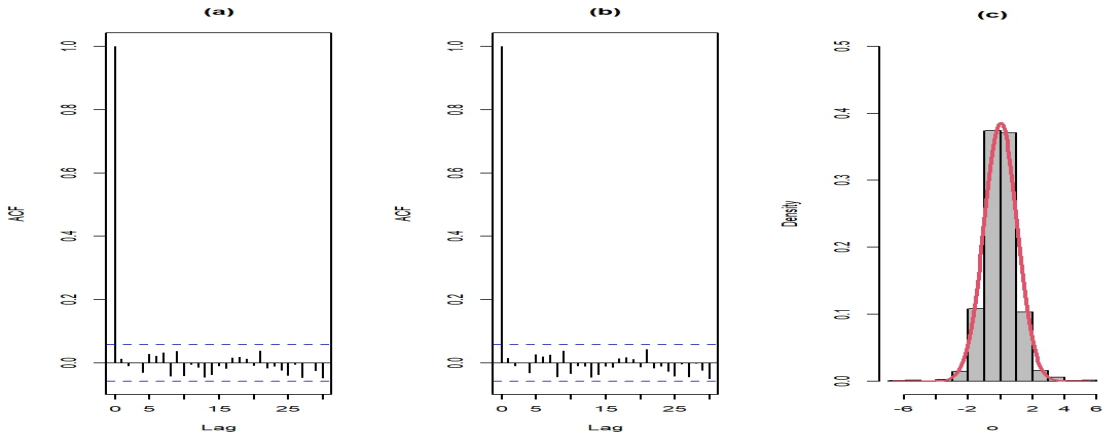

Figure 3.12: For GH data, (a). ACF of residuals for SV-MIN(1) model. (b). ACF of squared residuals for SV-MIN(1) model. (c). Histogram of residuals for SV-MIN(1) model.

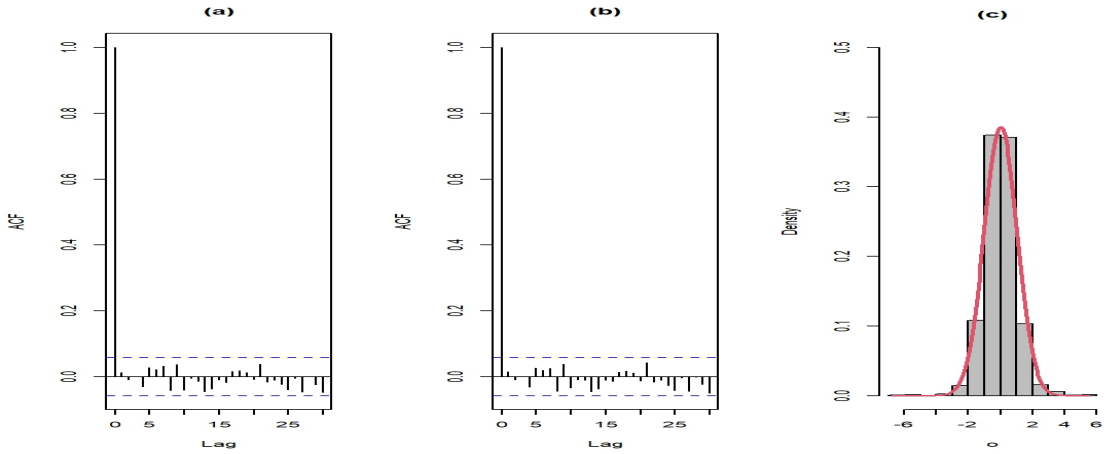

Figure 3.13: For GH data, (a). ACF of residuals for SV-EMARMIN(1) model. (b). ACF of squared residuals for SV-EMARMIN(1) model. (c). Histogram of residuals for SV-EMARMIN(1) model.

3.4.4 SV-EMARMIN(1)

The residual analysis was undertaken as indicated in Subsection 3.3.4. The ACF plot and histogram of the residuals are depicted in Figure 3.13. The Ljung-Box test with lag 20 confirmed no significant serial correlations in the residuals, with a p-value of 0.8865, and in the squared residuals, with a p-value of 0.3957. The histogram (Figure 3.13) shows that the residuals follow a normal distribution,

which was further validated by the Jarque-Bera test with a p-value of 0.6034. This proves the adequacy of the model, and we conclude that it performs satisfactorily. Next, we proceed to the out-of-sample performance of the GH dataset. The parameters were estimated for the time frame spanning from October 4, 2018, to May 24, 2023, and the out-of-sample analysis covers the period from May 25, 2023, to May 23, 2024 (250 trading days). The MAE and RMSE for each SV model are then calculated using the same approaches used for the USD/CAD dataset, and the results are shown in Table 3.3. The results reveal that, in comparison to the other SV models, the SV-EMARMIN(1) model has the lowest RMSE and MAE values, suggesting better predictive performance.

The VaR estimates at the 99 percentile for each model are also calculated, and the backtesting results over 250 days are,

(i) SV-EAR(1): 4 exceptions (Green zone).

(ii) SV-NEAR(1): 2 exceptions (Green zone).

(iii) SV-MIN(1): 3 exceptions (Green zone).

(iv) SV-EMARMIN(1):1 exception (Green zone).

These observed exceptions serve as a clear metric for assessing the performance of each model. All four models, SV-EAR(1), SV-NEAR(1), SV-MIN(1), and SV-EMARMIN(1) demonstrated strong accuracy in estimating VaR, with their results falling within the Green Zone. This indicates that these models are reliable for risk estimation at the 99% confidence level over a 250-day horizon. Figure 3.14 illustrates the plot of returns and VaR estimates for each model. It is evident from the figure that the SV-EMARMIN(1) model exhibited the highest accuracy with the fewest exceptions, followed by the SV-NEAR(1), SV-MIN(1), and SV-EAR(1) models. Consequently, the SV-EMARMIN(1) model outperforms the others in terms of forecasting accuracy and risk estimation.

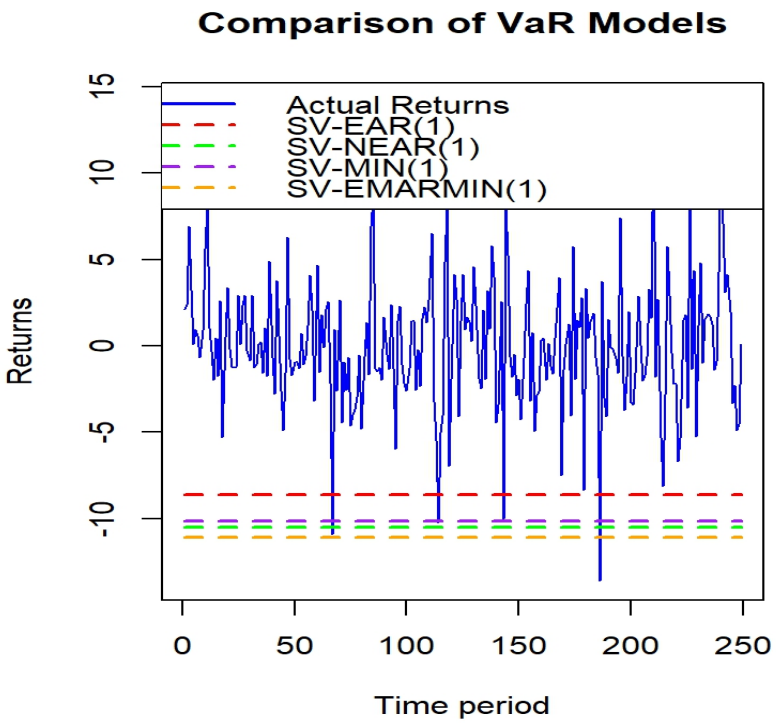

Figure 3.14: Daily returns and VaR estimates of GH data for each model.

3.5 Summary

A comprehensive analysis and comparison of the exponential Markov sequence-based SV models developed in Chapter 2 is conducted. The effectiveness of each model is demonstrated by analyzing two real financial datasets, and an approximate Kalman filtering approach is applied to perform comprehensive residual analyses and model diagnostics for SV-EAR(1) and SV-NEAR(1) models. On the other hand, for the SV-MIN(1) and SV-EMARMIN(1) models, a non-linear filtering method is employed, though, which worked very well. Furthermore, we compared the proposed SV models using MAE, RMSE, and VaR metrics, and found that the SV-EMARMIN(1) model performed best.

CHAPTER 4

Stochastic Volatility Model Generated by Induced Garima Distribution

4.1 Introduction

[1] In recent years, financial time series analysis has been gaining significant traction and has led to extensive research in this domain. As explained in Chapter 1, several models have been proposed to analyze the changing variance of financial asset returns. Although the classical normal-log-normal SV model has made tremendous contributions to volatility modeling, there are alternatives that offer notable improvements. Expansion of the basic SV model has been conducted mainly with respect to the refinement of the distributional aspects of the returns and error specifications of the model. The first-order Gaussian AR sequence is a quite appealing feature within those models, as it well recapitulates the dynamics of log-volatility. This focus on log-volatility has generated several Markovian sequences of non-negative random variables, now widely used in contemporary volatility modeling.

In Chapters 2 and 3, we explored various variants of exponential SV models with

[1] Some parts of this chapter are based on Jafna & Krishnarani (2024).

Laplace distributed returns, showcasing their efficacy in capturing the dynamics of volatility in financial time series. This chapter introduces a stationary Markov sequence of induced-Garima (i-Garima) random variables to model volatilities alongside an exploration of its statistical properties and applications in time series analysis. The SV model generated in this chapter has Laplace-mixture distributed returns, and the proposed model is motivated by the Lindley SV model, which has been widely discussed in Sri Ranganath (2018) and is specifically designed to handle the volatilities of the time-dependent process. The i-Garima distribution, introduced first by Singh & Das (2023), is a mixture of the exponential and gamma distributions which provides a flexible alternative for the analysis of time series models. The i-Garima distribution has better properties and is, therefore, suitable for time series applications since it can model a wide range of volatility behaviors, from short-term shocks to long-term persistence.

The chapter is structured as follows. Section 4.2 discusses the i-Garima distribution and its properties. Section 4.3 deals with the proposed i-Garima SV model and studies its characteristics and distributional properties. The estimation of the model parameters and simulation are carried out in Sections 4.4 and 4.5, respectively. The application of the model to two real data sets is employed in Section 4.6, and finally, the summary is given in Section 4.7.

4.2 Induced-Garima distribution

A random variable W follows i-Garima distribution if its pdf is given by,

$$f(w;\theta) = \frac{\theta}{\theta+3}(2+\theta+\theta w)e^{-\theta w}, \quad w>0, \quad \theta>0, \tag{4.1}$$

with corresponding cumulative distribution function,

$$F(w;\theta) = 1 - \left[1 + \frac{\theta w}{\theta + 3}\right] e^{-\theta w}, \quad w > 0, \quad \theta > 0.$$

This distribution is derived using the concept of induced distribution, hence it is referred to as the induced-Garima distribution. The i-Garima distribution can be expressed as a mixture of an exponential distribution with rate parameter θ and a gamma distribution with shape parameter 2 and rate θ, with mixing proportion $q = \frac{\theta+2}{\theta+3}$. That is, the pdf can be expressed as,

$$f(w;\theta) = qf_1(w) + (1-q)f_2(w),$$

where $f_1(w) = \theta e^{-\theta w}$, and $f_2(w) = \theta^2 w e^{-\theta w}$.

The r^{th} order moments about the origin are given as,

$$\mu'_r = \frac{r!}{\theta^r} \frac{(\theta + r + 3)}{(\theta + 3)}, \quad r = 1, 2, 3, \ldots.$$

The coefficient of skewness $\sqrt{\beta_1}$ and the coefficient of kurtosis β_2 are given as,

$$\sqrt{\beta_1} = \frac{\mu_3}{\mu_2^{\frac{3}{2}}} = \frac{2\left(\theta^3 + 12\theta^2 + 42\theta + 46\right)}{\left(\theta^2 + 8\theta + 14\right)^{\frac{3}{2}}},$$

$$\beta_2 = \frac{\mu_4}{\mu_2^2} = \frac{3\left(3\theta^4 + 48\theta^3 + 260\theta^2 + 592\theta + 488\right)}{\left(\theta^2 + 8\theta + 14\right)^2},$$

indicating that for varying values of θ, the distribution is positively skewed and leptokurtic. The i-Garima distribution is recognized as a second-order induced Lindley distribution and has significant applications in modeling lifetime data. However, there has been limited research on its application in time series analysis. Hence, in the following sections, we explore the use of the i-Garima distribution in time series analysis, particularly in the context of modeling volatility.

4.3 Induced-Garima stochastic volatility model

In this section, we develop an SV model based on a first-order i-Garima Markov sequence and discuss its properties. Let X_t denote the return of a financial asset at time t. We define the SV model as in (2.1), where $\{Y_t,\ t \geq 1\}$ is an iid sequence of standard normal random variables. Additionally, we define the volatility process as,

$$w_t = \phi w_{t-1} + \eta_t, \quad t = 1, 2, \ldots, \quad 0 < \phi < 1, \tag{4.2}$$

under the assumption that $\{w_t,\ t \geq 1\}$ follows an i-Garima distribution, as specified by the pdf given in (4.1). The sequence $\{Y_t\}$ is assumed to be independent of both the volatility sequence $\{w_t\}$ and the innovation sequence $\{\eta_t\}$ for every t. The first step to be addressed here is the identification of the distribution of the innovation random variable η_t provided w_t follows the i-Garima distribution. We can use the Laplace transforms to determine the distribution of the innovation random variable η_t since $\{w_t\}$ is a stationary process characterized by an additive structure.

The Laplace transform of the stationary process $\{w_t\}$ following the i-Garima distribution is expressed as,

$$\Phi_w(s) = \frac{\theta(3\theta + \theta^2 + 2s + s\theta)}{(3+\theta)(\theta+s)^2}, \tag{4.3}$$

and using the AR model in (4.2), the Laplace transform of η_t is obtained as,

$$\Phi_\eta(s) = \frac{\Phi_w(s)}{\Phi_w(\phi s)}. \tag{4.4}$$

The equations (4.3) and (4.4) yields the Laplace transform of η_t as,

$$\Phi_\eta(s) = \frac{(3\theta + \theta^2 + 2s + s\theta)(\theta + \phi s)^2}{(3\theta + \theta^2 + 2s\phi + s\theta\phi)(\theta + s)^2}.$$

Thus, the distribution of η_t is determined by applying the partial fraction decomposition method and the properties of inverse Laplace transforms and is identified as,

$$f_\eta(w) = \phi\delta(w) + (1-\phi)r(w). \tag{4.5}$$

That is, η_t is expressed as a mixture of two distributions, where $\delta(w)$ is the Dirac Delta function defined by,

$$\delta(w) = \begin{cases} +\infty, & if \quad w = 0, \\ 0, & if \quad w \neq 0, \end{cases}$$

and $r(w)$ has the pdf,

$$\begin{aligned} r(w) = &\left(\frac{3\theta^2\phi^2 - \theta^2\phi^3 - 3\theta^2\phi + \theta^2 - 3\theta\phi^3 + 11\theta\phi^2 - 13\theta\phi + 5\theta - 2\phi^3 + 8\phi^2 - 12\phi + 6}{(1-\phi)(\theta(1-\phi) + 3 - 2\phi)^2}\right) \\ &\times \theta\exp(-\theta w) + \frac{1-\phi}{(\theta(1-\phi) + 3 - 2\phi)}\theta^2 w\exp(-\theta w) \\ &- \frac{\phi}{(\theta(1-\phi) + 3 - 2\phi)^2}\left(\frac{\theta^2 + 3\theta}{2\phi + \theta\phi}\right)\exp\left(-\frac{\theta^2 + 3\theta}{2\phi + \theta\phi}\right)w, \end{aligned}$$

with $\theta > 0, \quad w \geq 0$, which shows that $r(w)$ is a mixture of an exponential distribution with parameter θ, a gamma distribution with shape parameter 2 and rate parameter θ, and an exponential distribution with parameter $(\frac{\theta^2+3\theta}{2\phi+\theta\phi})$. The mean and variance of the innovation sequence η_t are respectively given as,

$$E(\eta_t) = \frac{\theta + 4}{\theta(\theta + 3)}(1-\phi), \tag{4.6}$$

and

$$\text{Var}\,(\eta_t) = \frac{(1-\phi^2)\,(\theta^2+8\theta+14)}{\theta^2(\theta+3)^2}. \tag{4.7}$$

Next, we study and discuss the statistical properties of the proposed i-Garima SV model.

4.3.1 Properties

The characteristic function of X_t is given by,

$$\begin{aligned}
\Phi_X(s) &= E\left(e^{(isX_t)}\right) \\
&= E\left(e^{(isY_t\sqrt{w_t})}\right) \\
&= \int_0^\infty E\left(e^{\left(is\sqrt{w}Y_t\right)}\right) f_w(w)dw \quad [\because w_t = w] \\
&= \int_0^\infty \left(e^{\left(\frac{-s^2w}{2}\right)}\right) \frac{\theta}{\theta+3}(2+\theta+\theta w)e^{-\theta w}dw \\
&= \frac{\theta}{\theta+3}\left(\frac{2\theta}{2\theta+s^2}\right) + \frac{2}{\theta+3}\left(\frac{2\theta}{2\theta+s^2}\right) + \frac{1}{\theta+3}\left(\frac{2\theta}{2\theta+s^2}\right)^2 \\
&= \frac{\theta+2}{\theta+3}\left(\frac{2\theta}{2\theta+s^2}\right) + \frac{1}{\theta+3}\left(\frac{2\theta}{2\theta+s^2}\right)^2 \\
&= \frac{\theta+2}{\theta+3}L_1 + \frac{1}{\theta+3}L_2.
\end{aligned} \tag{4.8}$$

Thus $\{X_t\}$ is a stationary Markov sequence whose marginal distribution has the characteristic function given in (4.8), where L_1 is an iid random variable with Laplace distribution having pdf,

$$f_L(x) = \sqrt{\frac{\theta}{2}}\exp(-\sqrt{2\theta}|x|) \quad -\infty < x < \infty, \quad \theta > 0,$$

and L_2 is the sum of two independent Laplace distributed random variables having the pdf given above. This indicates that the returns follow a Laplace-mixture distribution, which is particularly useful in capturing several important character-

istics observed in financial data.

Given the return series, the model in (2.1) makes it evident that the odd moments of $\{X_t\}$ are zero and its even moments are expressed as,

$$\begin{aligned} E\left(X_t^{2r}\right) &= E\left(Y_t^{2r}\right) E\left(w_t^r\right) \\ &= \left(\frac{r!(\theta+r+3)}{\theta^r(\theta+3)}\right) \prod_{j=1}^{r}(2j-1); \quad r=1,2,\ldots. \end{aligned}$$

The second-order moments are,

$$E\left(X_t^2\right) = \mathrm{Var}\left(X_t\right) = \frac{\theta+4}{\theta(\theta+3)},$$

and

$$E\left(X_t^2 X_{t-1}^2\right) = \frac{\phi(\theta^2+8\theta+14)+(\theta+4)^2}{\theta^2(\theta+3)^2}.$$

The variance and covariance of the squared return series are obtained as,

$$\mathrm{Var}\left(X_t^2\right) = \frac{5\theta^2+40\theta+74}{\theta^2(\theta+3)^2},$$

and

$$\gamma_k\left(X_t^2\right) = \phi^{|k|}\frac{\theta^2+8\theta+14}{\theta^2(\theta+3)^2}.$$

The kurtosis of the returns X_t is,

$$K_X = 6\frac{(\theta^2+8\theta+15)}{\theta^2+8\theta+16} > 3, \tag{4.9}$$

which indicates that the distribution is leptokurtic. Typically, kurtosis associated with returns reflects the time-varying nature of volatility, and from Figure 4.1 we can see that as θ increases, the kurtosis increases and stabilizes.

The structure of the model in (2.1) reveals that the ACF of $\{X_t\}$ is zero while the

ACF of $\{X_t^2\}$ is significant. The ACF of $\{X_t^2\}$ is obtained as,

$$\begin{aligned}\rho_{X_t^2}(k) &= Corr\left(X_t^2, X_{t-k}^2\right) \\ &= \phi^{|k|}\frac{\theta^2+8\theta+14}{5\theta^2+40\theta+74}.\end{aligned}$$

This is illustrated in Figure 4.2, and it shows that for various parameter values, the ACF is an exponentially decaying function of the lags. This behavior is indicative of the fact that past squared returns have a declining effect on the current squared return, which reflects the nature of persistence in volatility commonly seen in financial time series data.

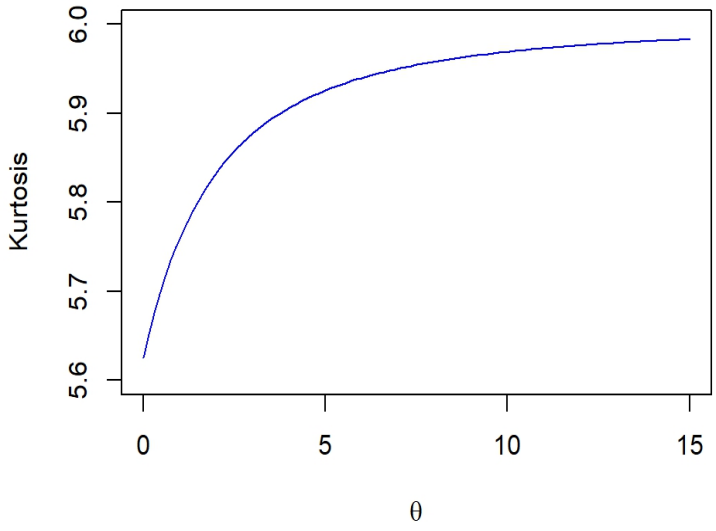

Figure 4.1: The plot of kurtosis of return X_t.

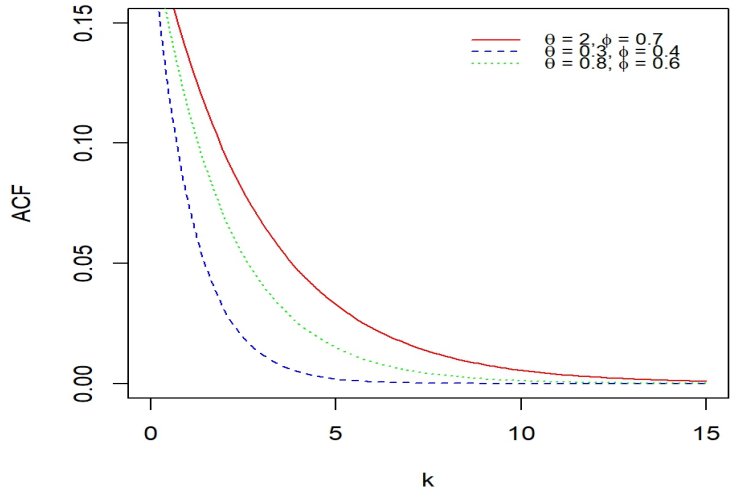

Figure 4.2: The ACF of squared returns for different combinations of the parameters.

In the next section, we will address the estimation of the unknown parameters of the i-Garima SV model.

4.4 Estimation of the parameters

The estimation of the parameters is carried out using the GMM technique as mentioned in Subsection 1.6.4.1. Let $(x_1, x_2, \ldots, x_n)$ are the observed return series of length n from i-Garima SV model given in (2.1) and let the moment function is $g(x_t, x_{t-1}, \mathbf{\Lambda})$, where $\mathbf{\Lambda} = (\phi, \theta)^T$ is the parameter vector to be estimated. The estimates are obtained by solving (2.15), and the moment function of this model is defined as,

$$g\left(x_t, x_{t-1}, \mathbf{\Lambda}\right) = \begin{pmatrix} x_t^2 - \frac{\theta+4}{\theta(\theta+3)} \\ x_t^2 x_{t-1}^2 - \frac{\phi(\theta^2+8\theta+14)+(\theta+4)^2}{\theta^2(\theta+3)^2} \end{pmatrix}.$$

Using (2.15), we solve the following equations numerically to obtain $\hat{\phi}$ and $\hat{\theta}$. That is,

$$\bar{x}_2 = \frac{\sum_{t=1}^{n} x_t^2}{n} = \frac{\theta + 4}{\theta(\theta + 3)},$$

and

$$\bar{x}_{22} = \frac{\sum_{t=2}^{n} x_t^2 x_{t-1}^2}{n-1} = \frac{\phi(\theta^2 + 8\theta + 14) + (\theta + 4)^2}{\theta^2(\theta + 3)^2},$$

yielding $\hat{\theta}$ and $\hat{\phi}$ as,

$$\begin{aligned} \hat{\theta} &= \frac{1 - 3\bar{x}_2 \pm \sqrt{9\bar{x}_2^2 + 10\bar{x}_2 + 1}}{2\bar{x}_2}, \\ \hat{\phi} &= \frac{\bar{x}_{22}\left(\hat{\theta}^2(\hat{\theta} + 3)^2\right) - (\hat{\theta} + 4)^2}{\hat{\theta}^2 + 8\hat{\theta} + 14}. \end{aligned} \tag{4.10}$$

4.4.1 Asymptotic properties of estimators

The asymptotic properties of the GMM estimators discussed in Subsection 1.6.4.1 and Theorem 2.3.1 also hold for the i-Garima SV model.

We have w_t is ergodic, stationary, and has finite moments; likewise, the sequence $\{X_t\}$ given in (2.1) also possesses these properties. Also, all moments of $\{X_t\}$ and $\{w_t\}$ are finite and $\frac{\partial g(x_t, x_{t-1}, \mathbf{\Lambda})}{\partial \mathbf{\Lambda}}$ exist and are continuous for all values of $\mathbf{\Lambda}$. Thus, our i-Garima SV model satisfies the regularity criterion specified in Subsection 1.6.4.1.

Next, we derive the elements of the proposed model's dispersion matrix to determine the estimators' asymptotic SE.

Let

$$\Gamma_{(k)} = \begin{pmatrix} \gamma_{11}^{(k)} & \gamma_{12}^{(k)} \\ \gamma_{21}^{(k)} & \gamma_{22}^{(k)} \end{pmatrix}, \quad k = 0, \pm 1, \pm 2, \ldots,$$

with $\Gamma_{(k)} = \Gamma_{(-k)}$, $k = 1, 2, \ldots$. Then the matrix S is obtained by $S = \Gamma_{(0)} + 2\sum_{k=1}^{\infty} \Gamma_{(k)}$.

For $k = 0$, we found the elements of $\Gamma_{(0)} = E(\omega_t \omega_t')$ as,

$$\gamma_{11}^{(0)} = \frac{5\theta^2 + 40\theta + 74}{\theta^2(\theta+3)^2},$$
$$\gamma_{12}^{(0)} = \gamma_{21}^{(0)} = \frac{A_1}{\theta^3(\theta+3)^2},$$
$$\gamma_{22}^{(0)} = \frac{216\phi^2(\theta+7)(\theta+3)^2 + 108\phi(1-\phi)(\theta+4)(\theta+6)(\theta+3) + A_2}{\theta^4(\theta+3)^3} - A_3^2,$$

where

$$A_1 = 296 + 234\theta + 60\theta^2 + 5\theta^3 + 280\phi + 23\theta\phi + 60\theta^2\phi + 5\theta^3\phi + 276\phi^2 + 252\theta\phi^2 + 72\theta^2\phi^2 + 6\theta^3\phi^2,$$
$$A_2 = 18(\theta+5)\left((1-\phi^2)(\theta^2+8\theta+14) + (\theta+4)^2(1-\phi)^2\right),$$
$$A_3 = \frac{\phi(\theta^2+8\theta+14) + (\theta+4)^2}{\theta^2(\theta+3)^2}.$$

For $k = 1, 2, \ldots,$ the elements of $\Gamma_{(k)}$ are,

$$\gamma_{11}^{(k)} = \phi^{|k|}\frac{\theta^2+8\theta+14}{\theta^2(\theta+3)^2},$$
$$\gamma_{12}^{(k)} = \phi^{k+2}a_3 + 2\phi^{k+1}a_2b_1 + \phi^k a_1 b_2 + a_2 b_1 \sum_{i=0}^{k-1}\phi^{i+1} + a_1 b_1^2 \sum_{i=0}^{k-1}\phi^i - \phi a_1 a_2 - a_1^2 b_1,$$
$$\gamma_{21}^{(k)} = \phi^{2k-1}a_3 + \phi^k a_2 b_1 \sum_{i=0}^{k-2}\phi^i + \phi^{k-1}a_2 b_1 \sum_{i=0}^{k-1}\phi^i + a_1 b_2 \phi^{2k-3} + a_1 b_1^2 \sum_{i=0}^{k-1}\phi^i \sum_{i=0}^{k-2}\phi^i - \phi a_1 a_2 - a_1^2 b_1,$$
$$\gamma_{22}^{(k)} = \phi^{2k+2}a_4 + a_3 b_1\left(3\phi^{2k+1} + \phi^{k+1} + 2\sum_{i=1}^{k-1}\phi^{i+k+1}\right) + \phi^{2k}(3a_2b_2 + a_1b_3) + \sum_{i=0}^{k-1}\phi^i \sum_{i=0}^{k-2}\phi^i(a_1 b_1^3 + \phi a_2 b_1^2) + a_2 b_1^2\left(\phi^k + 2\sum_{i=1}^{k-1}\phi^{i+k}\right) - \phi a_1 a_2 - a_1^2 b_1,$$

where

$$a_1 = \frac{\theta+4}{\theta(\theta+3)}, \quad a_2 = \frac{2(\theta+5)}{\theta^2(\theta+3)}, \quad a_3 = \frac{6(\theta+6)}{\theta^3(\theta+3)}, \quad b_1 = \frac{\theta+4}{\theta(\theta+3)}(1-\phi),$$
$$b_2 = \frac{(1-\phi^2)(\theta^2+8\theta+14) + (\theta+4)^2(1-\phi)^2}{\theta^2(\theta+3)^2}, \quad b_3 = E(\eta_t^3).$$

The matrix D is obtained using $D = E\left[\frac{\partial g(x_t,\mathbf{\Lambda})}{\partial \mathbf{\Lambda}}\right]$ and its corresponding elements are,

$$
\begin{aligned}
D_{11} &= \frac{\theta^2 + 8\theta + 12}{\theta^2(\theta+3)^2}, \\
D_{12} &= \frac{-96 - 88\theta - 24\theta^2 - 2\theta^3 - 84\phi - 80\theta\phi - 24\theta^2\phi - 2\theta^3\phi}{\theta^3(\theta+3)^3}, \\
D_{21} &= 0, \\
D_{22} &= -\frac{\theta^2 + 8\theta + 4}{\theta^2(\theta+3)^2}.
\end{aligned}
$$

The asymptotic dispersion matrix is $\frac{1}{N}(\Sigma)$, where $\Sigma = [DS^{-1}D']^{-1}$ and the diagonal elements of Σ are used to compute the asymptotic SE of the estimators. In the next section, we validate this through simulation analysis.

4.5 Simulation study

A simulation study is carried out with samples of sizes 100, 500, 2000, and 3000 to study the performance of the estimators. The algorithm for simulation analysis is as follows,

1. Generate samples of i-Garima Markov sequence using innovation random variable defined in (4.5).
2. Simulate sample of returns sequences X_t using this.
3. Solve the moment equations in (4.10) to obtain the estimates.
4. Repeat the process 1000 times for a fixed set of the parameter values.
5. Compute the mean estimates and their associated RMSE and SE.

Based on the simulated observations, the mean estimates and their corresponding RMSE and SE obtained are detailed in Table 4.1. It is evident from the table

that the bias, RMSE, and SE decrease as the sample size increases, indicating the accuracy and stability of the estimation method. This suggests that the estimators are more accurate with larger sample sizes, highlighting the robustness of the i-Garima SV model in practical applications.

Table 4.1: The estimates and the corresponding RMSE, and SE of the parameters for sample sizes 100, 500, 2000, and 3000.

	True Values		**Mean estimate values with RMSE and SE**					
Sample size(n)	θ	ϕ	$\hat{\theta}$	**RMSE**	**SE**	$\hat{\phi}$	**RMSE**	**SE**
100	0.2	0.30	0.2072	0.0427	0.0324	0.2968	0.0043	0.0039
	0.1	0.60	0.1048	0.0230	0.0193	0.5935	0.0085	0.0079
	0.5	0.35	0.5169	0.1096	0.0985	0.3465	0.0048	0.0041
	0.7	0.50	0.7332	0.1579	0.0992	0.4947	0.0072	0.0065
	0.8	0.45	0.8439	0.1789	0.1020	0.4455	0.0060	0.0058
500	0.2	0.30	0.2010	0.0183	0.0165	0.2994	0.0007	0.0005
	0.1	0.60	0.1006	0.0098	0.0087	0.5987	0.0016	0.0012
	0.5	0.35	0.5071	0.0499	0.0358	0.3492	0.0009	0.0007
	0.7	0.50	0.7065	0.0678	0.0572	0.4990	0.0013	0.0011
	0.8	0.45	0.8076	0.0751	0.0673	0.4490	0.0012	0.0009
2000	0.2	0.30	0.2002	0.0097	0.0084	0.2998	0.0010	0.0008
	0.1	0.60	0.0999	0.0048	0.0035	0.5996	0.0009	0.0007
	0.5	0.35	0.5010	0.0246	0.0104	0.3498	0.0008	0.0005
	0.7	0.50	0.6999	0.0323	0.0271	0.4997	0.0005	0.0004
	0.8	0.45	0.8030	0.0378	0.0241	0.4497	0.0006	0.0003
3000	0.2	0.30	0.1998	0.0078	0.0063	0.2999	0.0002	0.0002
	0.1	0.60	0.1003	0.0039	0.0027	0.5997	0.0002	0.0002
	0.5	0.35	0.5002	0.0183	0.0094	0.3498	0.0001	0.0001
	0.7	0.50	0.6996	0.0266	0.0141	0.4998	0.0002	0.0001
	0.8	0.45	0.8011	0.0298	0.0127	0.4498	0.0002	0.0002

4.6 Data analysis

The application of the i-Garima SV model is demonstrated using two real data sets and is discussed in the following subsections.

4.6.1 Dataset 1

We consider the daily exchange rate returns of Euro to US Dollar (EURUSD) for the period starting from January 1, 2010, to March 29, 2024, using data taken from https://www.marketwatch.com. The daily exchange rate is denoted by P_t and the returns are computed using (3.2). The time series plots of both the original series and returns are shown in Figure 4.3, and the summary statistics of the returns are presented in Table 4.2.

Table 4.2: Summary statistics of the return series.

Statistics	**EURUSD**	**DXY**
Sample size	3715	2391
Std. Dev	0.5432	0.4373
Minimum	-2.8415	-2.1693
Maximum	3.0048	2.5807
Kurtosis	5.0559	5.2116
Ljung-Box p-value for returns.	0.6875	0.9895
Ljung-Box p-value for squared returns.	2.2×10^{-16}	2.2×10^{-16}

The ACF plot of returns (Figure 4.4) exhibits no autocorrelation, while the ACF plot of squared returns shows significant autocorrelation and decays gradually. Using the Ljung-Box portmanteau test, we confirm this, that is, there is no significant serial correlation in the returns, with a p-value of 0.6875. Whereas, for the squared returns, the test shows the presence of autocorrelation, with a p-value less than 0.05. This highlights the time-varying nature of volatility in the return series, thereby supporting the effectiveness of the i-Garima SV model in capturing this behavior. Furthermore, the kurtosis value is greater than 3, indicating that

the returns follow a leptokurtic distribution.

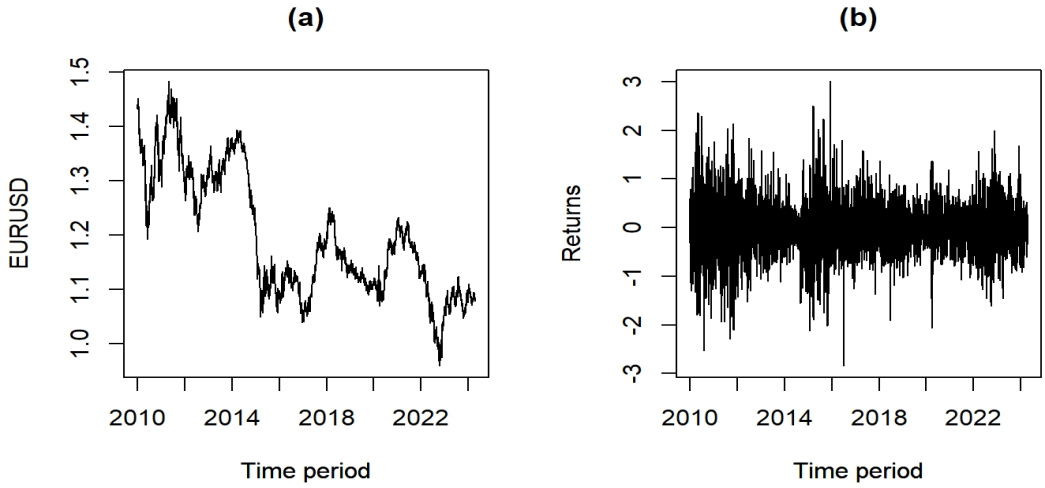

Figure 4.3: (a). EURUSD time series data. (b). Return series of the EURUSD data.

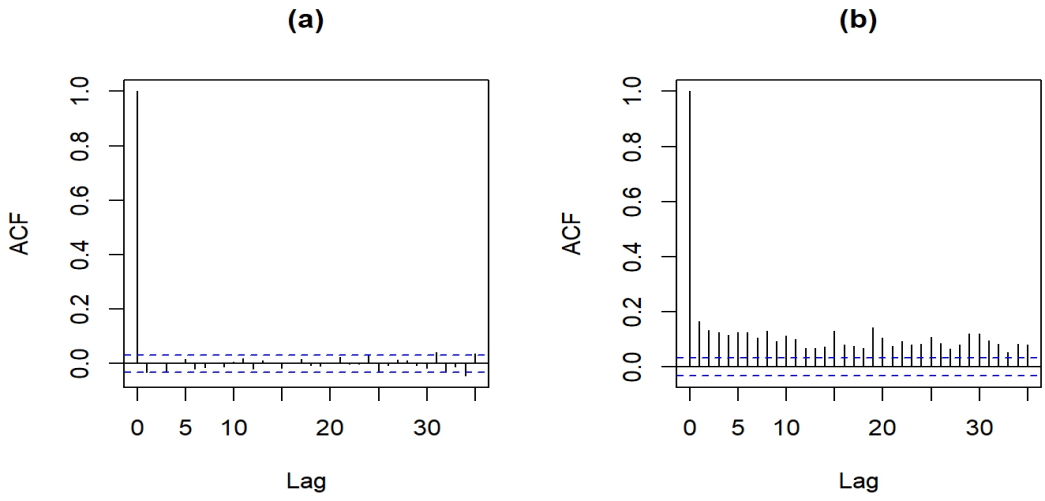

Figure 4.4: (a). ACF of EURUSD returns data. (b). ACF of EURUSD squared returns data.

The model parameters are next estimated using the GMM technique as mentioned in Section 2.3, and the estimates obtained are given in Table 4.3. We also

compare the performance of the i-Garima SV model with the Lindley SV model (Sri Ranganath (2018)) using the above data set. For that, the parameter estimates of the Lindley SV model are also provided in Table 4.3. The estimated values of $\hat{\phi}$ in Table 4.3 suggest significant volatility persistence in return series.

Table 4.3: Estimates of the model parameters and their corresponding SE for both the data sets.

Data Set	**Model**	$\hat{\theta}$	**SE**	$\hat{\phi}$	**SE**
EURUSD	i-Garima SV Model	3.8851	0.0172	0.6796	0.0068
	Lindley SV Model	4.0589	0.0185	0.6956	0.0072
DXY	i-Garima SV Model	4.7181	0.0098	0.4023	0.0043
	Lindley SV Model	4.8865	0.0094	0.4090	0.0045

After estimating the parameters, the next step is model diagnostic checking to ensure that the model's assumptions in (2.1) are consistent with our analyzed data. Since our model in (2.1) is expressed in terms of unobservable volatilities w_t, the model diagnostics become quite challenging. We use the Kalman filtering discussed in Chapter 1, which allows us to rewrite the model (2.1) in state-space form. We estimate the unobservable volatilities w_t by approximating the distribution of η_t given in (4.2) by a normal distribution. Once the volatilities are estimated, the residuals are computed using them.

The state space representation of the i-Garima SV model is given by (3.3). We have $w_t = \phi w_{t-1} + \eta_t$, where η_t is assumed to follow a normal distribution with mean given in (4.6) and variance as in (4.7). By presuming normal distribution to approximate τ_t, (3.3) transforms into a standard dynamic linear model. Let $\bar{w}_{t|t-1}$, $\Lambda_{t|t-1}$, $\bar{w}_{t|t}$, $\Lambda_{t|t}$ denote the predicted value of w_t and its variance at time $t-1$ and t respectively. These are computed and updated iteratively using the following equations,

Prediction:

$$\bar{w}_{t|t-1} = \phi \bar{w}_{t-1|t-1} + \frac{(\theta+4)(1-\phi)}{\theta(\theta+3)},$$
$$\Lambda_{t|t-1} = \phi^2 \Lambda_{t-1|t-1} + \frac{(1-\phi^2)\,(\theta^2+8\theta+14)}{(\theta^2(\theta+3)^2)},$$

Updating:

$$\bar{w}_{t|t} = \bar{w}_{t|t-1} + \frac{\Lambda_{t|t-1}}{g_t}\left[\log X_t^2 + 1.27 - \log \bar{w}_{t|t-1}\right],$$
$$\Lambda_{t|t} = \Lambda_{t|t-1}\left(1 - \frac{\Lambda_{t|t-1}}{g_t}\right),$$

where $g_t = \Lambda_{t|t-1} + \frac{\pi^2}{2}$. The initial values for the system are chosen as $\Lambda_0 = \frac{\theta^2+8\theta+14}{\theta^2(\theta+3)^2}$ and $w_0 = \frac{\theta+4}{\theta(\theta+3)}$ and the parameters θ and ϕ in the above system are updated by their respective estimates $\hat{\theta}$ and $\hat{\phi}$. The residuals are then obtained using $\hat{Y}_t = \frac{X_t}{\sqrt{\bar{w}_t}}$ and further residual analysis is done using this sequence. Figure 4.5 depicts the plots of ACF of the residuals and squared residuals showing the absence of significant serial correlations. This is validated using the Ljung-Box test, that is, for residuals, the p-value obtained is 0.9064, and for squared residuals, the p-value is 0.3461, suggesting no significant serial correlations in them.

Finally, we check whether the residual series follows standard normal distribution by superimposing the histogram of residuals by the density of standard normal variate. From Figure 4.5, it is found that normal distribution is a good fit for residuals. This is further confirmed using the Jarque-Bera test yielding a p-value of 0.5623. Thus, we have analyzed the model's adequacy and observed that it performs satisfactorily.

Now, for comparison of the Lindley SV model and the i-Garima SV model, the Kolmogorov-Smirnov (K-S) statistic values are computed for the above data set. The results show that the i-Garima SV model yields slightly higher p-values for the K-S test compared to the Lindley SV model (See Table 4.4). This indicates that the i-Garima SV model is not only competitive but may also serve as a better

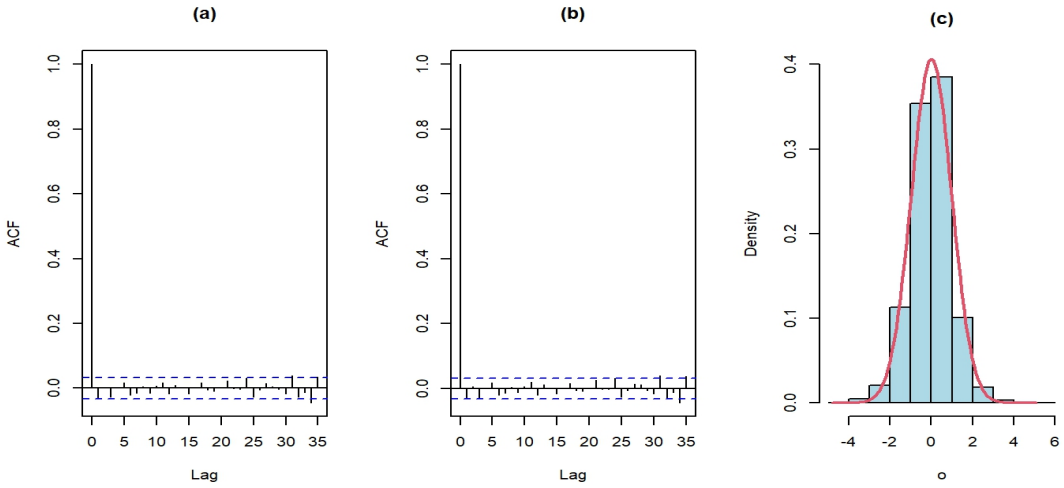

Figure 4.5: For EURUSD data, (a). ACF of residuals. (b). ACF of squared residuals. (c). Histogram of residuals.

alternative to the Lindley SV model in capturing the volatility dynamics in financial time series. Also, we compute an out-of-sample analysis using the squared returns for both models. The parameters were estimated for the period from January 1, 2010, to March 29, 2024, and out-of-sample analysis was carried out for the period from April 1, 2024, to October 31, 2024, covering 155 trading days. The one-step-ahead prediction of w_{t+j} given $X_{t+j-1}, X_{t+j-2}, \ldots$, is determined by $\hat{w_{t+j}} = E\left(w_{t+j} \mid X_{t+j-1}, X_{t+j-2} \ldots\right)$ and the predictions for $j = 1, 2, \ldots, 155$, are computed by estimating the model parameters at each point in the post-sample period.

For the Lindley SV model and i-Garima SV model the one-step-ahead predictions are calculated as follows,

➤ Lindley SV model,

$$E\left(w_{t+1} \mid X_t, X_{t-1} \ldots\right) = \phi w_t + \frac{\theta + 2}{\theta(\theta + 1)}(1 - \phi).$$

➤ i-Garima SV model,

$$E\left(w_{t+1} \mid X_t, X_{t-1} \ldots\right) = \phi w_t + \frac{\theta + 4}{\theta(\theta + 3)}(1 - \phi).$$

Based on these prediction values, the MAE and RMSE values are computed, and Table 4.4 demonstrates that the i-Garima SV model achieves lower MAE and RMSE values compared to the Lindley SV model, indicating its superior performance.

Table 4.4: The K-S statistic, corresponding p-value, MAE, and RMSE for both data sets.

Data Set	Model	K-S	p-value	MAE	RMSE
EURUSD	i-Garima SV Model	0.0390	0.2055	0.5672	0.6148
	Lindley SV Model	0.0436	0.1011	0.5885	0.6871
DXY	i-Garima SV Model	0.0237	0.3245	0.5217	0.4639
	Lindley SV Model	0.0291	0.2608	0.5611	0.5136

4.6.2 Dataset-2

We analyze the opening index data of the US Dollar Index future (DXY) for the period from January 2, 2015, to March 29, 2024 (https://www.marketwatch.com). Following the same methodology presented in Subsection 4.6.1, we perform a comprehensive data analysis for this dataset. The time series plots of the original series and returns are shown in Figure 4.6, and the summary statistics are presented in Table 4.2. The ACF plots of returns and squared returns depicted in Figure 4.7 indicate that the returns show no autocorrelation while the squared returns exhibit significant autocorrelation. This is confirmed using the Ljung-Box test, and the p-values for both returns and squared returns are given in Table 4.2.

Moreover, the kurtosis value suggests that the returns are leptokurtic.

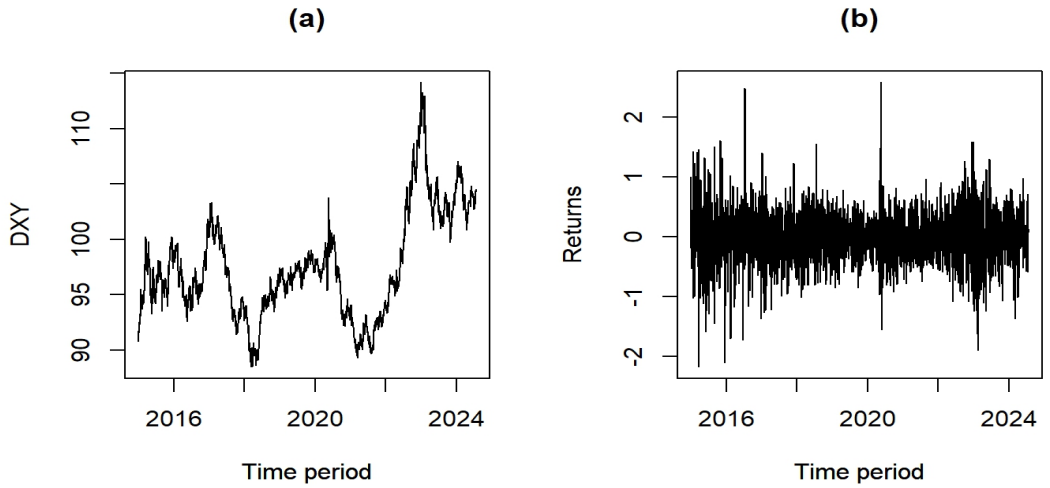

Figure 4.6: (a). DXY time series data. (b). Return series of the DXY data.

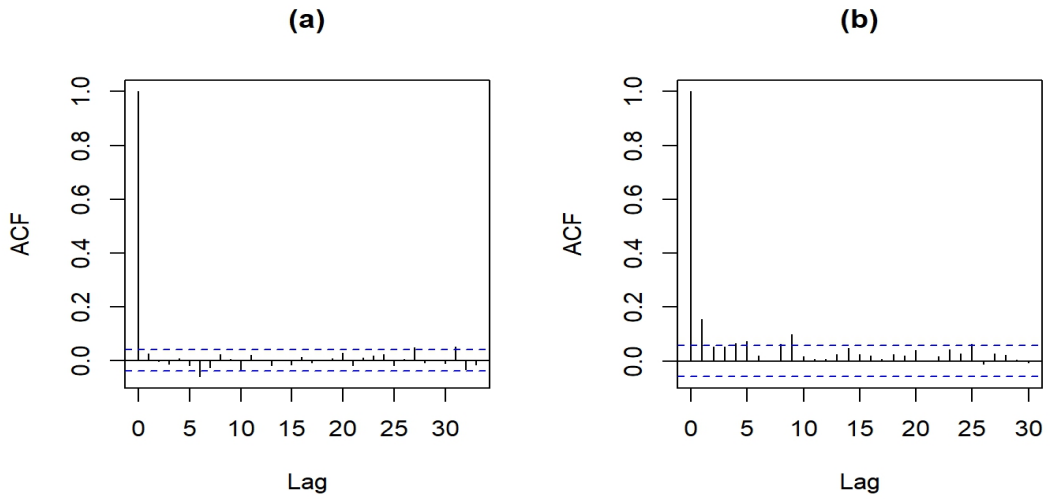

Figure 4.7: (a). ACF of DXY returns data. (b). ACF of DXY squared returns data.

The estimated parameters for both the i-Garima and Lindley SV models are presented in Table 4.3. The model diagnostics are also carried out as described

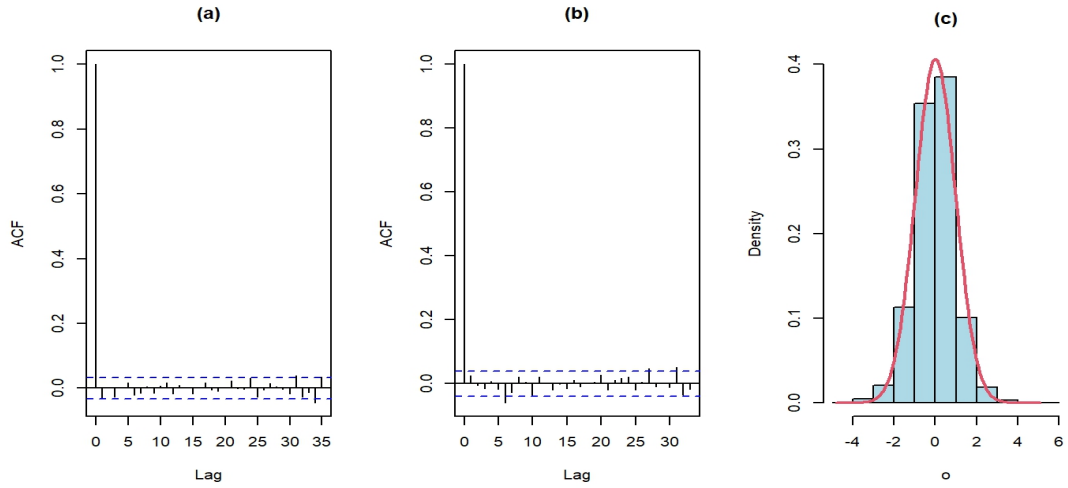

Figure 4.8: For DXY data, (a). ACF of residuals. (b). ACF of squared residuals. (c). Histogram of residuals.

in Subsection 4.6.1 and the residuals are computed. The histogram, ACF of residuals, and squared residuals are shown in Figure 4.8. This clearly shows that both residuals and squared residuals have insignificant autocorrelation. The Ljung-Box test further supports this, with a p-value of 0.8182 for the residuals and 0.4217 for the squared residuals, indicating no significant serial correlation. The normality of residuals is confirmed using the Jarque-Bera test with a p-value of 0.4563. Thus, confirming the adequacy of the proposed model.

The out-of-sample analysis is then carried out as described in the previous Subsection. It is carried out for a period starting from April 1, 2024, to October 31, 2024 (155 trading days). The MAE and RMSE values are then computed and are presented in Table 4.4, alongside the K-S statistic values. The results show that the i-Garima SV model has the lowest MAE and RMSE values, indicating its better forecasting performance compared to the Lindley SV model.

4.7 Summary

In this chapter, a stationary sequence of i-Garima random variables is introduced to model SV with Laplace-mixture distributed returns. Parameter estimation is achieved effectively through the GMM, while an approximate Kalman filtering technique is employed for model diagnostics. Simulation and data analysis demonstrate that the developed model successfully captures key characteristics of financial time series. A comparison with the existing Lindley SV model is also carried out, and our model acts as a potential alternative to the Lindley SV model.

CHAPTER 5

Application of Stochastic Volatility Models in Speech Enhancement

5.1 Introduction

SV models are, in general, most widely employed in financial econometrics for modeling time-varying volatility in asset returns. In the preceding chapters, we have explored their application in a financial setup. However, despite this widespread application of SV models in the context of financial time series, their potential in other domains remains largely unexplored. Hence, in this chapter, we aim to extend the application of SV models beyond financial data and explore their effectiveness in signal processing, especially in speech enhancement.

Speech enhancement aims to improve the clarity and intelligibility of speech signals that have been degraded by noise, with applications spanning telecommunications, hearing aids, and automatic speech recognition. In the past few decades, substantial research has been focused on tackling challenges in speech enhancement. One of the basic challenges has been that of how to model the speech signals properly in the Short-time Fourier transform (STFT) domain. A robust speech enhancement system involves two significant components: estimating the

noise power spectrum and estimating the speech signal itself. Traditional methods for speech enhancement rely on spectral domain estimators such as the MMSE of short-time spectrum amplitude (Ephraim & Malah (1984)), MMSE of log-spectral amplitude (Ephraim & Malah (1985)), Optimal modified log-spectral amplitude (OMLSA) (Cohen & Berdugo (2001)), etc. For noise power estimate, methods such as Improved minima controlled recursive averaging (IMCRA) (Cohen (2003)), minimal statistics-based estimation (Martin (2001)), etc., are frequently used. Nielsen et al. (2023) recently used the Gaussian SV model for noise estimation. These spectral-domain estimators rely on a priori estimation of the signal-to-noise ratio (SNR), commonly achieved using the decision-directed method (Ephraim & Malah (1985)).

Since the STFT expansion coefficients of speech signals display characteristics like heavy tails and volatility clustering where large magnitudes tend to follow large magnitudes, and small magnitudes follow small ones, while the phase remains uncorrelated, Cohen (2006, 2004); Atkins & Cohen (2016) suggested employing the ARCH and GARCH models for statistically modeling these speech signals in the time-frequency domain. Although these models have been widely employed, they come with certain limitations, and one of the most flexible and effective alternatives is the SV model. As we have already discussed, SV models treat variance as an unobserved, time-varying stochastic process and hence it offers greater adaptability in capturing the complex and dynamic volatility patterns of speech signals, particularly in noisy environments. This makes SV models a more robust and reliable choice for speech signal modeling.

Utilizing the SV models for speech signals greatly enhances their adaptability to the natural fluctuations within speech. This can make SV models ideally suited to applications such as speech enhancement and speaker recognition. The SV models can improve speech recognition systems' robustness and accuracy by cap-

turing speaker-specific variations in speech characteristics such as formants and pitch. This is especially useful in noisy environments or with speakers with variable speech patterns. Therefore, in this chapter, we apply SV models to statistically model speech signals in the time-frequency domain with the aim to capture these distinctive characteristics and improve the accuracy of speech processing.

Tran et al. (2010) developed a speech enhancement approach combining an IMCRA noise power spectrum estimator with an OMLSA speech power spectrum estimator. Building on this foundation, we propose a method that integrates SV models with OMLSA and IMCRA techniques. The performance of the suggested SV-based model compared to GARCH-based methods is also evaluated in this chapter, using metrics like log-spectral distortion (LSD), perceptual evaluation of speech quality (PESQ) (as per ITU-T P.862), short-time objective intelligibility (STOI) (Taal et al. (2010)), and entropy.

The chapter is organized as follows. Section 5.2 gives an overview of the performance metrics used in this chapter, and Section 5.3 outlines the problem formulation and objectives. Section 5.4 introduces the SV model in the STFT domain and its estimation approach. Section 5.5 gives a summary of the IMCRA noise estimation technique, including an appropriate speech presence probability function to control noise spectrum adaptation. Section 5.6 describes the OMLSA method for speech enhancement. Finally, Section 5.7 provides an analysis of the proposed method and experimental results validating its effectiveness, and Section 5.8 summarises the study.

5.2 Speech quality and intelligibility metrics

This section provides a summary of the main objective metrics used to assess the quality and intelligibility of speech signals in this chapter.

➤ **Log-spectral distortion:**

The LSD in dB is defined by,

$$\text{LSD} = \left[\frac{1}{||\mathcal{H}_1||} \sum_{tk \in \mathcal{H}_1} \left(20 \log_{10} |X_{t,k}| - 20 \log_{10} \left| \hat{X}_{t,k} \right| \right)^2 \right]^{\frac{1}{2}},$$

where $\mathcal{H}_1 = \{(t,k) : 20 \log_{10} |X_{t,k}| > \nu\}$ denotes the set of time-frequency bins that contain the speech signal, $||\mathcal{H}_1||$ is its cardinality, and we have $\nu = \max_{tk} \{20 \log_{10} |X_{t,k}|\} - 50$ limits the dynamic range of the log-spectrum to 50 dB.

➤ **Perceptual evaluation of speech quality:**

The PESQ (Rix et al. (2001)) was recently standardized by the International Telecommunications Union as Recommendation P.862. It is an objective measure based on the comparison of the speech signal's perceptual quality before and after degradation and involves several steps, including signal preprocessing, psychoacoustic modeling, and a comparison of the signals in a perceptually relevant domain.

➤ **Short-time objective intelligibility:**

STOI is an objective metric that is used to predict speech signal intelligibility, especially in reverberant and noisy environments. An intelligibility score can be calculated by computing the correlation between the short-time temporal envelopes of the degraded and clean speech signals over overlapping time frames. A higher STOI score indicates better speech intelligibility, and the scores range from 0 to 1.

➤ **Entropy:**

Entropy (Shannon (1948)) measures the uncertainty or randomness observed

in a signal. In the context of signal processing, differential entropy (Nath (1968)) is used to quantify the variability or spread of a continuous signal. For the continuous valued signals, the differential entropy is generally defined as,

$$H\left(X_{t,k}\right) = \frac{1}{2}\int f(x)\log f(x)dx,$$

where $f(x)$ is the pdf of continuous random variable $X_{t,k}$. If the signals are modeled using a Gaussian distribution, that is $X_{t,k} \sim N\left(0, \sigma^2\right)$, then the differential entropy is given by,

$$H\left(X_{t,k}\right) = \frac{1}{2}\log\left(2\pi e\sigma^2\right).$$

where e is the base of the natural logarithm. A higher entropy value shows a greater degree of randomness or noise in the signal, while a lower value indicates more structure and less uncertainty.

In the following section, we define the problem that forms the basis of this chapter and outline the key objectives.

5.3 Problem formulation

Let the speech signal be denoted by $x(n)$ and uncorrelated additive noise signals by $d(n)$, where n is the discrete time index. The observed noisy speech signal is given by $y(n) = x(n) + d(n)$, which is divided into overlapping frames by using a window function. These signals are then analyzed using the STFT, having the representation,

$$Y_{t,k} = \sum_{n=0}^{N-1} y(n + tM)h(n)\mathrm{e}^{-\mathrm{j}(2\pi/N)nk},$$

where k is the frequency bin index, t is the time frame index, h is an analysis window of size N (Hanning window), and M is the framing step. The STFT of noisy speech signal is written as, $Y_{t,k} = X_{t,k} + D_{t,k}$ where $X_{t,k}$ and $D_{t,k}$ denote the STFT of the clean speech and noise signal, respectively. Let $H_0^{t,k}$ and $H_1^{t,k}$ denote respectively, the hypotheses for speech absence and presence in the noisy spectral coefficient $Y_{t,k}$, and $p_{t,k}$ be the speech presence probability. The hypotheses are given as,

$$\begin{aligned} H_0^{t,k} &: Y_{t,k} = D_{t,k}, \\ H_1^{t,k} &: Y_{t,k} = X_{t,k} + D_{t,k}. \end{aligned} \tag{5.1}$$

The STFT coefficients of speech and noise signals are assumed to follow a complex Gaussian distribution (Ephraim & Malah (1984)). Therefore, the conditional pdf of the observed noisy speech signal $Y_{t,k}$ under both hypotheses are,

$$\begin{aligned} p\left(Y_{t,k} \mid H_0^{t,k}\right) &= \frac{1}{\pi w_{t,k}^d} \exp\left\{-\frac{|Y_{t,k}|^2}{w_{t,k}^d}\right\}, \\ p\left(Y_{t,k} \mid H_1^{t,k}\right) &= \frac{1}{\pi\left(w_{t,k}^d + w_{t,k}^x\right)} \exp\left\{-\frac{|Y_{t,k}|^2}{w_{t,k}^d + w_{t,k}^x}\right\}, \end{aligned}$$

where $w_{t,k}^x = E\left[X_{t,k}^2 \mid H_1^{t,k}\right]$ represent the variance of speech and $w_{t,k}^d = E\left[D_{t,k}^2\right]$ represent the variance of noise. Applying Bayes' rule to the conditional speech presence probability, we get,

$$p\left(H_1^{t,k} \mid Y_{t,k}\right) = \frac{p\left(Y_{t,k} \mid H_1^{t,k}\right) p\left(H_1^{t,k}\right)}{p\left(Y_{t,k} \mid H_1^{t,k}\right) p\left(H_1^{t,k}\right) + p\left(Y_{t,k} \mid H_0^{t,k}\right) p\left(H_0^{t,k}\right)}. \tag{5.2}$$

We denote $q_{t,k} = p\left(H_0^{t,k}\right)$ as the a priori probability for speech absence, and the generalized likelihood ratio is expressed by,

$$\mathcal{L}_{t,k} = \frac{(1-q_{t,k})p\left(Y_{t,k} \mid H_1^{t,k}\right)}{q_{t,k}p\left(Y_{t,k} \mid H_0^{t,k}\right)},$$

and speech presence probability,

$$\begin{aligned} p_{t,k} &= p\left(H_1^{t,k} \mid Y_{t,k}\right), \\ &= \left\{1 + \frac{q_{t,k}}{1-q_{t,k}}(1+\xi_{t,k})\exp(-v_{t,k})\right\}^{-1}, \end{aligned} \tag{5.3}$$

where

$$\xi_{t,k} = \frac{w_{t,k}^x}{w_{t,k}^d}, \tag{5.4}$$

$$\gamma_{t,k} = \frac{|Y_{t,k}|^2}{w_{t,k}^d}, \tag{5.5}$$

$$v_{t,k} = \frac{\xi_{t,k}\gamma_{t,k}}{1+\xi_{t,k}}. \tag{5.6}$$

$\xi_{t,k}$ and $\gamma_{t,k}$ denote a priori and a posteriori SNRs.

The primary objectives of this chapter are,

1. To derive an appropriate gain function for estimating the clean speech signal $\hat{X}_{t,k}$.

2. To obtain estimates for the speech spectral variance $\hat{w}_{t,k}^x$, and noise spectral variance $\hat{w}_{t,k}^d$.

3. To obtain estimates for a priori speech absence probability $\hat{q}_{t,k}$ and a priori SNR $\hat{\xi}_{t,k}$ under speech presence probability.

4. To develop a speech enhancement algorithm based on all of these.

The next sections outline the development of these estimators and the speech enhancement technique using the SV model.

5.4 Speech variance estimation

5.4.1 Gaussian stochastic volatility model

Volatility clustering is a key characteristic of speech signals within the STFT domain. When examining a time series of successive expansion coefficients in a specific frequency bin, although successive phrases are nearly uncorrelated, the magnitudes of these coefficients exhibit significant correlation. In this context, large magnitudes are likely to follow large magnitudes, and small magnitudes tend to follow small ones, even though the phase remains unpredictable. This clustering indicates that variations in the speech spectral coefficients are not directly observable, even in ideal conditions without noise (i.e., $D_{t,k} = 0$ for all t and k). In view of this hidden nature, we treat the speech spectral variance, $w^x_{t,k}$, as random variables. That is, here we utilize an SV model to characterize the speech spectral coefficients $X_{t,k}$ as well as their conditional variances.

We assume that the spectral speech coefficients $X_{t,k}$ are generated as follows,

$$\begin{aligned} X_{t,k} =& \sqrt{w^x_{t,k}}\epsilon_{t,k}, \\ =& \exp\left\{\Gamma^x_{t,k}/2\right\}\epsilon_{t,k}, \end{aligned}$$

where $\Gamma^x_{t,k} = \ln\left(w^x_{t,k}\right)$, $\left\{\epsilon_{t,k} \mid \mathrm{H}_0^{t,k}\right\}$ are identically zero, and $\left\{\epsilon_{t,k} \mid \mathrm{H}_1^{t,k}\right\}$ are statistically independent complex Gaussian random variables with zero mean, unit variance, and have iid real and imaginary parts. Under hypothesis $\mathrm{H}_1^{t,k}$, the expansion coefficients $\left\{X_{t,k} \mid \mathrm{H}_1^{t,k}\right\}$ are conditionally zero-mean, statistically independent Gaussian random variables given their variances $w^x_{t,k}$. Additionally, the

real and imaginary components of $\left\{X_{t,k} \mid \mathrm{H}_1^{t,k}\right\}$ are also conditionally iid given $w_{t,k}^x$. The volatility sequences in the SV model described above are assumed to follow a first-order Gaussian AR process on the log-variance, defined by,

$$\Gamma_{t,k}^x = \alpha + \phi(\Gamma_{t-1,k}^x - \alpha) + \eta_{t,k}, \tag{5.7}$$

where $\eta_{t,k}$ follows $N\left(0, \sigma_\eta^2\right)$. The SV model is then defined as,

$$\begin{aligned} X_{t,k} \mid \Gamma_{t,k}^x &\sim N\left(0, \exp^{\Gamma_{t,k}^x}\right), \\ \Gamma_{t,k}^x \mid \Gamma_{t-1,k}^x, \alpha, \phi, \sigma_\eta &\sim N\left(\alpha + \phi\left(\Gamma_{t-1,k}^x - \alpha\right), \sigma_\eta^2\right), \\ \Gamma_{0,k}^x \mid \alpha, \phi, \sigma_\eta &\sim N\left(\alpha, \sigma_\eta^2 / \left(1 - \phi^2\right)\right), \end{aligned}$$

where $N\left(\alpha, \sigma_\eta^2\right)$ denotes the normal distribution with mean α and variance σ_η^2 and, $\mathbf{\Lambda} = (\alpha, \phi, \sigma_\eta^2)^T$ is the vector of parameters associated with it. Here α indicates the level of log-variance, ϕ $(0 < \phi < 1)$ reflects the persistence of log-variance. The estimation of the model parameters $\mathbf{\Lambda}$ is our next focus.

5.4.2 Estimation of model parameters

We use a Bayesian method via the MCMC algorithm for estimation. In the context of SV, the R package *stochvol* (Kastner (2016)) provides a fully Bayesian implementation of heteroskedasticity modeling. With the use of MCMC samplers, it does inference by drawing the posterior distribution of parameters and latent variables, which can subsequently be used to predict future volatilities. We calculate the latent volatilities and the SV model's parameters using this package. To execute this, the prior distribution for the parameter vector $\mathbf{\Lambda}$ needs to be specified, and the relevant values are then passed as inputs to the main sampling function *svsample*. The output of the function *svsample* yields the parameters

$\mathbf{\Lambda}$ as well as the latent log-volatilities, which correspond to the variances of the speech spectral coefficients. After estimating $w^x_{t,k}$, the next goal is to estimate the a priori SNR $\xi_{t,k}$ using (5.4).

In the next section, a detailed overview of the estimation of the noise power spectrum is presented.

5.5 Noise spectrum estimation.

5.5.1 Improved minima controlled recursive averaging

The IMCRA (Cohen (2003)) approach for spectral noise power estimate is summarized in this section, for a better understanding of the theory behind it. In this case, the noise estimate is determined by averaging the spectral power values of previous noisy speech. For recursive averaging, a time-varying frequency-dependent smoothing parameter that is modified by the speech presence probability is utilized. The output is then multiplied by a constant to adjust for bias after recursive averaging.

In the IMCRA technique, the noisy power spectrum is smoothed both in the frequency and time domains. This indicates that there is a significant correlation between the speech presence in adjacent frequency bins of succeeding frames. Two iterations of smoothing and minimal tracking constitute this technique. The first iteration provides the identification of rough speech activity in each frequency band and is given by,

$$\begin{aligned} S^f_{t,k} &= \sum_{i=-\mathrm{w}}^{w} b(i)|Y_{t,(k-i)}|^2, \\ S_{t,k} &= \alpha_s S_{(t-1),k} + (1-\alpha_s)\, S^f_{t,k}, \\ S^{\min}_{t,k} &= \min\left(S_{t',k} \mid t-D+1 \le t' \le t\right), \end{aligned}$$

where $S^f_{t,k}$ denote the noisy power spectrum in frequency domain and $S_{t,k}$ is the noisy power spectrum in time domain. Define,

$$I_{t,k} = \begin{cases} 1, & \text{if } \gamma^{\min}_{t,k} < \gamma_0 \text{ and } \zeta_{t,k} < \zeta_0 \text{ (speech is absent)}, \\ 0, & \text{otherwise (speech is present)}, \end{cases}$$

where α_s is the smoothing parameter ($0 < \alpha_s < 1$), $\gamma^{\min}_{t,k}$, γ_0, $\varsigma_{t,k}$, and ς_0 are derived as in Cohen (2003), $b(i)$ denote Hanning window function of length $2w + 1$ with $w = 1$ and D is search windows. The D sample windows are partitioned into U subwindows of V samples in such a way that $UV = D$. In the second iteration, smoothing omits relatively strong speech elements,

$$\tilde{S}_{t,k} = \begin{cases} \frac{\sum_{i=-w}^{w} b(i) I_{t,(k-i)} |Y_{t,(k-i)}|^2}{\sum_{i=-w}^{w} b(i) I_{t,(k-i)}}, & \text{if} \quad \sum_{i=-w}^{w} I_{t,(k-i)} \neq 0, \\ \tilde{S}_{(t-1),k}, & \text{otherwise .} \end{cases}$$

The spectral power of noisy speech in the time domain $\tilde{S}_{t,k}$ is smooth even after the elimination of strong speech components, and $\tilde{S}^{min}_{t,k}$ is estimated using the "minimum tracking" procedure.

$$\begin{aligned} \tilde{S}_{t,k} &= \alpha_s \tilde{S}_{t-1,k} + (1 - \alpha_s)\, \tilde{S}^f_{t,k}, \\ \tilde{S}^{min}_{t,k} &= \min\left(\tilde{S}_{t',k} \mid t - D + 1 \leq t' \leq t\right). \end{aligned}$$

The a priori speech absence probability $\hat{q}_{t,k}$ is computed using,

$$\hat{q}_{t,k} = \begin{cases} 1, & \text{if } \tilde{\gamma}^{\min}_{t,k} \leq 1 \text{ and } \tilde{\zeta}_{t,k} < \zeta_0, \\ \frac{(\gamma_1 - \tilde{\gamma}^{\min}_{t,k})}{(\gamma_1 - 1)}, & \text{if } 1 < \tilde{\gamma}^{\min}_{t,k} < \gamma_1 \text{ and } \tilde{\zeta}_{t,k} < \zeta_0, \\ 0, & \text{otherwise,} \end{cases}$$

where $\tilde{\gamma}_{t,k}^{\min}$, γ_1 and $\tilde{\zeta}_{t,k}$, ς_0 are calculated as in Cohen (2003). The posteriori speech presence probability $\hat{p}_{t,k}$ is then determined using these values and the Bayesian formula provided in (5.3).

In this approach, noise estimation is achieved by recursively averaging past spectral power values of the noisy speech during periods when speech is absent. We define the following condition,

$$H_0^{t,k} : \bar{w}_{t+1,k}^d = \alpha_d \bar{w}_{t,k}^d + (1-\alpha_d)\,|Y_{t,k}|^2,$$
$$H_1^{t,k} : \bar{w}_{t+1,k}^d = \bar{w}_{t,k}^d,$$

where $0 < \alpha_d < 1$ is the smoothing parameter. Under conditions of speech presence uncertainty, the recursive averaging is performed using the conditional speech presence probability as follows,

$$\begin{aligned}\bar{w}_{t+1,k}^d &= \bar{w}_{t,k}^d p_{t,k} + [\alpha_d \bar{w}_{t,k}^d + (1-\alpha_d)|Y_{t,k}|^2](1-p_{t,k}),\\ \bar{w}_{t+1,k}^d &= \tilde{\alpha}_d \bar{w}_{t,k}^d + (1-\tilde{\alpha}_d)|Y_{t,k}|^2,\end{aligned}$$

where $\tilde{\alpha}_d = \alpha_d + (1-\alpha_d)p_{t,k}$ is a time-varying frequency-dependent smoothing parameter. When speech is present, the noise spectral estimate is close to the previous noise spectral estimate, making $\tilde{\alpha}_d$ close to 1. Conversely, in the absence of speech, $\tilde{\alpha}_d$ is close to α_d, ensuring the noise spectral estimate remains close to the recursively averaged past spectral power values of the noisy speech. However, the speech presence probability also influences the clean speech spectral estimate, leading to a bias toward higher values to avoid speech distortion (Cohen (2003)), and we have,

$$\hat{w}_{t+1,k}^d = \beta \bar{w}_{t+1,k}^d,$$

where $\hat{w}_{t+1,k}^d$ represents the estimated noise spectral power, and β is the bias

factor.

The OMLSA estimator employed for the signal estimation is addressed in the next section.

5.6 Signal estimation

5.6.1 Optimal modified log-spectral amplitude

In spectral enhancement problems, the main approach employed is to derive an estimator $\hat{X}_{t,k}$ for the speech spectral coefficients such that the expected value of a certain distortion measure is minimized. The clean speech signal is typically estimated by applying a specific gain function to each spectral component of the noisy speech signal, expressed as,

$$\hat{X}_{t,k} = G_{t,k} Y_{t,k}.$$

In this study, we utilize the OMLSA estimator (Cohen & Berdugo (2001)), which has demonstrated superior performance compared to many existing speech enhancement techniques. In this method to obtain the estimate of spectral speech amplitude, we need to minimize the objective function,

$$E\left\{(\log A_{t,k} - \log \hat{A}_{t,k})^2\right\},$$

where $A_{t,k} = |X_{t,k}|$ is the spectral speech amplitude and $\hat{A}_{tk}$ is the optimal estimate of spectral speech amplitude, given by,

$$\hat{A}_{t,k} = \exp\left\{E[\log A_{t,k}|Y_{t,k}]\right\}. \tag{5.8}$$

Based on the hypothesis model given in (5.1), we can write,

$$E[\log A_{t,k}|Y_{t,k}] = E[\log A_{t,k}|Y_{t,k}, H_1^{t,k}]p_{t,k} + E[\log A_{t,k}|Y_{t,k}, H_0^{t,k}](1 - p_{t,k}).$$

Thus, the OMLSA estimator in (5.8) is,

$$\begin{aligned}\hat{A}_{tk} &= (\exp\left\{E[\log A_{tk}|Y_{tk}, H_1^{tk}]\right\})^{p_{tk}} \times (\exp\left\{E[\log A_{tk}|Y_{tk}, H_0^{tk}]\right\})^{1-p_{tk}}, \\ &= G_{tk}|Y_{tk}|, \end{aligned} \tag{5.9}$$

where $G_{t,k}$ is the spectral gain function.
In speech absence, the gain is constrained to be larger than a threshold G_{min}, a constant smaller than 1. Hence,

$$\exp\left\{E[\log A_{t,k}|Y_{t,k}, H_0^{t,k}]\right\} = G_{min}|Y_{t,k}|. \tag{5.10}$$

In speech presence we have,

$$\exp\left\{E[\log A_{t,k}|Y_{t,k}, H_1^{t,k}]\right\} = G_{\mathrm{H}_1^{t,k}}|Y_{t,k}|, \tag{5.11}$$

where

$$G_{\mathrm{H}_1^{t,k}} = \frac{\xi_{t,k}}{1+\xi_{t,k}} \exp\left(\frac{1}{2}\int_{v_{t,k}}^{\infty} \frac{\mathrm{e}^{-t}}{t}\ \mathrm{d}t\right).$$

Using (5.10) and (5.11) we get the overall specral gain function as,

$$G_{t,k} = \left\{G_{\mathrm{H}_1^{t,k}}\right\}^{p_{t,k}} G_{min}^{1-p_{t,k}}. \tag{5.12}$$

Thus the OMLSA estimator in (5.9) is,

$$\hat{A}_{t,k} = \left\{G_{\mathrm{H}_1^{t,k}}\right\}^{p_{t,k}} G_{min}^{1-p_{t,k}}|Y_{t,k}|. \tag{5.13}$$

So to compute the spectral gain, it is essential to estimate the a priori SNR. The method for estimating the a priori SNR using our SV model is already detailed in Subsection 5.4.1.

5.7 Experimental results

The application of the suggested model in speech enhancement is demonstrated in this section. For evaluating the performance of the suggested model, three objective quality metrics are used, namely, LSD, PESQ score (ITU-T P.862), and STOI. The speech signals for evaluation were sourced from the TIMIT database (Garofolo et al. (1993)), and we considered only 30 different utterances from 30 different speakers (half male and half female). They are sampled at 16 kHz and corrupted by white Gaussian noise with SNR in the range $[0, 20]$ dB. These noisy signals are then transformed into the STFT domain using a half-overlapping Hanning analysis window of 512 samples length (32 ms) and 128 samples frame update step.

The OMLSA-IMCRA parameter estimators are set to the values provided in Table 5.1 and the SV model parameters for each speaker are estimated individually from the clean speech signal of that speaker using the R programming, as described in Section 5.4. These estimated values are presented in Table 5.2. Following this, each noisy speech signal is subjected to the speech enhancement method based on the SV model, OMLSA, and IMCRA estimate.

Table 5.1: Fixed parameter values used for implementing OMLSA-IMCRA estimators at a sampling rate of 16kHz.

$D = 120$	$\gamma_0 = 4.6$	$\gamma_1 = 3$	$B_{\min} = 1.66$
$w = 1$	$\alpha_s = 0.9$	$U = 8$	$V = 15$
$\zeta_0 = 1.67$	$\alpha_d = 0.85$	$\beta = 1.47$	b : Hanning window

Table 5.2: Parameter estimates of SV speech estimators.

$\phi = 0.98$	$\alpha = 20$	$\sigma_\eta = 0.28$

For comparison, we also considered a speech enhancement approach using the GARCH model introduced by Cohen (2004). In GARCH(1,1) modeling, the conditional variance of the spectral coefficients of speech is defined as,

$$\hat{w}^x_{t,k} = w_{min} + \alpha_0 |X_{t-1,k}|^2 + \beta_0 (\hat{w}^x_{t-1,k} - w_{min}),$$

where $w_{min} > 0$, $\alpha_0 \geq 0$, $\beta_0 \geq 0$, and $\alpha_0 + \beta_0 < 1$. These parameters are also estimated independently for each speaker.

Table 5.3 presents the results of LSD, PESQ, and STOI values obtained using both methods. The results demonstrate that the SV modeling approach consistently yields lower LSD and higher STOI and PESQ scores compared to the GARCH model. This indicates that the SV model offers superior performance in enhancing speech quality and intelligibility. These outcomes highlight the effectiveness of SV modeling in accurately estimating speech variance, particularly in noisy environments, making it a more reliable method for speech enhancement.

Table 5.3: LSD, PESQ, and STOI values obtained by using OMLSA and IMCRA estimation with different speech variance estimation methods - GARCH and SV modeling.

Input SNR (dB)	**GARCH modeling method**			**SV modeling method**		
	LSD	**PESQ**	**STOI**	**LSD**	**PESQ**	**STOI**
0	4.3573	2.5221	0.8475	4.1645	2.8534	0.8557
5	3.3046	2.8562	0.8837	3.0732	2.9952	0.8943
10	2.2949	3.3251	0.9438	2.0195	3.7935	0.9564
15	1.7837	3.7192	0.9749	1.2310	3.9149	0.9849
20	1.2105	3.8517	0.9872	1.0387	3.9996	0.9963

The entropy associated with the noisy speech signal and enhanced signals is also calculated for validation. For the noisy speech signal, the entropy is found as -4.3122, and after applying the speech enhancement techniques, the entropy values were observed to decrease, indicating a reduction in signal uncertainty and noise. Specifically, the entropy for the speech signal enhanced using the GARCH model is obtained as -5.0700, while the speech signal enhanced using our SV modeling technique has a lower value of -5.0891. This reduction in value of entropy for both models highlights their effectiveness in suppressing noise and improving signal structure, with the SV modeling approach demonstrating marginally better performance in terms of minimizing uncertainty in the speech signal.

The SV modeling technique may also be useful in determining the quality of the speech signals and may serve as a foundation for further research in individual speech recognition. The variability in speech due to health-related factors depends upon the severity of the disease affecting key characteristics such as pitch, tone, and articulation. Therefore, the SV modeling approach holds potential for applications in speech enhancement and speaker identification within the healthcare sector.

5.8 Summary

In the STFT domain, we have developed a novel method for statistically modeling speech signals. The speech signals are modeled using the SV model, where the conditional variances of the STFT expansion coefficients are treated as a stochastic process. It provides an explicit model for the conditional distribution as well as the conditional variance of the expansion coefficients, accounting for the heavy-tailed nature of the STFT expansion coefficients. These spectral speech variances are estimated using a Bayesian method via the MCMC algorithm implemented

by an R package. Additionally, the study incorporates the OMLSA technique for speech enhancement and the IMCRA method for estimating noise spectral coefficients. The performance of the OMLSA and IMCRA estimators, when paired with variance estimation based on either SV or GARCH modeling, is compared. The results demonstrate that our SV-based model outperforms the GARCH model across three objective quality measures, establishing it as a robust statistical model for enhancing speech quality. Also, the entropy value of noisy speech, enhanced speech using the SV-based model, and the GARCH model suggests that the SV-based speech enhancement possesses a lower entropy value, suggesting its better performance and improved signal structure compared to others.

CHAPTER 6

Two-Dimensional Stochastic Volatility Model and its Applications

6.1 Introduction

In digital image processing, one of the main challenges is image enhancement, particularly when noise reduces image quality during transmission or capture. The resolution of imaging sensors and the characteristics of the transmission channel are some factors that might cause a received image to differ greatly from the original. This challenge is particularly significant in medical imaging techniques like ultrasound, where interference from sound waves causes speckle noise, which deteriorates clarity and makes diagnostic analysis more difficult. Hence, effective image denoising techniques are necessary to reduce noise and enhance the quality of a variety of image types, including satellite and astronomical images as well as medical imaging like computed tomography, magnetic resonance imaging, and ultrasound scans.

In the previous chapter, we explored and studied the application of SV models in speech signal processing. Now, we try to broaden this SV framework to image processing, specifically in the context of image denoising. Image denoising aims to re-

store the original image by minimizing noise while retaining essential features like textures and edges. Recent studies suggest that image wavelet coefficients show heavy-tailed distributions, underscoring the necessity for sophisticated non-linear models that can handle spatially complicated and non-Gaussian data. Hence, to effectively model these statistical wavelet coefficients, several methods were introduced. One among them is the 2-D GARCH model described in Subsection 1.7.2. The 2-D GARCH model has been applied for image denoising, anomaly detection, and speckle suppression in ultrasound images (Amirmazlaghani & Amindavar (2007a); Noiboar & Cohen (2007); Amirmazlaghani & Amindavar (2007b)), and these models have proven to be effective in enhancing image quality and identifying anomalies.

Classical image denoising methods, such as median filtering and Gaussian smoothing, frequently cause the loss of small details. In order to overcome these constraints, we suggest a unique method that applies the concepts of SV models to the wavelet coefficients of noisy images and efficiently reduces noise while maintaining important details. We extend the 1-D SV models to a novel 2-D SV model and investigate its potential uses, especially in noise reduction of images and speckle suppression in ultrasound images. We use the Kalman filtering technique to estimate the hidden volatilities, and it offers an iterative refinement of estimates, resulting in more accurate noise reduction. The performance of the proposed 2-D SV model for image denoising is assessed and compared with several existing denoising techniques by using various image quality metrics.

The chapter is structured as follows. Section 6.2 provides a summary of the performance metrics utilized in this chapter to evaluate the image quality. Section 6.3 and its subsections introduce the newly developed 2-D SV model and study its properties and estimation techniques. Section 6.4 discusses the image-denoising algorithm based on the proposed model, and Section 6.5 presents an analysis of

the developed method, along with experimental results demonstrating its effectiveness. Finally, Section 6.6 provides a summary of the chapter.

6.2 Image quality metrics

This section provides a concise overview of the key metrics used in this chapter for evaluating image denoising and speckle suppression techniques. These metrics help in quantifying structural preservation, image quality, and edge retention.

- **Mean squared error:**

  The most popular quality metric, mean squared error (MSE), is calculated by averaging the squared intensity differences between the restored and reference images. A smaller MSE indicates more effective noise reduction. It is mathematically given by,

$$\text{MSE} = \frac{1}{n}\sum_{i=1}^{n}(\hat{X}_i - X_i)^2,$$

  where, X_i is the original image and $\hat{X}_i$ is the restored image.

- **Peak signal-to-noise ratio:**

  The peak signal-to-noise ratio (PSNR) metric is calculated as,

$$\text{PSNR} = 10\log_{10}\left(\frac{\text{MAX}^2}{\text{MSE}}\right),$$

  where MAX is the maximum pixel value of the image and MSE is the mean square error. The PSNR metric reflects the speckle noise level, with higher PSNR values indicating better denoising performance.

- **Mean structural similarity index measure:**

  The mean structural similarity index measure (MSSIM) is a perceptual met-

ric used to assess how similar two images are structurally. It assesses image quality based on luminance, texture, and structural information. In general, images with higher MSSIM values (close to 1) are more similar than images with lower values.

➤ **Structural content:**

Structural content (SC) measures similarity between images by focusing on regions with significantly low-level structural information. It is used to assess the quality of structural content in an image. Generally, higher SC values denote lower image quality.

➤ **Pratt's figure of merit:**

Pratt's figure of merit (FOM) is an index used to assess the edge preservation in an image (Pratt (1977)). It measures how well the edges are preserved in the recovered image compared with the reference image. Values close to 1 imply better edge preservation, whereas values close to 0 imply poor edge retention.

➤ **Q index:**

The Q index is another quality metric used to measure the restoring image performance (Wang & Bovik (2002)). It reveals the overall image quality and might be useful when assessing complex tasks of noise reduction and denoising.

In the following section, we introduce a novel 2-D SV model, explore its properties, and discuss its estimation.

6.3 Two-Dimensional stochastic volatility model

The 1-D SV model is defined as in (2.1) and the volatility sequences $\{w_t\}$ are generated by a Gaussian AR(1) process given as,

$$w_t = \phi w_{t-1} + \eta_t; \quad t = 1, 2, \ldots; \quad 0 < \phi < 1,$$

with $\eta_t \sim N\left(0, \sigma_\eta^2\right)$. The sequence $\{Y_t\}$ is independent of $\{w_t\}$ and the innovation sequence $\{\eta_t\}$ for every t. These 1-D SV models are used for modeling 1-D signals. Now, we extend this SV model to 2-D and define X_{ij} to be a 2-D stochastic process defined as,

$$X_{ij} = \sqrt{w_{ij}} Y_{ij}, \tag{6.1}$$

where $Y_{ij} \sim N(0, 1)$ is an iid 2-D stochastic process independent of conditional variance w_{ij} and $\{w_{ij}\}$ is assumed to be generated by a 2-D AR(1) given in (1.7), where $w_{i-1,j}$, $w_{i,j-1}$, $w_{i-1,j-1}$ denotes the latent variance at positions $(i-1, j)$,$(i, j-1)$ and $(i-1, j-1)$ respectively and ϕ_{00}, ϕ_{01}, ϕ_{10}, ϕ_{11} represents the 2-D AR(1) parameters that governs the dependencies of the current volatility on the volatility of neighboring pixels. This formulation accounts for the modeling of heteroskedastic noise, where the variance can vary across several image regions and we assume, $\eta_{ij} \sim N\left(0, \sigma_{\eta_{ij}}^2\right)$. The information set is represented by $\mathcal{F}_{ij} = \{X_{00}, ..., X_{i-1,j-1}, w_{00}, ..., w_{i-1,j-1}\}$ and X_{ij} is conditionally distributed as,

$$X_{ij} \mid \mathcal{F}_{i,j} \sim N(0, w_{ij}).$$

Here the parameter vector to be estimated is denoted by $\mathbf{\Lambda} = \left(\phi_{00}, \phi_{01}, \phi_{10}, \phi_{11}, \sigma_{\eta_{ij}}^2\right)$. The autocorrelation structure of the 2-D SV model is characterized by the 2-D AR(1) process governing w_{ij}. Given the 2-D AR(1) form in (1.7), the ACF of

$w_{ij}, \rho_w(\Delta i, \Delta j)$ at lag $(\Delta i, \Delta j)$ is described by the Yule-Walker equations for 2-D processes. For smaller lags, we have,

$$\rho_w(1,0) \approx \phi_{10}, \quad \rho_w(0,1) \approx \phi_{01}, \quad \rho_w(1,1) \approx \phi_{11}.$$

These autocorrelations reflect how the volatility of neighboring points influences the volatility at a given location. From (6.1), the ACF of X_{ij}^2, $\rho_{x^2}(\Delta i, \Delta j)$ is largely governed by the autocorrelation in w_{ij} provided Y_{ij} follows iid Gaussian noise. The ACF of X_{ij}^2 is approximated as,

$$\rho_{X^2}(\Delta i, \Delta j) \approx \frac{\text{Cov}\left[X_{ij}^2, X_{i+\Delta i, j+\Delta j}^2\right]}{\text{Var}\left[X_{ij}^2\right]} \approx \rho_w(\Delta i, \Delta j).$$

The model parameters $\mathbf{\Lambda}$ are then estimated using the Kalman filtering technique adapted for 2-D space and are described in the next subsection.

6.3.1 Estimation of the parameters

The state-space representation of the 2-D SV model provides an effective framework for modeling and denoising the wavelet coefficients of images. It allows capturing the underlying volatility structure in the presence of noise and is given by,

$$\log(X_{ij}^2) = -1.2704 + \log(w_{ij}) + \tau_{ij}, \tag{6.2}$$

where, $\tau_{ij} = \log(Y_{ij}^2) + 1.2704$ with $E(\tau_{ij}) = 0$, and $Var(\tau_{ij}) = \frac{\pi^2}{2}$ and the volatility sequences $\{w_{ij}\}$ follows the 2-D AR(1) process as discussed above.

The Kalman filter, as discussed in Chapter 1 (Subsection 1.6.4.3), is a widely used optimal recursive estimator that estimates the hidden states in state-space models. So we employ the Kalman filtering of 2-D space to estimate the model parameters as well as the hidden volatility from the noisy wavelet coefficients. The Kalman

filtering (Wu & Kundu (1992)) consists of two main steps: prediction and update.

Prediction step:

Here we calculate the predicted hidden volatility w_{ij}^p and the predicted error covariance P_{ij}^p as,

$$\begin{aligned} w_{ij}^p &= \phi_{00} + \phi_{01} w_{i,j-1}^p + \phi_{10} w_{i-1,j}^p + \phi_{11} w_{i-1,j-1}^p, \\ P_{ij}^p &= \phi_{01}^2 P_{i,j-1}^p + \phi_{10}^2 P_{i-1,j}^p + \phi_{11}^2 P_{i-1,j-1}^p + \sigma_{\eta_{ij}}^2. \end{aligned}$$

Update step:

The Kalman gain K is computed under this step, and it determines the weight given to the new observation $log(X_{ij}^2)$ when updating the estimate of the hidden volatility. It is given by $K = \frac{P_{ij}^p}{P_{ij}^p + \pi^2/2}$. The updated hidden volatility w_{ij}^u and the updated error covariance P_{ij}^u are then obtained as,

$$\begin{aligned} w_{ij}^u &= w_{ij}^p + K[log(X_{ij}^2) - log(w_{ij}^p) + 1.2704], \\ P_{ij}^u &= (1 - K) P_{ij}^p. \end{aligned}$$

The next step after applying the Kalman filter is to optimize the model parameters to enhance the accuracy of the estimates. This is carried out by constructing a likelihood function based on the observed data and the Kalman filter updates. We define the sample space as a 2-D lattice of size $M \times N$, denoted by $\Phi = \{ij \mid 1 \leq i \leq M, 1 \leq j \leq N\}$, and the likelihood function is given by,

$$L(\mathbf{\Lambda}) = \prod_{ij \in \Phi} f\left(X_{ij} \mid \mathcal{F}_{ij}, \mathbf{\Lambda}\right). \tag{6.3}$$

Then the log-likelihood function is,

$$\log L(\mathbf{\Lambda}) = -\frac{1}{2}\sum_{i,j\in\Phi}\left[\log\left(P_{ij}^{\mathrm{p}} + \frac{\pi^2}{2}\right) + \frac{\left(\log\left(X_{ij}^2\right) - \log\left(w_{ij}^{\mathrm{p}}\right) + 1.2704\right)^2}{P_{ij}^{\mathrm{p}} + \frac{\pi^2}{2}}\right].$$

The model parameters are then estimated by maximizing the log-likelihood function. It ensures that the parameters are adjusted to best fit the observed data, resulting in more accurate and robust denoising. Next, we discuss the image-denoising algorithm associated with this 2-D SV model.

6.4 Image denoising algorithm

In this section, we try to develop an MMSE estimator based on the 2-D SV model to retrieve the signal component of wavelet coefficients in noisy images. The 2-D SV model may capture the key characteristics of wavelet coefficients, like their non-stationary behavior, heavy-tailed marginal distribution, and the dependencies between coefficients. Let $x = z + \eta$ be the observed image, such that z and η are the original image and additive noise, respectively. The image denoising technique based on the suggested model is outlined below, and a block diagram illustrating the algorithm is depicted in Figure 6.1.

Initially, the discrete wavelet transform (DWT) is applied to the noisy image in order to extract the subbands across various orientations and scales. The DWT of z, η, and x are denoted by Z_n, $\mathcal{N}_n$, and X_n, respectively, for an arbitrary subband denoted by n. Therefore, we have,

$$X_{ij}^n = Z_{ij}^n + \mathcal{N}_{ij}^n. \tag{6.4}$$

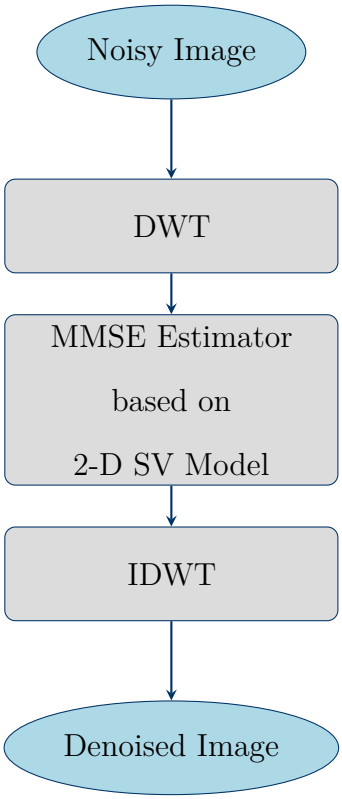

Figure 6.1: Block diagram of the image denoising process using 2-D SV model.

The MMSE estimator based on the 2-D SV model is then obtained as follows. Let $\sigma^2_{X^n_{ij}} = w_{ij}$ represent the conditional variance of $X_{ij}, \sigma^2_{\mathcal{N}^n_{ij}}$ is the variance of noise, and $\sigma^2_{Z^n_{ij}}$ denote the conditional variance of Z^n_{ij}, defined as $\sigma^2_{X^n_{ij}} - \sigma^2_{\mathcal{N}^n_{ij}}$. In some image denoising applications, the input noise variance $\sigma^2_{\mathcal{N}^n_{ij}}$ is known; otherwise, it can be estimated based on the approach suggested by Donoho & Johnstone (1994). Next, we consider an estimator for Z^n_{ij}, given $\sigma^2_{Z^n_{ij}}$ and the noisy wavelet coefficients X^n_{ij}, which minimizes the expected distortion,

$$\min_{\hat{Z}^n_{ij}} E\left\{d\left(Z^n_{ij}, \hat{Z}^n_{ij}\right) \mid \sigma^2_{Z^n_{ij}}, X^n_{ij}\right\}.$$

Specifically, we rely on the MMSE estimator given by,

$$\min_{\hat{Z}^n_{ij}} E\left\{\left|Z^n_{ij} - \hat{Z}^n_{ij}\right|^2 \mid \sigma^2_{Z^n_{ij}}, X^n_{ij}\right\},$$

where,

$$\hat{Z}_{ij}^{n} = E\left(Z_{ij}^{n} \mid \sigma_{Z_{ij}^{n}}^{2}, X_{ij}^{n}\right),$$

for which $f\left(Z_{ij}^{n} \mid X_{ij}^{n}, \sigma_{Z_{ij}^{n}}^{2}\right)$ need to be obtained. We have,

$$f\left(Z_{ij}^{n} \mid X_{ij}^{n}, \sigma_{Z_{ij}^{n}}^{2}\right) = \frac{f\left(Z_{ij}^{n} \mid \sigma_{Z_{ij}^{n}}^{2}\right) f\left(X_{ij}^{n} \mid Z_{ij}^{n}, \sigma_{Z_{ij}^{n}}^{2}\right)}{f\left(X_{ij}^{n} \mid \sigma_{Z_{ij}^{n}}^{2}\right)},$$

where,

$$\begin{aligned} f\left(Z_{ij}^{n} \mid \sigma_{Z_{ij}^{n}}^{2}\right) &\sim N\left(0, \sigma_{Z_{ij}^{n}}^{2}\right), \\ f\left(X_{ij}^{n} \mid \sigma_{Z_{ij}^{n}}^{2}\right) &\sim N\left(0, \sigma_{Z_{ij}^{n}}^{2} + \sigma_{\mathcal{N}_{ij}^{n}}^{2}\right), \\ f\left(X_{ij}^{n} \mid Z_{ij}^{n}, \sigma_{Z_{ij}^{n}}^{2}\right) &\sim N\left(Z_{ij}^{n}, \sigma_{\mathcal{N}_{ij}^{n}}^{2}\right). \end{aligned}$$

Thus we have,

$$\begin{aligned} \hat{Z}_{ij}^{n} &= \frac{\sigma_{Z_{ij}^{n}}^{2}}{\sigma_{Z_{ij}^{n}}^{2} + \sigma_{\mathcal{N}_{ij}^{n}}^{2}} X_{ij}^{n} \\ &= \frac{\sigma_{X_{ij}^{n}}^{2} - \sigma_{\mathcal{N}_{ij}^{n}}^{2}}{\sigma_{X_{ij}^{n}}^{2}} X_{ij}^{n} \\ &= \beta_{ij} X_{ij}^{n}. \end{aligned}$$

The MMSE estimates of each subband are computed, and lastly, the denoised image is reconstructed using the inverse DWT(IDWT).

This algorithm can also be used for the suppression of speckle noise in ultrasound images. Speckle noise, unlike additive noise, is multiplicative, making it more difficult to eliminate, as its intensity varies with the image intensity. In the multiplicative case, the noisy signal is modeled as $x = z.\eta$, which can then be logarithmically transformed into additive noise, producing $\ln x = \ln z + \ln \eta$. Further, the DWT can be applied to these logarithmic noisy images, and by following in the similar way discussed above, the MMSE estimates can be obtained. Finally, the IDWT results are applied to the logarithmic denoised image, which can then be transformed exponentially to produce the final denoised image.

Next, we evaluate the performance of this algorithm on various images and compare it with the existing models.

6.5 Experimental results

6.5.1 Image denoising

Here we demonstrate the application of the developed model for image denoising. The denoising algorithm outlined earlier was applied to several natural grayscale images, including Hill (512×512), Lena (512×512), Boat (512×512), and House (256×256), under varying levels of Gaussian noise.

For each subband, the image denoising algorithm using the 2-D SV model is applied, and subsequently, parameter estimates and volatilities are calculated. The initial values for the iterative Kalman filtering technique are set as $\phi_{00} = 0.0001$, $\phi_{01} = 0.0001$, $\phi_{10} = 0.0001$, $\phi_{11} = 0.0001$, and $\sigma^2_{\eta_{ij}} = 0.001$. The MMSE estimates are then computed for each subband, followed by reconstruction of the denoised images using the IDWT.

For comparison, we also considered image denoising methods based on the 2-D GARCH model discussed in Amirmazlaghani & Amindavar (2007a), the adaptive thresholding technique described by Gnanadurai & Sadasivam (2008), and the Wiener filter introduced by Jassim et al. (2023). To evaluate the quality of the reconstructed image, the PSNR values for each method are computed and are presented in Table 6.1. Figure 6.2 shows the original Lena image, the noisy image, and the denoised images obtained by the Wiener filter, adaptive thresholding, the 2-D GARCH model, and the 2-D SV model.

The results in Table 6.1 indicate that compared to conventional denoising approaches, the developed 2-D SV method significantly increases the PSNR and

performs better. Next, we examine the effectiveness of our method for speckle suppression in ultrasound images.

Table 6.1: PSNR values (in dB) for various denoising methods applied to different images corrupted by Gaussian noise.

Image	noise	noisy	Wiener	Adaptive	2-D GARCH	2-D SV
Hill	15	24.64	28.47	27.32	28.52	29.49
	20	22.17	27.75	26.09	28.11	28.55
	25	20.24	25.73	24.80	29.52	27.69
	30	18.75	24.58	24.02	26.90	27.14
Lena	15	24.62	32.01	30.94	33.31	33.94
	20	22.11	29.73	29.61	31.45	31.80
	25	20.16	28.53	28.72	30.10	30.81
	30	18.61	26.97	28.12	28.81	29.32
Boat	15	24.65	28.61	28.37	29.11	29.43
	20	22.19	27.73	26.98	28.07	28.93
	25	20.28	26.52	25.61	27.12	27.79
	30	18.74	25.43	25.01	26.10	26.39
House	15	24.61	30.35	30.02	30.76	31.12
	20	22.18	28.96	28.49	29.17	30.19
	25	20.22	28.11	27.71	28.81	29.47
	30	18.65	2713	26.12	28.01	28.66

6.5.2 Speckle suppression

The developed model is first applied to synthetic images degraded by multiplicative speckle noise and then to real ultrasound medical images. We utilize Daubechies wavelets (Db4) with two decomposition levels along with the 2-D SV model. Initially, synthetic images are analyzed to assess the algorithm's performance across varying levels of speckle variance (0.01, 0.02, 0.06).

The proposed algorithm is applied to the synthetic images, and for comparison, we also consider the 2-D GARCH method (Amirmazlaghani & Amindavar (2007b)). The MSE, PSNR, MSSIM, SC, FOM, and the Q index are computed for both

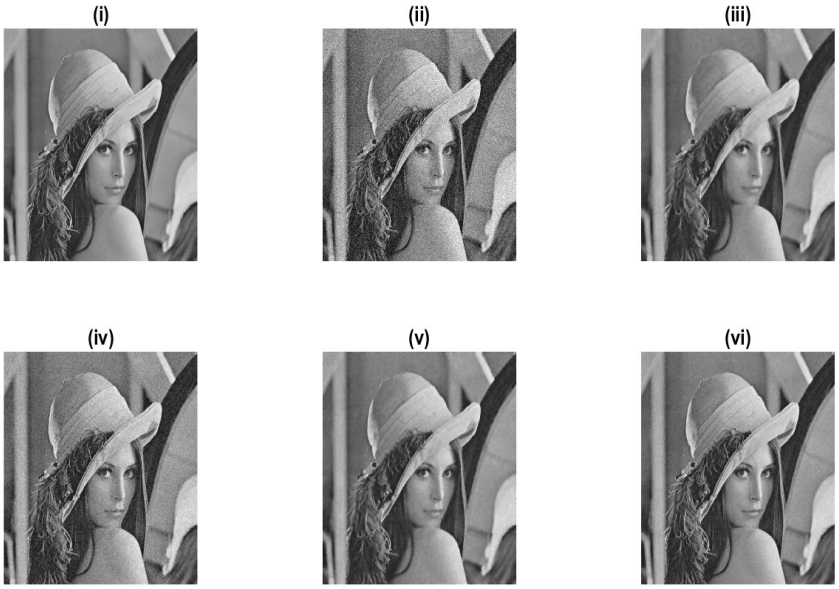

Figure 6.2: (i) Original Lena image, (ii) Noisy image, (iii)Weiner denoised image, (iv) Adaptive denoised image, (v) 2-D GARCH-based denoised image, and (vi) 2-D SV-based denoised image.

the 2-D SV and 2-D GARCH methods, and the results are summarized in Table 6.2. Figure 6.3 illustrates the visual quality evaluation of the synthetic image before and after filtering, showing that the suggested method outperforms the other. Finally, the 2-D SV method is applied to a real medical ultrasound image for qualitative visual assessment, as shown in Figure 6.4. Although the ultrasound images lack standardized quality metrics for qualitative evaluation, the visual outcomes for both synthetic and real images consistently demonstrate that the developed approach excels in reducing speckle noise while preserving edge details. Thus, the image denoising technique based on our 2-D SV model proves to be an effective algorithm for noise reduction as well as speckle suppression in ultrasound images. Moreover, its adaptability extends beyond medical imaging, making it a promising approach for reducing noise in video processing and enhancing texture analysis. By leveraging the dynamic nature of the SV model, this method can preserve es-

sential structural details while effectively mitigating noise across various imaging applications.

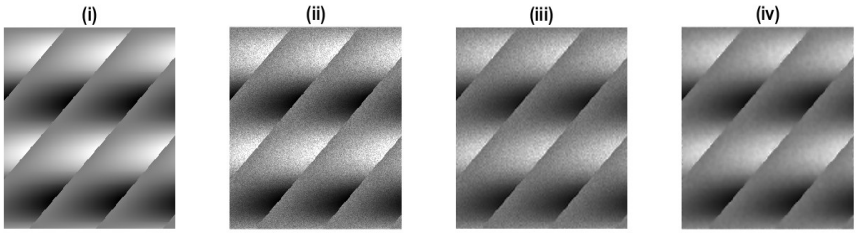

Figure 6.3: (i) Original synthetic image, (ii) Synthetic noisy image with speckle variance 0.02, (iii) Restored image with 2-D GARCH model, (iv) Restored image by 2-D SV model.

Table 6.2: Performance metrics for the synthetic image comparing 2-D GARCH and 2-D SV models.

Metric	**2-D GARCH**	**2-D SV**
MSE	0.0662	0.0306
PSNR (dB)	59.9247	63.2766
MSSIM	0.9972	0.9987
SC	1.0058	1.0054
FOM	0.5956	0.7025
Q index	0.8677	0.9488

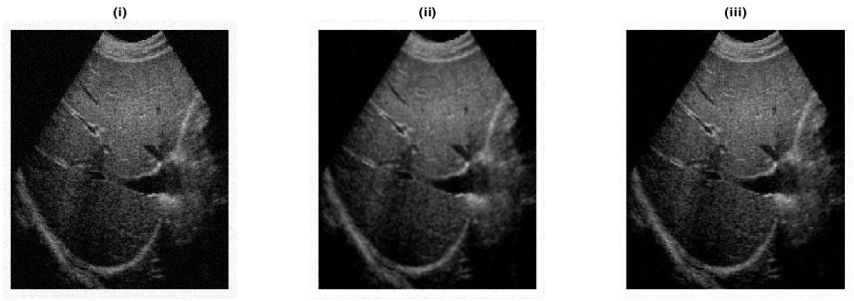

Figure 6.4: (i) Noisy ultrasound image, (ii) 2-D GARCH-based denoised image, (iii) 2-D SV-based denoised image.

6.6 Summary

In this chapter, we have developed and thoroughly analyzed a novel 2-D SV model, focusing on its statistical properties and parameter estimation. The estimation of the model parameters is carried out using the Kalman filtering technique. This new statistical model is later applied to model the wavelet coefficients of images, especially in image denoising and speckle suppression. An MMSE estimator based on this proposed framework is then developed and evaluated by conducting experiments on several natural images. These experiments at different noise levels showed that our image-denoising technique significantly outperformed existing techniques, thereby underlining its high efficiency and robustness. Furthermore, the algorithm can also be utilized for identifying original images in forensic studies and enhancing image quality in the healthcare sector, particularly in Magnetic Resonance Imaging and Computed Tomography scans.

CHAPTER 7

Spatial Moving Average Process driven Spatial Stochastic Volatility Model

7.1 Introduction

Volatility modeling is a significant field of time series analysis, particularly in financial econometrics, geostatistics, and environmental science. While traditional volatility models have been extremely effective in modeling univariate and multivariate time series, many real-world processes change over multiple geo-referenced locations. These processes exhibit spatial or spatiotemporal interdependencies where the volatility at one location is influenced by the volatility at neighboring locations. Examples include regional economic fluctuations, environmental processes such as pollution dispersion, and financial market volatility, all of which have spatially correlated patterns and cannot be modeled by conventional models. This emphasizes the requirement of spatial and spatiotemporal volatility models that capture spatial interdependencies explicitly. Recognizing this challenge, researchers have extended SV models into the spatial domain.

As we have highlighted in Chapter 1 (Subsection 1.7.3), Robinson (2009) and Taşpınar et al. (2021) made significant developments in spatial econometrics by

introducing spatial SV models. These SV models enhance the ability to capture intricate spatial dynamics by incorporating more stochastic components into the volatility process. These spatial SV models are based on a spatial AR process that aggregates spillover effects from higher-order neighbors to enable the global transmission of shocks (Anselin (2003); LeSage & Pace (2009)). This AR structure, however, may not be optimal in all situations, especially where empirical evidence indicates that shock transmission is extremely localized with effects remaining confined to a specific region rather than spreading broadly. In such cases, a spatial MA process (Hepple (1995); Fingleton (2008a,b)) offers a more appropriate alternative, as it better captures localized dependencies.

Building on this foundation, this chapter introduces a spatial SV model driven by a spatial MA process. The spatial MA process offers a flexible and robust framework for modeling spatial dependencies by allowing the volatility at each location to be influenced by a weighted average of its neighbors. This refinement enhances the model's capacity to capture spatially dependent volatility patterns, offering a comprehensive tool for analyzing processes characterized by both spatial and temporal complexity.

The chapter is structured as follows. Section 7.2 introduces a new spatial SV model driven by the spatial MA process and discusses its properties. Section 7.3 outlines the Bayesian MCMC method used for the estimation of parameters, and Section 7.4 investigates the finite sample performance of these proposed algorithms using Monte Carlo simulations. Section 7.5 focuses on the empirical application of the model, and lastly, Section 7.6 provides a summary of the chapter.

7.2 Spatial stochastic volatility model

We have already defined the spatial SV model generated by the spatial AR model in (1.8). Now, we develop a spatial SV model driven by a spatial MA process. Define $\{x_i\}$ for $i = 1, 2, \ldots, n$ as the outcome variable given by,

$$x_i = e^{\frac{1}{2}w_i} y_i, \tag{7.1}$$

where $\{y_i\}_{i=1}^n \overset{\text{iid}}{\sim} N(0,1)$ and the volatility sequence $\{w_i\}$ is assumed to be generated by a first-order spatial MA process given by,

$$w_i - \mu_w = \theta \sum_{j=1}^{n} g_{ij}\eta_j + \eta_i, \tag{7.2}$$

where μ_w represents the constant mean, $\{g_{ij}\}_{i=1}^n$ denotes non-stochastic spatial weights, and $\{\eta_i\} \overset{\text{iid}}{\sim} N(0, \sigma_\eta^2)$. Also, $\{\eta_i\}$ and $\{y_j\}$ are assumed to be independent for all i, j. The scalar parameter θ is the spatial MA parameter. It measures how the nearby locations influence data at one location through a spatially structured error component.

Define $\mathbf{w} = (w_1, \ldots, w_n)'$ as the $n \times 1$ vector of log-volatilities, $\eta = (\eta_1, \ldots, \eta_n)'$ as the $n \times 1$ vector of disturbance terms, and $\mathbf{G} = (g_{ij})$ as the $n \times n$ non-stochastic spatial weights matrix that has zero diagonal elements, then (7.2) becomes,

$$\begin{aligned} \mathbf{w} - \boldsymbol{l}_n\mu_w =& \theta\mathbf{G}\eta + \eta \\ =& (\theta\mathbf{G} + \boldsymbol{I}_n)\eta \\ =& \mathbf{A}(\theta)\eta. \end{aligned} \tag{7.3}$$

where $\mathbf{A}(\theta) = \theta\mathbf{G} + \boldsymbol{I}_n$, $\boldsymbol{l}_n$ is the $n \times 1$ vector of ones, and $\boldsymbol{I}_n$ is the $n \times n$ identity matrix. We have the parameter space of θ bounded, with the bounds

defined by the eigenvalues of the spatial weight matrix $\mathbf{G}$. The parameter space is usually restricted to $\{\theta : \theta\lambda_i < 1\}$, where λ_i represents the eigenvalues of $\mathbf{G}$ for $i = 1, 2, \ldots, n$.

The conditional variance of x_i given w_i is,

$$\text{Var}\left(x_i \mid w_i\right) = e^{w_i},$$

indicating the conditional variance of x_i is space-varying. Also, $E\left(x_i x_j\right) = 0$ for all $i \neq j$ revealing no spatial correlations among x_i's. Since $y_i \overset{\text{iid}}{\sim} N(0,1)$, we have the odd moments of x_i is zero.

Let $\mathbf{M}_i(\theta)$ represents the row vector of $\mathbf{A}(\theta)$ and $r \in \mathbb{N}$ is an even number. The even moments of x_i are obtained as,

$$\begin{aligned} E\left(x_i^r\right) &= E\left(e^{\frac{1}{2}w_i r}\right) E\left(y_i^r\right) \\ &= e^{\frac{\mu_w r}{2} + \frac{r^2\sigma_\eta^2}{8}\|\mathbf{M}_i(\theta)\|^2} \mu_{(r)}, \end{aligned}$$

where $\mu_{(r)} = \frac{r!}{2^{r/2} \times (r/2)!}$. This yields $\left(\text{E}\left(x_i^4\right) / \left[E\left(x_i^2\right)\right]^2\right) - 3 = 3\left(e^{\sigma_\eta^2\|\mathbf{M}_i(\theta)\|^2} - 1\right) > 0$, indicating x_i follows a distribution with leptokurtic nature.

Further,

$$\begin{aligned} \text{Cov}\left(x_i^r, x_j^r\right) &= E\left(e^{\frac{r}{2}(w_i+w_j)}\right) E\left(y_i^r\right) E\left(y_j^r\right) - E\left(e^{\frac{r}{2}w_i}\right) E\left(y_i^r\right) E\left(e^{\frac{r}{2}w_j}\right) E\left(y_j^r\right) \\ &= \mu_{(r)}^2 e^{\mu_w r + \frac{\sigma_\eta^2 r^2}{8}\left(\|\mathbf{M}_i(\theta)\|^2 + \|\mathbf{M}_j(\theta)\|^2 + 2\mathbf{M}_i'(\theta)\mathbf{M}_j(\theta)\right)} \\ &\quad - \mu_{(r)}^2 e^{\frac{\mu_w r}{2} + \frac{\sigma_\eta^2 r^2}{8}\|\mathbf{M}_i(\theta)\|^2} e^{\frac{\mu_w r}{2} + \frac{\sigma_\eta^2 r^2}{8}\|\mathbf{M}_j(\theta)\|^2} \\ &= \mu_{(r)}^2 \left[e^{\mu_w r + \frac{\sigma_\eta^2 r^2}{8}\left(\|\mathbf{M}_i(\theta)\|^2 + \|\mathbf{M}_j(\theta)\|^2\right)} \left(e^{\frac{\sigma_\eta^2 r^2}{8} 2\mathbf{M}_i'(\theta)\mathbf{M}_j(\theta)} - 1 \right) \right]. \end{aligned}$$

This suggests that x_i's are spatially dependent.

For example, assume that we have two spatial locations indexed by i and j, with their associated row vectors as $\mathbf{M}_i(\theta) = (1, 2)$, $\mathbf{M}_j(\theta) = (1, 1)$ and if we take,

$r = 2$ we have $\mu_{(2)} = 1$, and let $\sigma_\eta^2 = 0.2$, and $\mu_w = 2$, then the covariance of x_i^2, x_j^2 is obtained as 90.4 indicating strong positive spatial dependence among them. This suggests that the volatility at one spatial location influences the volatility at a neighboring location, reinforcing the spatial structure embedded in the model. The strength of this dependence is influenced by the choice of parameters, such as σ_η^2 and μ_w, where higher values of σ_η^2 amplify the effect of spatial correlation. In the next section, we discuss the posterior analysis of each parameter of our spatial SV model.

7.3 Estimation of the parameters

7.3.1 Posterior analysis

We employ the Bayesian technique introduced by Taşpınar et al. (2021) for estimation. To carry out this Bayesian analysis, we first reformulate the spatial SV model into a linear state-space representation. In particular, we restructure the model to ensure that the resulting estimation equation becomes linear in the log-volatility w_i. This is achieved by first squaring both sides of equation (7.1) and subsequently applying the natural logarithm, resulting in,

$$x_i^* = w_i + y_i^*, \tag{7.4}$$

where $x_i^* = \log x_i^2$, $y_i^* = \log y_i^2$, and also y_i^* has a $\log \chi_1^2$ distribution with pdf,

$$f\left(y_i^*\right) = \frac{1}{\sqrt{2\pi}} \exp\left(-\frac{1}{2}\left(e^{y_i^*} - y_i^*\right)\right), \quad -\infty < y_i^* < \infty, \quad i = 1, 2, \ldots, n,$$

such that $E\left(y_i^*\right) \approx -1.2704$, and $\mathrm{Var}\left(y_i^*\right) = \pi^2/2$.

Let $\mathbf{x}^* = \left(x_1^*, \ldots, x_n^*\right)'$ denote the $n \times 1$ vector of the transformed dependent

variable, and $\mathbf{y}^* = (y_1^*, \ldots, y_n^*)'$ be the $n \times 1$ vector of the transformed disturbance terms. Then, (7.4) changes to,

$$\mathbf{x}^* = \mathbf{w} + \mathbf{y}^*.$$

The distribution of y_i^* is approximated by a 10-component Gaussian mixture distribution (Taşpınar et al. (2021)) having pdf,

$$f\left(y_i^*\right) \approx \sum_{j=1}^{m} c_j \times \zeta\left(y_i^* \mid \mu_j, \sigma_j^2\right),$$

where $\zeta\left(y_i^* \mid \mu_j, \sigma_j^2\right)$ represents the Gaussian density function with mean μ_j and variance σ_j^2, c_j is the probability of j th mixture component and m is the number of components (in our case $m = 10$). We express the 10-component Gaussian mixture distribution using an auxiliary random variable $b_i \in \{1, 2, \ldots, 10\}$, which serves as the mixture component indicator. That is, we assume

$$y_i^* \mid (b_i = j) \sim N\left(\mu_j, \sigma_j^2\right),$$

and

$$p\left(b_i = j\right) = c_j, \quad j = 1, 2, \ldots, 10, \quad i = 1, 2, \ldots, n.$$

Thus, given the component indicator variable $\mathbf{b} = (b_1, \ldots, b_n)$, the model in (7.4) becomes conditionally linear and Gaussian. The parameters of the 10-component Gaussian mixture distribution are presented in Table 7.1 (Omori et al. (2007)).

Table 7.1: The 10-component Gaussian mixture approximation for $\log \chi_1^2$.

Components	c_j	μ_j	σ_j^2
1	0.00609	1.92677	0.11265
2	0.04775	1.34744	0.17788
3	0.13057	0.73504	0.26768
4	0.20674	0.02266	0.40611
5	0.22715	-0.85173	0.62699
6	0.18842	-1.97278	0.98583
7	0.12047	-3.46788	1.57469
8	0.05591	-5.55246	2.54498
9	0.01575	-8.68384	4.16591
10	0.00115	-14.65000	7.33342

For our suggested spatial SV model, we assume the following independent prior distributions. That is,

$$\sigma_\eta^2 \sim \text{IG}\left(a_{0\eta}, b_{0\eta}\right), \quad \theta \sim \text{Uniform}\left(-1, 1\right), \quad \mu_w \sim N\left(\mu_{0w}, V_{\mu w}\right),$$

where $\text{IG}\left(a_{0\eta}, b_{0\eta}\right)$ represents the inverse gamma distribution with shape parameter $a_{0\eta}$ and scale parameter $b_{0\eta}$, and $\text{Uniform}\left(-1, 1\right)$ represents the uniform distribution.

The joint posterior distribution $p\left(\mathbf{w}, \mathbf{b}, \sigma_\eta^2, \mu_w, \theta \mid \mathbf{x}^*\right)$ is therefore,

$$p\left(\mathbf{w}, \mathbf{b}, \sigma_\eta^2, \mu_w, \theta \mid \mathbf{x}^*\right) \propto p\left(\mathbf{x}^* \mid \mathbf{w}, \mathbf{b}\right) \times p\left(\mathbf{w} \mid \sigma_\eta^2, \mu_w, \theta\right) \times p(\mathbf{b}) \times p\left(\sigma_\eta^2\right) \times p\left(\mu_w\right) \times p(\theta), \tag{7.5}$$

where $p\left(\mathbf{x}^* \mid \mathbf{w}, \mathbf{b}\right)$ is the conditional likelihood function of (7.4).

Let $\mathbf{d}_b = \left(\mu_{b_1}, \ldots, \mu_{b_n}\right)'$ and $\mathbf{\Sigma}_b = \text{Diag}\left(\sigma_{b_1}^2, \ldots, \sigma_{b_n}^2\right)$. Then, $y^* \mid \mathbf{b} \sim N\left(\mathbf{d}_b, \mathbf{\Sigma}_b\right)$. Hence from (7.2) and (7.4) we have,

$$\mathbf{x}^* \mid \mathbf{b}, \mathbf{w} \sim N\left(\mathbf{w} + \mathbf{d}_b, \mathbf{\Sigma}_b\right),$$

$$\mathbf{w} \mid \sigma_\eta^2, \mu_w, \theta \sim N\left(\boldsymbol{l}_n \mu_w, \sigma_\eta^2 \mathbf{A}(\theta)\mathbf{A}(\theta)'\right).$$

The Gibbs sampler algorithm used to generate random draws from $p\left(\mathbf{w}, \mathbf{b}, \sigma_\eta^2, \mu_w, \theta \mid \mathbf{x}^*\right)$ is described below.

1. Sampling step for $\mathbf{b}$:

$$p\left(b_i = j \mid x_i^*, w_i\right) = \frac{c_j \times \zeta\left(x_i^* \mid w_i + \mu_j, \sigma_j^2\right)}{\sum_{k=1}^{10} c_k \times \zeta\left(x_i^* \mid w_i + \mu_k, \sigma_k^2\right)}, \quad j = 1, \ldots, 10, \quad i = 1, \ldots, n.$$

   Here, the denominator is the normalizing constant.

2. Sampling step for $\mathbf{w}$:

$$\mathbf{w} \mid \mathbf{x}^*, \mathbf{b}, \sigma_\eta^2, \mu_w, \theta \sim N\left(\widehat{\mathbf{w}}, \widehat{\mathbf{W}}_w^{-1}\right),$$

   where

$$\widehat{\mathbf{W}}_w = \mathbf{\Sigma}_b^{-1} + \frac{1}{\sigma_\eta^2}\left(\mathbf{A}(\theta)\mathbf{A}(\theta)'\right)^{-1},$$

   and

$$\widehat{\mathbf{w}} = \widehat{\mathbf{W}}_w^{-1}\left(\mathbf{\Sigma}_b^{-1}\left(\mathbf{x}^* - \mathbf{d}_b\right) + \frac{\mu_w}{\sigma_\eta^2}\left(\mathbf{A}(\theta)\mathbf{A}(\theta)'\right)^{-1}\boldsymbol{l}_n\right).$$

3. Sampling step for σ_η^2 :

$$\sigma_\eta^2 \mid \mathbf{w}, \mu_w, \theta \sim \mathrm{IG}\left(a_{0\eta} + \frac{n}{2}, b_{0\eta} + \frac{1}{2}\left(\mathbf{w} - \boldsymbol{l}_n\mu_w\right)'\left(\mathbf{A}(\theta)\mathbf{A}(\theta)'\right)^{-1}\left(\mathbf{w} - \boldsymbol{l}_n\mu_w\right)\right).$$

4. Sampling step for μ_w :

$$\mu_w \mid \mathbf{w}, \sigma_\eta^2, \theta \sim N\left(\widehat{\mu}_{0w}, \widehat{V}_{\mu w}^{-1}\right),$$

   where

$$\widehat{V}_{\mu w} = V_{\mu w}^{-1} + \frac{1}{\sigma_\eta^2}\boldsymbol{l}_n'\left(\mathbf{A}(\theta)\mathbf{A}(\theta)'\right)^{-1}\boldsymbol{l}_n,$$

and

$$\widehat{\mu}_{0w} = \widehat{V}_{\mu w}^{-1} \left(\frac{1}{\sigma_\eta^2} \boldsymbol{l}_n' \left(\mathbf{A}(\theta)\mathbf{A}(\theta)' \right)^{-1} \mathbf{w} + V_{\mu w}^{-1} \mu_{0w} \right).$$

5. Sampling step for θ :

$$p\left(\theta \mid \mathbf{w}, \mu_w, \sigma_\eta^2\right) \propto |\mathbf{S}(\theta)|^{-1} \times \exp\left(-\frac{1}{2\sigma_\eta^2} \left(\mathbf{w} - \boldsymbol{l}_n \mu_w \right)' \left(\mathbf{A}(\theta)\mathbf{A}(\theta)' \right)^{-1} \left(\mathbf{w} - \boldsymbol{l}_n \mu_w \right) \right).$$

This does not correspond to any known density function. Hence, to sample from it, we apply the Metropolis-Hastings algorithm (LeSage & Pace (2009)). In this method, a candidate value $\tilde{\theta}$ is generated at iteration h as,

$$\tilde{\theta} = \theta^{(h-1)} + z_\theta \times N(0,1),$$

where z_θ is the tuning parameter. This candidate value $\tilde{\theta}$ is accepted with probability,

$$p\left(\tilde{\theta}, \theta^{(h-1)}\right) = \min\left(1, \frac{p\left(\tilde{\theta} \mid \mathbf{w^{(h-1)}}, \sigma_\eta^{2(h-1)}, \mu_w^{(h-1)}\right)}{p\left(\theta^{(h-1)} \mid \mathbf{w^{(h-1)}}, \sigma_\eta^{2(h-1)}, \mu_w^{(h-1)}\right)} \right).$$

Remark 7.3.1. To compute the inverse of $(\mathbf{A}(\theta)\mathbf{A}(\theta)')$, where $\mathbf{A}(\theta) = \theta\mathbf{G} + \mathbf{I_n}$, we use Cholesky factorization. First, we decompose the matrix as,

$$\mathbf{A}(\theta)\mathbf{A}(\theta)' = \mathbf{C}\mathbf{C}',$$

where $\mathbf{C}$ is lower triangular. This decomposition enables efficient computation of the inverse using forward and backward substitution. For sampling, generate $\mathbf{u} \sim N(\mathbf{0}, \mathbf{I}_n)$, then solve $\mathbf{C}\boldsymbol{\xi} = \mathbf{u}$, and set $\boldsymbol{\xi} = \mathbf{C}^{-1}\mathbf{u}$.

Remark 7.3.2. To reduce the computational burden when sampling $\mathbf{w}$, we first compute the Cholesky factor $\mathbf{C}$ such that $\mathbf{C}'\mathbf{C} = \widehat{\mathbf{W}}_w$. Next, we solve for $\widehat{\mathbf{w}}$ using,

$$\mathbf{C}'\mathbf{C}\widehat{\mathbf{w}} = \boldsymbol{\Sigma}_b^{-1} \left(\mathbf{x}^* - \mathbf{d}_b \right) + \frac{\mu_w}{\sigma_\eta^2} \left(\mathbf{A}(\theta)\mathbf{A}(\theta)' \right)^{-1} \boldsymbol{l}_n,$$

for $\widehat{\mathbf{w}}$. Once we have $\widehat{\mathbf{w}}$, we can sample from $N\left(\widehat{\mathbf{w}}, \widehat{\mathbf{W}}_w^{-1}\right)$ by first drawing $\mathbf{u} \sim N(\mathbf{0}, \mathbf{I}_n)$ and solving $\mathbf{C}\boldsymbol{\xi} = \mathbf{u}$ for $\boldsymbol{\xi}$. Finally, we set $\mathbf{w} = \widehat{\mathbf{w}} + \boldsymbol{\xi}$, following the method proposed by Chan & Jeliazkov (2009).

In the next section, we validate this estimation algorithm using Monte Carlo simulations.

7.4 Simulation study

In this section, we consider a Monte Carlo study to examine the sampling properties of the Bayesian analysis mentioned above. The data generating process is as described in (7.1) and (7.2) such that y_i and η_i are independently generated from normal distributions. Row-standardized rook and queen contiguity weights matrices are considered for the spatial weights matrix $\mathbf{G}$. In queen contiguity, we set $g_{ij} = 1$ if the j-th observation is adjacent to or shares a boundary with the i-th observation, and for rook contiguity, we set $g_{ij} = 1$ if the j-th observation is adjacent (left, right, above, or below) to the i-th observation.

First, we generate samples of sizes n=100 and 400 using (7.1) and (7.2). The parameter values are chosen as $\theta = (0.1, 0.2, 0.4, 0.6, 0.8)$, $\mu_w = 2$, and $\sigma_\eta^2 = 2$. The number of resamples is fixed to 50, and the Markov chain has 12,000 draws, with the first 2,000 draws accounting for the burn-in period. We consider $\theta \sim \text{Uniform}(-1, 1)$, $\mu_w \sim N(0, 10)$, $\sigma_\eta^2 \sim \text{IG}(2, 2)$ as the prior distributions. The process is repeated R=50 times for this set of parameter values. Figure 7.1 shows some representative trace plots to assess the adequacy of the chain length and its mixing properties, that is, the convergence of MCMC samplers. The red dotted lines in these trace plots represent the estimated posterior means. The simulation results for θ, μ_w, and σ_η^2 are presented in Table 7.2 along with their average bias and RMSE. And let w_{ji}^r be the ith log-volatility calculated in the jth

repetition and rth pass from the sampler. Then the grand RMSE in this context is calculated by,

$$\text{RMSE} = \left[\frac{1}{50 \times R \times n} \sum_{i=1}^{n} \sum_{j=1}^{50} \sum_{r=1}^{R} \left(w_{ji}^{r} - \widehat{w}_{ji}^{r} \right)^2 \right]^{1/2}.$$

Table 7.2: Simulation results for different values of θ when $\mu_w = 2$, and $\sigma_\eta^2 = 2$ for samples of sizes 100 and 400.

n	Weights	$\widehat{\theta}$			$\widehat{\sigma}_\eta^2$		$\widehat{\mu}_w$		$\widehat{w}$	
		θ	**Bias**	**RMSE**	**Bias**	**RMSE**	**Bias**	**RMSE**	**MAE**	**RMSE**
100	Queen	0.1	0.0041	0.0538	-0.0023	0.0504	0.0030	0.0271	0.7027	0.7985
		0.2	0.0052	0.0734	0.0028	0.0581	0.0032	0.0395	0.8162	0.9823
		0.4	-0.0084	0.0947	0.0057	0.1273	0.0039	0.0730	0.8851	1.0017
		0.6	-0.0097	0.1083	0.0128	0.1591	0.0084	0.0869	0.9129	1.1075
		0.8	0.0681	0.1120	0.0538	0.2746	0.0156	0.1927	1.2133	1.8794
	Rook	0.1	0.0033	0.0413	-0.0018	0.0401	0.0024	0.0170	0.7003	0.7756
		0.2	0.0045	0.0687	0.0022	0.0468	0.0030	0.0202	0.8025	0.9462
		0.4	0.0072	0.0891	0.0050	0.0978	0.0035	0.0711	0.8123	0.9976
		0.6	-0.0083	0.0996	0.0111	0.1462	0.0077	0.0813	0.9045	1.0937
		0.8	0.0546	0.1035	0.0522	0.2641	0.0102	0.1916	1.2057	1.7987
400	Queen	0.1	0.0023	0.0310	-0.0011	0.0383	0.0022	0.0145	0.5426	0.5349
		0.2	0.0029	0.0406	0.0019	0.0396	0.0026	0.0227	0.5991	0.6812
		0.4	0.0037	0.0481	0.0025	0.0721	0.0031	0.0514	0.7168	0.9331
		0.6	-0.0043	0.0564	0.0095	0.0973	0.0052	0.0637	0.7814	0.9674
		0.8	0.0356	0.0907	0.0182	0.1015	0.0093	0.0914	0.9124	1.1017
	Rook	0.1	0.0015	0.0291	-0.0009	0.0311	0.0013	0.0138	0.5161	0.5278
		0.2	0.0027	0.0367	0.0014	0.0372	0.0020	0.0191	0.5517	0.6196
		0.4	0.0030	0.0416	0.0021	0.0713	0.0027	0.0456	0.6332	0.8995
		0.6	0.0037	0.0492	0.0087	0.0900	0.0041	0.0571	0.6910	0.9277
		0.8	0.0298	0.0894	0.0102	0.1100	0.0084	0.0921	0.9213	1.1026

The RMSE and MAE values of the log-volatility are also presented in Table 7.2. The results suggest that the simulation outcomes are invariant with respect to queen and rook weight matrices, indicating that the performance of the algorithms remains unaffected by the choice of spatial weight matrix specification. Furthermore, from Table 7.2 we can infer that the Bayesian estimator performs

satisfactorily. For smaller values of θ, the RMSE and bias are relatively low for all parameters, while higher values of θ are associated with increased RMSE and bias. Also, as the sample size increases, the RMSE and bias decrease, ensuring the stability of the model. Additionally, traceplots for another set of parameter values are also depicted in Figure 7.2, providing a thorough insight into their behavior over the iterations.

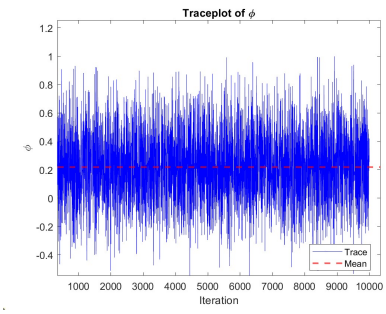

(a) Traceplot of $\theta = 0.2$.

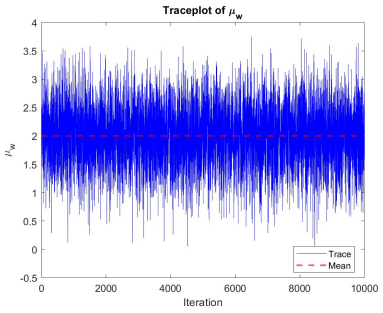

(b) Traceplot of $\mu_w = 2$.

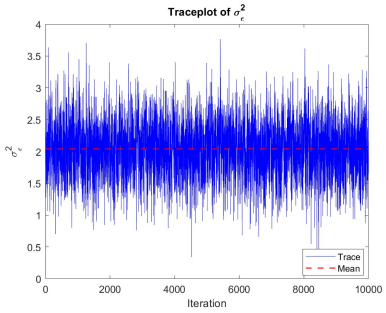

(c) Traceplot of $\sigma_\eta^2 = 2$.

Figure 7.1: Traceplots of parameters $(\theta, \mu_w, \sigma_\eta^2) = (0.2, 2, 2)$ for rook weight matrix.

7.5 Data analysis

In this section, we study the application of the suggested spatial SV model by analyzing the stock market dynamics. The dataset under study comprises the stock market values (in USD) for 74 countries, during the years 2022 and 2023. The data set is sourced from https://datacatalog.worldbank.org/home. These stock

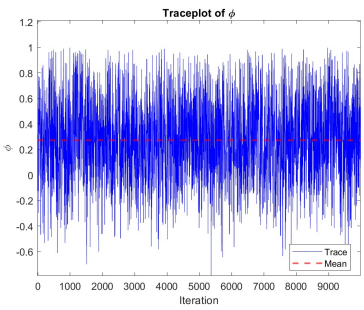

(a) Traceplot of $\theta = 0.3$.

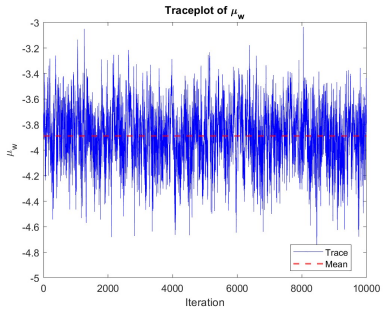

(b) Traceplot of $\mu_w = -4$.

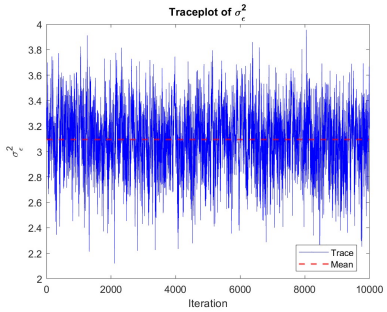

(c) Traceplot of $\sigma_\eta^2 = 3$.

Figure 7.2: Traceplots of parameters $(\theta, \mu_w, \sigma_\eta^2) = (0.3, -4, 3)$ for queen weight matrix.

market values reflect the performance of various stock exchanges or indices within each country, offering insights into both the temporal and spatial patterns of financial volatility on a global scale.

Annual returns are computed as the first differences in the logarithm of annual stock prices. Figure 7.3 illustrates the scatter plots of returns and squared returns. Here, the returns and squared returns are classified as low or high depending on whether they fall below or exceed their respective sample averages. To examine the spatial correlation in returns and squared returns, we conduct the Moran's I test, using weight matrices based on rook contiguity. Although both queen and rook contiguity matrices were evaluated in the simulation study, we focus on rook matrices here, as both matrices produced consistent results in the simulation analysis. The Moran's I test results summarized in Table 7.3 suggest that both returns and squared returns show significant positive spatial autocorrelation.

Notably, the test statistics are higher for squared returns, suggesting a moderate spatial dependence in market volatility.

Table 7.3: Moran I test results using rook contiguity matrices.

	Moran I test statistic	**p-value**
Retuns	0.4889	0.0012
Squared returns	0.4922	0.0010

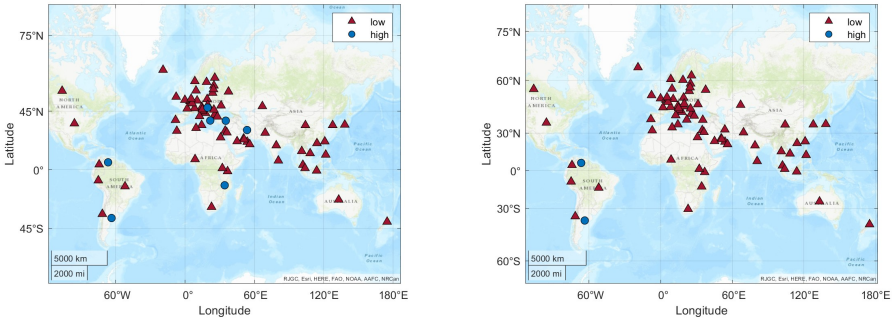

(a) Returns **(b)** Squared Returns

Figure 7.3: Scatter plots of returns and squared returns.

The model parameters are estimated using the Bayesian MCMC technique discussed earlier and are given in Table 7.4.

Table 7.4: Parameter estimates of the model

	Statistic	$\widehat{\theta}$	$\widehat{\mu_w}$	$\widehat{\sigma_\eta^2}$	$\widehat{w}$**(log-volatility)**
Rook	Mean	0.2171	-3.7627	3.4545	-3.7913
	Standard deviation	0.0293	0.1224	0.0883	0.1357

Furthermore, Table 7.5 shows the returns and estimated volatilities for each country. From this table, it is clear that countries such as Venezuela (4.9449), Argentina (1.9441), Malawi (0.5352), Iran (0.4283), and Turkey (0.4700) have high conditional variances, which could be due to economic instability, political uncertainty, and structural challenges. For example, the variance of Venezuela is extremely high, indicating a very volatile market, which may reflect severe

economic turbulence and uncertainty. On the other hand, countries like Korea (0.0941), Luxembourg (0.1128), and Singapore (0.1080) have relatively low conditional variances, which means a stable or predictable market. This may be partly because these countries enjoy strong institutional frameworks and well-established financial systems.

Table 7.5: Returns and estimated volatilities of 74 countries.

Country	Returns	Estimated volatility	Country	Returns	Estimated volatility
United Arab Emirates	0.1173	0.1974	Sri Lanka	-0.0238	0.1129
Argentina	3.033	1.9441	Lithuania	0.0886	0.1744
Australia	-0.028	0.1158	Luxembourg	-0.0219	0.1128
Austria	0.0307	0.1181	Latvia	0.1475	0.2175
Belgium	-0.0163	0.1076	Morocco	0.2069	0.2592
Bulgaria	0.1471	0.2294	North Macedonia	0.0178	0.1248
Bahrain	0.0142	0.1105	Malta	0.0258	0.1227
Bosnia and Herzegovina	-0.0369	0.1297	Malawi	0.5976	0.5352
Brazil	0.0767	0.1915	Malaysia	-0.0788	0.1600
Canada	-0.04	0.1232	Nigeria	-0.1273	0.2034
Switzerland	0.0357	0.1226	Netherlands	0.0982	0.1826
Chile	0.1754	0.2391	Norway	-0.0646	0.1465
China	-0.0664	0.1441	New Zealand	-0.0586	0.1382
Colombia	0.1044	0.2051	Oman	0.0851	0.1658
Germany	0.1559	0.2253	Pakistan	-0.2764	0.3157
Denmark	0.162	0.2317	Peru	0.076	0.1802
Egypt, Arab Rep.	0.1571	0.2223	Philippines	-0.053	0.1349
Estonia	0.0414	0.1277	Poland	0.1629	0.2369
Finland	-0.0471	0.1412	Portugal	0.0736	0.1676
France	0.1344	0.2031	Qatar	-0.1885	0.2508
United Kingdom	0.0238	0.1175	Romania	0.0973	0.1767
Greece	0.3808	0.3841	Russian Federation	-0.3095	0.3395
Hong Kong	-0.066	0.1463	Saudi Arabia	-0.0815	0.1597
Croatia	0.1759	0.2361	Singapore	0.0213	0.1080
Hungary	0.2145	0.2828	Slovakia	-0.1067	0.1818
Indonesia	-0.0395	0.1252	Slovenia	0.0799	0.1628
India	0.0455	0.1311	Sweden	-0.0392	0.1233
Ireland	0.1988	0.2633	Thailand	-0.0549	0.1448
Iran, Islamic Rep.	0.4213	0.4283	Tunisia	0.1182	0.1981
Iceland	-0.1741	0.2359	Turkey	0.5056	0.4700
Israel	-0.1763	0.2412	Taiwan	-0.0132	0.1056
Italy	0.2034	0.2548	Uganda	-0.1955	0.2609
Jordan	0.0049	0.1000	Ukraine	-0.1488	0.2193
Japan	0.0446	0.1232	United States	0.0373	0.1360
Kazakhstan	0.1973	0.2809	Venezuela, RB	9.5453	4.9449
Kenya	-0.2444	0.2828	Viet Nam	-0.1381	0.2076
Korea, Rep.	0.0023	0.0941	South Africa	-0.0514	0.1426

The data show clear regional clustering patterns: emerging markets and developing economies, such as Argentina, Malawi, and Turkey, tend to have higher

variances, which reflect the increased volatility and risk associated with these markets. On the other hand, developed nations like Luxembourg, Singapore, and Korea show lower variances, which indicates that they are less susceptible to financial shocks and have stronger economic stability. These trends highlight the disparities in risk management capabilities, institutional resilience, and susceptibility to global political and economic shocks.

In addition, the model's spatial dimension reveals significant regional interdependencies and spillover effects. Neighboring countries may possess comparable volatility characteristics due to common geopolitical factors, regional economic integration, or similar economic conditions. For example, geographically proximate countries such as those in Latin America or the Middle East exhibit similar volatility, underscoring the significance of taking spatial relationships when analyzing financial markets. Figure 7.4 presents a graphical representation of these estimated volatilities of the 74 countries.

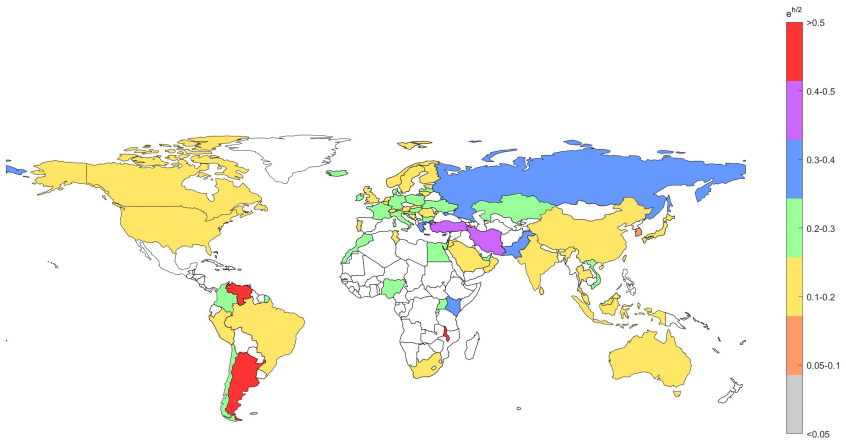

Figure 7.4: Estimated conditional volatilities.

These findings underscore the necessity of customised policy interventions in

countries that have higher conditional variances to reduce economic risks. They also emphasize the significance of monitoring regional dynamics and spillover effects for more in-depth risk assessment and global policy formulation.

7.6 Summary

A spatial SV model generated by a spatial MA process is introduced. The model is re-specified as a linear Gaussian state-space model for estimation, and the log-volatility equation is used as the state equation. Parameters are estimated through a Bayesian approach via the MCMC algorithm. A simulation study is carried out, and it suggests the good performance of the Bayesian estimator, demonstrating its stability and reliability in finite samples. The empirical application of the proposed model is shown in an analysis of stock market values for 74 countries, exhibiting widespread volatility variations. Large variances in countries such as Venezuela and Argentina indicate economic instability, whereas smaller variances in countries such as Luxembourg and Singapore indicate greater market stability. Further, regional clustering patterns and spillover effects distinguish typical volatility patterns among neighboring countries. These findings demonstrate the model's ability to capture global financial market dynamics and depict it as an effective tool for risk assessment and policy-making.

CHAPTER 8

Final Conclusions and Recommendations for Future Research

8.1 Introduction

This chapter concludes the study by summarizing its key findings, contributions, and potential directions for future research. The research highlights the developments in SV modeling and its wide range of applications in various fields. It also tackles the limitations of conventional SV models by developing novel frameworks that incorporate non-Gaussian distributions, alternative volatility structures, and advanced estimating methods. The study also broadens the application of SV models beyond financial analysis by showcasing their efficiency in image denoising, speech enhancement, and spatial analysis, underscoring their versatility in handling intricate real-world data. In addition to synthesizing the study's core contributions, the chapter also outlines future research directions, paving the way for further advancements in SV modeling and its interdisciplinary applications.

8.2 Summary of the thesis

This thesis mainly dealt with the construction and development of new SV models that expand the traditional frameworks by incorporating non-Gaussian distributions and other forms of volatility dynamics, making them more adaptable across various domains. It also explored the application of SV models beyond financial contexts, particularly in signal processing, thereby helping to bridge the gap between time series modeling and signal processing applications. The key findings of the research are summarized below.

The first chapter introduced some fundamental concepts, along with the Box-Jenkins methodology, linear time series models, financial time series models, and spatial models. It also provided a comprehensive review of existing literature and outlined the objectives and significance of the study. Thus, the chapter laid down the necessary theoretical foundation for the methodologies and models developed in subsequent chapters.

In Chapter 2, a novel SV model with Laplace-distributed returns was developed by using various non-Gaussian time series models. While most of the existing SV models were based on a standard AR framework, this study broadened the class by integrating alternative volatility structures, marking a significant contribution to the field. Specifically, the volatility sequences were generated by using an exponential minification model, a new exponential AR model, and an exponential mixture of AR and minification processes. The estimation of model parameters and simulation studies were conducted, and it confirmed that the developed SV models were both reliable and stable.

Chapter 3 explored the real-time applications of all the SV models developed in Chapter 2. Their effectiveness was demonstrated by analyzing two real financial datasets, and a comparative study among the models was also conducted. The

results indicated that the SV model generated based on the mixture of AR and minification processes outperformed the others, and this conclusion was supported by risk assessment measures, demonstrating how these advanced volatility models could enhance risk management strategies and improve volatility forecasts.

In Chapter 4, a new SV model with Laplace mixture-distributed returns was developed, where the volatility sequences were generated using an i-Garima Markov sequence. The i-Garima distribution, which is a mixture of exponential and gamma distributions, could effectively capture the heavy-tailed characteristics commonly found in financial data. Hence, an i-Garima AR(1) sequence was constructed and utilized to develop a novel SV model based on it. The statistical properties were discussed, and the parameters were estimated using GMM. A simulation analysis was conducted to assess its reliability, and the application of the model was examined using two real data sets. The results showed that the model successfully captured the key features of financial time series, demonstrating its effectiveness in modeling real-world data. Moreover, a comparative study with an existing SV model confirmed that it served as a promising alternative.

Since SV models are primarily applied only in financial contexts, Chapter 5 extended and developed their application to signal processing, specifically in speech enhancement. Speech signals were modeled using SV frameworks, and a speech enhancement technique was developed by integrating the SV model with the IMCRA technique and the OMLSA estimator. The performance of this proposed technique was evaluated experimentally and compared with existing conventional speech enhancement methods. The results demonstrated that the SV model-based approach outperformed other methods, thereby highlighting its effectiveness in enhancing speech quality. These SV modeling techniques can also be employed to diagnose or monitor speech-related disorders and in emotion detection systems. Further, they can be employed in speaker recognition systems to capture the

variation in voice signals among different speakers by modeling the volatility of speaker-specific variables such as formants, pitch, etc. Thus, the SV modeling technique provides a versatile framework for capturing the variations in speech signals

In Chapter 6, a new 2-D SV model was put forth and applied to image processing. The estimation of the model parameters was performed using Kalman filtering in a 2-D space, and this statistical framework was then applied to model the wavelet coefficients of images, particularly for image denoising and speckle suppression. Based on this framework, an MMSE estimator and an image-denoising algorithm were set up. Experiments on various natural images at different noise levels were conducted, and the results demonstrated that the proposed image-denoising technique significantly outperformed existing methods, highlighting its efficiency and robustness. Beyond image denoising, the 2-D SV model also offers significant potential for a range of other applications. It can be employed in texture analysis, where its ability to capture the stochastic nature of image textures can lead to improvements in segmentation and classification tasks. In video processing, the 2-D SV model can be used to reduce noise and preserve details, especially in low-light conditions. Additionally, the model can be applied to financial data analysis, where it can be used to model volatility surfaces, leading to more accurate predictions and better risk assessments.

Chapter 7 is focused on exploring the application of SV models in capturing complex spatial dynamics. A new spatial SV model driven by a spatial MA process was developed. The model's properties were analyzed, and parameter estimation was performed using a Bayesian approach via the MCMC algorithm. Its effectiveness was evaluated through simulation studies and real data applications. The results demonstrated that the developed SV model successfully captured spatial volatility dynamics and structures, making it a valuable tool for spatial data

analysis. Beyond this, our spatial SV model can be applied in various other domains. In environmental sciences, it can be used to model spatial variability in climate patterns or pollution levels. In medical imaging and remote sensing, the model can aid in detecting spatial patterns and anomalies, improving data-driven decision-making.

8.3 Contributions

This research offers contributions to methodological developments, theoretical breakthroughs, as well as real-world applications.

- **Theoretical advancements**

  The research introduced and developed novel SV models in 1-D, 2-D, and spatial frameworks, offering more flexible and generalized approaches to model time-varying volatility across various domains. The study expanded the traditional SV frameworks by integrating non-Gaussian distributions and other volatility structures, thereby making them more adaptive to complex real-world data. The development of these alternative volatility structures marks a significant contribution, broadening the scope of SV modeling beyond the AR frameworks typically used in the literature. The proposed models and estimation methods offer a more comprehensive approach to handling non-Gaussian, heavy-tailed, and dynamic volatility structures, making them highly relevant for both academia and industry.

- **Methodological innovations**

  Advanced statistical methods were used to enhance the efficiency and accuracy of SV model estimation. The research applied robust parameter estimation methods in non-Gaussian environments, Kalman filtering for state-space estimation in 1-D and 2-D volatility models, a non-linear filtering

method, and Bayesian inference using MCMC methods. These methods guaranteed accurate estimation and improved the applicability of the proposed models in practice.

- **Cross domain applications**

  Although SV models are classically applied in financial time series analysis, this study pushed their application to speech processing, medical imaging, image denoising, and spatial modeling, proving their applicability outside finance. By being able to extend SV models outside their traditional field, this study fills the gap between time series modeling, spatial analysis, and signal processing, providing a unified statistical framework for analyzing complex, dynamic, and noisy data across various fields.

- **Performance Benchmarking**

  The effectiveness of the proposed SV frameworks was rigorously evaluated through comparative analyses with existing models across multiple domains. These evaluations demonstrate that the suggested SV models offer significant improvements in capturing complex stochastic dynamics, ensuring more robust predictions and enhanced performance across diverse applications.

8.4 Recommendations for future research

Based on the findings of this study, several potential directions for future research are suggested below.

- Future research may involve alternative distributional assumptions, such as heavy-tailed or skewed distributions for volatility and errors to enhance model flexibility. Also, integrating deep learning techniques with SV models may improve volatility forecasting capabilities.

- The proposed SV-based speech model can be extended to more complex noise environments, such as reverberant and non-stationary noise conditions. Further, other non-Gaussian distributional assumptions for the model may enhance its effectiveness. They can be applied to speaker recognition systems, monitoring speech-related disorders, and in emotion detection systems.

- The 2-D SV model can be extended to multi-resolution or multi-scale representations, making it suitable for advanced applications such as medical imaging and hyperspectral image analysis. Adaptive estimation techniques can further improve performance under different noise conditions. Further integrating with deep learning techniques such as convolutional neural networks and recurrent neural networks may build hybrid models that can be useful for image classification.

- Further development of spatial and spatiotemporal SV models may enable better modeling of volatility patterns in geospatial and network data. For instance, spatial volatility models driven by other alternative structures and other distributional characteristics assumptions can be considered.

- The SV framework holds potential beyond finance, speech, and image processing. Future research can explore applications in environmental modeling, epidemiology, and climate studies, where time-varying volatility plays a crucial role.

- Efficient estimation techniques can be explored to improve computational scalability, particularly for high-dimensional and large-scale datasets.

Publications, Presentations, and Awards

List of published/accepted works:

1. Fathima Jafna & Krishnarani, S. D. (2024). Induced Garima Stochastic Volatility Models. *Austrian Journal of Statistics*, **53**(1), 104–119. (https://doi.org/10.17713/ajs.v53i1.1650)

2. Krishnarani, S. D. & Fathima Jafna. (2024). Exponential stochastic volatility model with Laplace returns and its variants. *Communications in Statistics - Simulation and Computation*, 1–30. (https://doi.org/10.1080/03610918.2024.2376873)

3. Fathima Jafna, & Krishnarani, S. D. (2025). Stochastic Volatility Models for Speech Signals. To appear in *International Journal of Speech Technology*.

List of works under review:

1. Fathima Jafna, & Krishnarani, S. D. (2024). Two-Dimensional Stochastic Volatility Model and its Application in Image Denoising.

2. Fathima Jafna, & Krishnarani, S. D. (2025). Spatial Stochastic Volatility Models: A Bayesian Approach with Spatial Moving Average Process.

Presentations in Conferences/Seminars:

1. *Induced Garima stochastic volatility models*, International Conference on Statistics, Probability, Data Science and Related Areas (ICSPDS 2023) in conjunction with the 42th Annual Convention of Indian Society for Probability and Statistics (ISPS) jointly organized by the Department of Statistics, CUSAT, and ISPS, 4-6 January 2023.

2. *Laplace stochastic volatility model and its variants*, International Conference on Statistical Sciences and Stochastic Modelling-ICSSSM 2023 organized by the Department of Statistics, University of Calicut, Thenhipalam, Malappuram, 16-17 February 2023.

3. *Speech enhancement using stochastic volatility models*, Ninth International Conference on "Recent Trends in Statistical Theory and Applications-2024" (WSTA-2024) organized by the Department of Statistics, School of Physical & Mathematical Sciences, University of Kerala, jointly with International Statistics Fraternity (ISF), Kerala Statistical Association (KSA), and Statistics Fraternity Kerala (SFK), June 29 - July 02, 2024.

4. *Two-dimensional stochastic volatility models for image processing*, Annual Conference of International Indian Statistical Association 2024, held at Cochin University of Science and Technology, jointly organized by the Department of Statistics, Cochin University of Science and Technology, and International Indian Statistical Association, 27-31 December 2024.

5. *Spatial Stochastic Volatility Models: A Bayesian Approach with Spatial Moving Average Process*, International Conference on Connecting Theory and Practice in Mathematics, Statistics, and Data Science (ICMSD-2025) jointly organized by the Department of Mathematics, School of Advanced Sciences,

VIT-AP University, in collaboration with the Department of Mathematics and Statistics, Faculty of Science and Technology, The University of the West Indies, St. Augustine, West Indies, 15-17 March 2025.

Awards:

- **Prof. K.C.S Pillai Best Paper Presentation Award-2024**, for the paper entitled *"Speech enhancement using stochastic volatility models"*, in the Ninth International Conference on "Recent Trends in Statistical Theory and Applications-2024" (WSTA - 2024), June 29 - July 02, 2024, organized by Department of Statistics, School of Physical & Mathematical Sciences, University of Kerala, jointly with the International Statistics Fraternity (ISF), Kerala Statistical Association (KSA) and Statistics Fraternity Kerala (SFK).

References

[1] Abraham, B., Balakrishna, N., & Sivakumar, R. (2006). Gamma stochastic volatility models. *Journal of Forecasting*, 25(3), 153–171.

[2] Aksasse, B. & Radouane, L. (1999). Two-dimensional autoregressive (2-D AR) model order estimation. *IEEE Transactions on Signal Processing*, 47(7), 2072–2077.

[3] Amirmazlaghani, M. & Amindavar, H. (2007a). Image denoising using two-dimensional GARCH model. In *2007 14th International Workshop on Systems, Signals and Image Processing and 6th EURASIP Conference focused on Speech and Image Processing, Multimedia Communications and Services* (pp. 397–400).

[4] Amirmazlaghani, M. & Amindavar, H. (2007b). Speckle suppression in medical ultrasound images using two dimensional GARCH model. In *2007 IEEE Pacific Rim Conference on Communications, Computers and Signal Processing* (pp. 585–588).

[5] Andersen, T. G., Chung, H.-J., & Sørensen, B. E. (1999). Efficient method of moments estimation of a stochastic volatility model: A Monte Carlo study. *Journal of Econometrics*, 91(1), 61–87.

[6] Andersson, J. (2001). On the normal inverse Gaussian stochastic volatility model. *Journal of Business & Economic Statistics*, 19(1), 44–54.

[7] Anselin, L. (2003). Spatial econometrics. In *A Companion to Theoretical Econometrics* chapter 14, (pp. 310–330). John Wiley & Sons, Ltd.

[8] Asai, M. & McAleer, M. (2005). Dynamic asymmetric leverage in stochastic volatility models. *Econometric Reviews*, 24(3), 317–332.

[9] Atkins, A. & Cohen, I. (2016). Speech enhancement using arch model. In *2016 IEEE International Workshop on Acoustic Signal Enhancement (IWAENC)* (pp. 1–5).

[10] Balakrishna, N. & Shiji, K. (2014). Stochastic volatility processes generated by Gumbel extreme value autoregressive model. *Journal of Indian Statistical Association*, 52(1), 45–64.

[11] Balakrishna, N. & Thekkedath, R. (2019). Modelling of stochastic volatility using Birnbaum-Saunders Markov sequence. *Statistics and Applications*, 17(1), 105–120.

[12] Barndorff-Nielsen, O. E. (1997). Normal inverse Gaussian distributions and stochastic volatility modelling. *Scandinavian Journal of Statistics*, 24(1), 1–13.

[13] Basel Committee on Banking Supervision (1996). *Supervisory Framework for the Use of "Backtesting" in Conjunction with the Internal Models Approach to Market Risk Capital Requirements*. Technical report, Bank for International Settlements.

[14] Bera, A. K. & Simlai, P. (2005). Testing spatial autoregressive model and

a formulation of spatial ARCH (SARCH) model with applications. In *Econometric Society World Congress* London.

[15] Berg, A., Meyer, R., & Yu, J. (2004). Deviance information criterion for comparing stochastic volatility models. *Journal of Business & Economic Statistics*, 22(1), 107–120.

[16] Black, F. & Scholes, M. (1973). The pricing of options and corporate liabilities. *Journal of Political Economy*, 81(3), 637–654.

[17] Bollerslev, T. (1986). Generalized autoregressive conditional heteroskedasticity. *Journal of Econometrics*, 31(3), 307–327.

[18] Bos, C. S. (2012). Relating stochastic volatility estimation methods. In *Handbook of Volatility Models and Their Applications* chapter 6, (pp. 147–174). John Wiley & Sons, Ltd.

[19] Box, G. & Jenkins, G. (1970). *Time Series Analysis: Forecasting and Control*. Holden-Day series in time series analysis and digital processing. Holden-Day.

[20] Box, G. E. P., Jenkins, G. M., Reinsel, G. C., & Ljung, G. M. (2015). *Time Series Analysis: Forecasting and Control*. Wiley Series in Probability and Statistics. Wiley, 5th edition.

[21] Broto, C. & Ruiz, E. (2004). Estimation methods for stochastic volatility models: A survey. *Journal of Economic Surveys*, 18(5), 613–649.

[22] Chan, J. C. (2013). Moving average stochastic volatility models with application to inflation forecast. *Journal of Econometrics*, 176(2), 162–172.

[23] Chan, J. C. & Jeliazkov, I. (2009). Efficient simulation and integrated

likelihood estimation in state space models. *International Journal of Mathematical Modelling and Numerical Optimisation*, 1(1-2), 101–120.

[24] Chausse, P. (2010). Computing generalized method of moments and generalized empirical likelihood with R. *Journal of Statistical Software*, 34(11), 1–35.

[25] Chib, S., Nardari, F., & Shephard, N. (2002). Markov chain Monte Carlo methods for stochastic volatility models. *Journal of Econometrics*, 108(2), 281–316.

[26] Chib, S., Nardari, F., & Shephard, N. (2006). Analysis of high dimensional multivariate stochastic volatility models. *Journal of Econometrics*, 134(2), 341–371.

[27] Choi, B. & Politis, D. N. (2007). Modeling 2-D AR processes with various regions of support. *IEEE Transactions on Signal Processing*, 55(5), 1696–1707.

[28] Choy, B., Wan, W. Y., & Chan, C. M. (2009). Bayesian student-t stochastic volatility models via scale mixtures. *Available at SSRN (August 18, 2009)*.

[29] Cliff, A. & Ord, J. (1973). *Spatial Autocorrelation*. London:Pion.

[30] Cohen, I. (2003). Noise spectrum estimation in adverse environments: Improved minima controlled recursive averaging. *IEEE Transactions on Speech and Audio Processing*, 11(5), 466–475.

[31] Cohen, I. (2004). Modeling speech signals in the time-frequency domain using GARCH. *Signal Processing*, 84(12), 2453–2459.

[32] Cohen, I. (2006). Speech spectral modeling and enhancement based on autoregressive conditional heteroscedasticity models. *Signal Processing*, 86(4), 698–709.

[33] Cohen, I. & Berdugo, B. (2001). Speech enhancement for non-stationary noise environments. *Signal Processing*, 81(11), 2403–2418.

[34] Cont, R. (2001). Empirical properties of asset returns: stylized facts and statistical issues. *Quantitative Finance*, 1(2), 223–236.

[35] Danielsson, J. (1994). Stochastic volatility in asset prices estimation with simulated maximum likelihood. *Journal of Econometrics*, 64(1-2), 375–400.

[36] Donoho, D. L. & Johnstone, I. M. (1994). Ideal spatial adaptation by wavelet shrinkage. *Biometrika*, 81(3), 425–455.

[37] Engle, R. F. (1982). Autoregressive conditional heteroscedasticity with estimates of the variance of United Kingdom inflation. *Econometrica*, 50(4), 987–1007.

[38] Engle, R. F. & Kraft, D. F. (1983). Multiperiod forecast error variances of inflation estimated from arch models. *Applied time series analysis of economic data*, (pp. 293–307).

[39] Engle, R. F. & Ng, V. K. (1993). Measuring and testing the impact of news on volatility. *The Journal of Finance*, 48(5), 1749–1778.

[40] Ephraim, Y. & Malah, D. (1984). Speech enhancement using a minimum-mean square error short-time spectral amplitude estimator. *IEEE Transactions on Acoustics, Speech, and Signal Processing*, 32(6), 1109–1121.

[41] Ephraim, Y. & Malah, D. (1985). Speech enhancement using a minimum mean-square error log-spectral amplitude estimator. *IEEE Transactions on Acoustics, Speech, and Signal Processing*, 33(2), 443–445.

[42] Fama, E. F. (1965). The behavior of stock market prices. *The Journal of Business*, 38(1), 34–105.

[43] Fingleton, B. (2008a). A generalized method of moments estimator for a spatial model with moving average errors, with application to real estate prices. *Empirical Economics*, 34(1), 35–57.

[44] Fingleton, B. (2008b). A generalized method of moments estimator for a spatial panel model with an endogenous spatial lag and spatial moving average errors. *Spatial Economic Analysis*, 3(1), 27–44.

[45] Gallant, A., Hsieh, D., & Tauchen, G. (1997). Estimation of stochastic volatility models with diagnostics. *Journal of Econometrics*, 81(1), 159–192.

[46] Garofolo, J., Lamel, L., Fisher, W., Fiscus, J., Pallett, D., & Dahlgren, N. (1993). Darpa timit acoustic-phonetic continuous speech corpus cd-rom TIMIT.

[47] Gaver, D. P. & Lewis, P. A. W. (1980). First-order autoregressive gamma sequences and point processes. *Advances in Applied Probability*, 12(3), 727–745.

[48] Gelfand, A. E. & Smith, A. F. (1990). Sampling-based approaches to calculating marginal densities. *Journal of the American statistical association*, 85(410), 398–409.

[49] Geman, S. & Geman, D. (1984). Stochastic relaxation, Gibbs distributions, and the Bayesian restoration of images. *IEEE Transactions on Pattern Analysis and Machine Intelligence*, PAMI-6(6), 721–741.

[50] Ghysels, E., Harvey, A. C., & Renault, E. (1996). 5 stochastic volatility. In *Statistical Methods in Finance*, volume 14 of *Handbook of Statistics* (pp. 119–191). Elsevier.

[51] Glosten, L. R., Jagannathan, R., & Runkle, D. E. (1993). On the relation between the expected value and the volatility of the nominal excess return on stocks. *The Journal of Finance*, 48(5), 1779–1801.

[52] Gnanadurai, D. & Sadasivam, V. (2008). An efficient adaptive thresholding technique for wavelet based image denoising. *World Academy of Science, Engineering and Technology, International Journal of Electrical, Computer, Energetic, Electronic and Communication Engineering*, 2(8), 1703–1708.

[53] Hansen, L. P. (1982). Large sample properties of generalized method of moments estimators. *Econometrica*, 50(4), 1029–1054.

[54] Harvey, A., Ruiz, E., & Shephard, N. (1994). Multivariate Stochastic Variance Models. *The Review of Economic Studies*, 61(2), 247–264.

[55] Hepple, L. W. (1995). Bayesian techniques in spatial and network econometrics: 1. model comparison and posterior odds. *Environment and Planning A: Economy and Space*, 27(3), 447–469.

[56] Hull, J. & White, A. (1987). The pricing of options on assets with stochastic volatilities. *The Journal of Finance*, 42(2), 281–300.

[57] Jacquier, E., Polson, N. G., & Rossi, P. E. (1994). Bayesian analysis of stochastic volatility models. *Journal of Business & Economic Statistics*, 12(4), 371–389.

[58] Jacquier, E., Polson, N. G., & Rossi, P. E. (2004). Bayesian analysis of stochastic volatility models with fat-tails and correlated errors. *Journal of Econometrics*, 122(1), 185–212.

[59] Jafna, F. & Krishnarani, S. D. (2024). Induced Garima stochastic volatility models. *Austrian Journal of Statistics*, 53(1), 104–119.

[60] Jarque, C. M. & Bera, A. K. (1980). Efficient tests for normality, homoscedasticity and serial independence of regression residuals. *Economics Letters*, 6(3), 255–259.

[61] Jassim, D. A., Jassim, S. I., & Alhayani, N. J. (2023). Image de-blurring and de-noising by using a Wiener filter for different types of noise. In *Proceedings of the 2nd International Conference on Emerging Technologies and Intelligent Systems* (pp. 451–460). Cham: Springer International Publishing.

[62] Joseph, A. (2009). *Marshall Olkin Distributions and Minification Processes*. PhD thesis, Mahatma Gandhi University.

[63] Kalman, R. E. (1960). A new approach to linear filtering and prediction problems. *Journal of Basic Engineering*, 82(1), 35–45.

[64] Kastner, G. (2016). Dealing with stochastic volatility in time series using the R package stochvol. *Journal of Statistical Software*, 69(5), 1–30.

[65] Kavungal, S. & Thekkedath, R. (2022). On normal-Laplace stochastic

volatility model. *Stochastics and Quality Control*, 37(2), 127–136.

[66] Kharfouchi, S. (2014). Inference for 2-D GARCH models. *Statistics & Probability Letters*, 92, 99–108.

[67] Kharfouchi, S. & Mili, W. (2023). Estimating 2-D GARCH models by quasi-maximum of likelihood. *Communications in Statistics - Theory and Methods*, 52(17), 6275–6286.

[68] Kim, S., Shephard, N., & Chib, S. (1998). Stochastic volatility: Likelihood inference and comparison with ARCH models. *The Review of Economic Studies*, 65(3), 361–393.

[69] Kitagawa, G. (1987). Non-Gaussian state-space modeling of nonstationary time series. *Journal of the American Statistical Association*, 82(400), 1032–1041.

[70] Krishnarani, S. D. (2007). *Study on Minification Processes*. PhD thesis, University of Calicut.

[71] Krishnarani, S. D. & Jafna, F. (2024). Exponential stochastic volatility model with Laplace returns and its variants. *Communications in Statistics - Simulation and Computation*, (pp. 1–30).

[72] Lawrance, A. J. & Lewis, P. A. W. (1981). A new autoregressive time series model in exponential variables (NEAR(1)). *Advances in Applied Probability*, 13(4), 826–845.

[73] LeSage, J. & Pace, R. K. (2009). *Introduction to Spatial Econometrics*. New York: Chapman and Hall/CRC, 1st edition.

[74] Liesenfeld, R. & Jung, R. C. (2000). Stochastic volatility models: Condi-

tional normality versus heavy-tailed distributions. *Journal of Applied Econometrics*, 15(2), 137–160.

[75] Liesenfeld, R. & Richard, J.-F. (2003). Univariate and multivariate stochastic volatility models: estimation and diagnostics. *Journal of Empirical Finance*, 10(4), 505–531.

[76] Liesenfeld, R. & Richard, J.-F. (2008). Improving mcmc, using efficient importance sampling. *Computational Statistics & Data Analysis*, 53(2), 272–288.

[77] Ljung, G. M. & Box, G. E. (1978). On a measure of lack of fit in time series models. *Biometrika*, 65(2), 297–303.

[78] Mandelbrot, B. B. (1997). The variation of certain speculative prices. In *Fractals and Scaling in Finance: Discontinuity, Concentration, Risk. Selecta Volume E* (pp. 371–418). New York: Springer.

[79] Martin, R. (2001). Spectral subtraction based on minimum statistics.

[80] Melino, A. & Turnbull, S. M. (1990). Pricing foreign currency options with stochastic volatility. *Journal of Econometrics*, 45(1-2), 239–265.

[81] Metropolis, N. & Ulam, S. (1949). The Monte Carlo method. *Journal of the American Statistical Association*, 44(247), 335–341.

[82] Meyer, R. & Yu, J. (2000). BUGS for a Bayesian analysis of stochastic volatility models. *The Econometrics Journal*, 3(2), 198–215.

[83] Moran, P. A. P. (1950). Notes on continuous stochastic phenomena. *Biometrika*, 37(1-2), 17–23.

[84] Muhammed Anvar, P., Balakrishna, N., & Abraham, B. (2019). Stochastic volatility generated by product autoregressive models. *Stat*, 8(1), e232.

[85] Nakajima, J. & Omori, Y. (2009). Leverage, heavy-tails and correlated jumps in stochastic volatility models. *Computational Statistics & Data Analysis*, 53(6), 2335–2353.

[86] Nakajima, J. & Omori, Y. (2012). Stochastic volatility model with leverage and asymmetrically heavy-tailed error using GH skew Student's t-distribution. *Computational Statistics & Data Analysis*, 56(11), 3690–3704.

[87] Nath, P. (1968). Inaccuracy and coding theory. *Metrika*, 13(1), 123–135.

[88] Nelson, D. B. (1991). Conditional heteroskedasticity in asset returns: A new approach. *Econometrica*, 59(2), 347–370.

[89] Nielsen, J. K., Christensen, M. G., & Boldt, J. B. (2023). An analysis of traditional noise power spectral density estimators based on the Gaussian stochastic volatility model. *IEEE/ACM Transactions on Audio, Speech, and Language Processing*, 31, 2299–2313.

[90] Noiboar, A. & Cohen, I. (2005). Two-dimensional garch model with application to anomaly detection. In *2005 13th European Signal Processing Conference* (pp. 1–4).

[91] Noiboar, A. & Cohen, I. (2007). Anomaly detection based on wavelet domain GARCH random field modeling. *IEEE Transactions on Geoscience and Remote Sensing*, 45(5), 1361–1373.

[92] Omori, Y., Chib, S., Shephard, N., & Nakajima, J. (2007). Stochastic

volatility with leverage: Fast and efficient likelihood inference. *Journal of Econometrics*, 140(2), 425–449.

[93] Otto, P., Doğan, O., Taşpınar, S., Schmid, W., & Bera, A. K. (2024). Spatial and spatiotemporal volatility models: A review. *Journal of Economic Surveys*.

[94] Otto, P., Schmid, W., & Garthoff, R. (2018). Generalised spatial and spatiotemporal autoregressive conditional heteroscedasticity. *Spatial Statistics*, 26, 125–145.

[95] Otto, P., Schmid, W., & Garthoff, R. (2021). Stochastic properties of spatial and spatiotemporal ARCH models. *Statistical Papers*, 62, 623–638.

[96] Popović, B. V., Ristić, M. M., & Balakrishna, N. (2017). A mixed stationary autoregressive model with exponential marginals. *Statistical Papers*, 58, 1125–1148.

[97] Pratt, W. K. (1977). *Digital Image Processing*. New York: Wiley.

[98] Raslain, S., Hachouf, F., & Kharfouchi, S. (2018). Using a generalised method of moment approach and 2D-generalised autoregressive conditional heteroscedasticity modelling for denoising ultrasound images. *IET Image Processing*, 12(11), 2011–2022.

[99] Rix, A., Beerends, J., Hollier, M., & Hekstra, A. (2001). Perceptual evaluation of speech quality (PESQ)-a new method for speech quality assessment of telephone networks and codecs. In *2001 IEEE International Conference on Acoustics, Speech, and Signal Processing. Proceedings (Cat. No.01CH37221)*, volume 2 (pp. 749–752).

[100] Robinson, P. M. (2009). Large-sample inference on spatial dependence. *The Econometrics Journal*, 12(S1), S68–S82.

[101] Ruiz, E. (1994). Quasi-maximum likelihood estimation of stochastic volatility models. *Journal of Econometrics*, 63(1), 289–306.

[102] Sato, T. & Matsuda, Y. (2017). Spatial autoregressive conditional heteroskedasticity models. *Journal of the Japan Statistical Society*, 47(2), 221–236.

[103] Shannon, C. E. (1948). A mathematical theory of communication. *The Bell System Technical Journal*, 27(3), 379–423.

[104] Shephard, N. (1996). *Statistical Aspects of ARCH and Stochastic Volatility*. London: (Edited by D.R. Cox, David V. Hinkley and Ole E. Barndorff-Neilsen). Chapman & Hall.

[105] Singh, B. P. & Das, U. D. (2023). On an induced distribution and its statistical properties. *REVSTAT-Statistical Journal*, 21(3), 303–319.

[106] Sri Ranganath, C. G. (2018). *Modelling and Analysis of Financial Time Series Using Some Non-Gaussian Models*. PhD thesis, Cochin University of Science and Technology.

[107] Sujith, P. & Balakrishna, N. (2023). Autoregressive inverse Gaussian process and the stochastic volatility modeling. *Communications in Statistics-Theory and Methods*, 52(10), 3574–3580.

[108] Taal, C. H., Hendriks, R. C., Heusdens, R., & Jensen, J. (2010). A short-time objective intelligibility measure for time-frequency weighted noisy speech. In *2010 IEEE International Conference on Acoustics, Speech*

and Signal Processing (pp. 4214–4217).

[109] Taşpınar, S., DoĞan, O., Chae, J., & Bera, A. K. (2021). Bayesian inference in spatial stochastic volatility models: An application to house price returns in chicago. *Oxford Bulletin of Economics and Statistics*, 83(5), 1243–1272.

[110] Tavares, L. V. (1980). An exponential markovian stationary process. *Journal of Applied Probability*, 17(4), 1117–1120.

[111] Taylor, S. (1986). *Modelling Financial Time Series*. New York, USA: John Wiley & Sons.

[112] Taylor, S. J. (1994). Modeling stochastic volatility: A review and comparative study. *Mathematical Finance*, 4(2), 183–204.

[113] Tran, T. D., Nguyen, Q. C., & Nguyen, D. K. (2010). Speech enhancement using modified IMCRA and OMLSA methods. In *International Conference on Communications and Electronics 2010* (pp. 195–200).

[114] Tsay, R. S. (2005). *Analysis of Financial Time Series*. New Jersey, USA: John Wiley & Sons.

[115] Varadhan, R. & Gilbert, P. (2009). BB: An R package for solving a large system of nonlinear equations and for optimizing a high-dimensional nonlinear objective function. *Journal of Statistical Software*, 32(4), 1–26.

[116] Wang, J. J., Choy, S. T. B., & Chan, J. S. (2013). Modelling stochastic volatility using generalized t distribution. *Journal of Statistical Computation and Simulation*, 83(2), 340–354.

[117] Wang, Z. & Bovik, A. (2002). A universal image quality index. *IEEE Signal Processing Letters*, 9(3), 81–84.

[118] Watanabe, T. (1999). A non-linear filtering approach to stochastic volatility models with an application to daily stock returns. *Journal of Applied Econometrics*, 14(2), 101–121.

[119] Wu, W.-R. & Kundu, A. (1992). Image estimation using fast modified reduced update Kalman filter. *IEEE Transactions on Signal Processing*, 40(4), 915–926.

[120] Zakoian, J.-M. (1994). Threshold heteroskedastic models. *Journal of Economic Dynamics and Control*, 18(5), 931–955.

[121] Zhang, Y. & Nadarajah, S. (2018). A review of backtesting for value at risk. *Communications in Statistics - Theory and Methods*, 47(15), 3616–3639.